THE FUEL CELL - STATUS AND BACKGROUND*

by

H. A. Liebhafsky and D. L. Douglas
General Electric Co., Schenectady, New York

ABSTRACT

A few historical remarks on fuel cell development and a brief review of chemical thermodynamics as applied to fuel cells will be given. Fuel cells will be classified on the basis of fuel costs; in particular, the hydrogen-oxygen cell developed at General Electric will be used as an example to compute performance of this type of cell.

* Manuscript not received in time for preprinting.

CARBONACEOUS FUEL CELLS*

by

H. H. Chambers and A.D.S. Tantram
Sondes Place Research Institute
Dorking, Surrey, England

ABSTRACT

A brief review of work at the Sondes Place Research Laboratory on high temperature fuel cells will be presented. Particular attention is given to the problem of the operation of high temperature fuel cells on carbonaceous fuels.

* Manuscript not received in time for preprinting.

Recd 14pp ms. Aug 28, 1959 by ORB

Not for Publication

Presented before the Division of Gas and Fuel Chemistry
American Chemical Society
Atlantic City, New Jersey, Meeting, September 13-18, 1959

The Hydrogen-Oxygen (Air) Fuel Cell with Carbon Electrodes

by Karl Kordesch

Research Laboratories
National Carbon Company
Division of Union Carbide Corporation
Cleveland, Ohio

Introduction

The reversal of water electrolysis on platinum electrodes in the first hydrogen-oxygen cell was demonstrated by W. Grove in 1839.[1] Early theoretical publications appeared shortly after 1900. Very extensive competitive efforts to build practical fuel cells started after World War I, ending in the mid-thirties without practical results. The improved heat engine, in spite of the efficiency limit set by Carnot's cycle, discouraged all efforts to construct fuel battery power plants. It is beyond the scope of this paper to mention all the various fuel cell constructions tried during this period. For a comprehensive summary, see the review written in 1933 by E. Baur and J. Tobler.[2]

Practical oxygen carbon electrodes became well known from experiments with air depolarized zinc batteries. Around 1930 G. W. Heise and E. A. Schumacher at the National Carbon Company[3] constructed long lasting "Air-Cells" with caustic electrolyte, more powerful than the earlier cells operating with ammonium chloride. But not before 1943, when W. G. Berl published his studies,[4] was the peroxide mechanism of the carbon oxygen electrode accepted.

After World War II scientists became strongly aware of the need to preserve fossil fuels by obtaining higher energy conversion efficiencies and fuel cell research was revived.

Again it is impossible to mention all the progress made in recent years on many different fuel cell systems, but fortunately most communications are already collected in survey publications and papers.[5,6,7]

As far as the carbon electrode fuel cell is concerned, O. Davtyan in Russia[8] experimented with catalyzed carbon electrodes with unconvincing results. E. Justi in Germany[9] worked initially with carbon, switching later to porous metal electrodes. The lack of durable catalysts and good carbon materials was obvious. The high pressure cell of F. T. Bacon seemed to be the only prospective fuel cell.[10]

In the meantime, realizing that the simplest gas element was a carbon electrode cell operating at room temperature on air, A. Marko and the author, at the University of Vienna, investigated catalyzing procedures which led to high current oxygen electrodes for alkaline cells.[11] A short time later F. Kornfeil,[7] F. Martinola[12] and H. Hunger[13] joined the research group. The performance of hydrogen-oxygen carbon fuel cells looked very promising, but it was still difficult to obtain reliable carbon material.

In 1955 the author joined the National Carbon Company and could make use of the carbon production experience accumulated at this organization. Together

with R. R. Witherspoon and J. F. Yeager, the present fuel cells have been developed.

In the following part of this paper the fundamental principles and the performance parameters of our cells will be stressed. Technical descriptions of the performance of practical batteries have already been presented by G. E. Evans at the Twelfth and Thirteenth Annual Power Sources Conferences of the U.S. Army Signal Research & Development Laboratories.[5]

The Characteristics of the National Carbon Fuel Cell

The construction of a laboratory type hydrogen-air fuel cell with two concentric electrodes is shown in Figure 1. The electrolyte is 30 per cent KOH. The cell produces electricity as soon as hydrogen is fed into the inner carbon tube. The outer tube is exposed to air. With more cells in series a common electrolyte circulation system is provided to remove water or carbonate if necessary. It should be noted that the CO_2-pickup from the air is astonishingly slow. The larger surface of the outer tube offsets the lower current density of the air electrode. With pure oxygen-hydrogen cells we prefer equal-surface electrodes to obtain proper cell balance. Tube bundle cells or plate cells are chosen in this case.

1. The Oxygen Electrode

The transporation of oxygen through the wall of the carbon tube determines the current of the electrode. Fick's law for linear diffusion allows a calculation of the pressure drop between gas side and electrolyte side of the carbon wall.[7] Under a number of operating conditions, it amounts to several percent of the applied gas pressure, depending on the load. No gas escapes into the electrolyte in a properly operating cell. The pore structure is chosen such that a large pressure differential is required to produce gas bubbles on the electrolyte-carbon interface. Penetration of the electrolyte into the carbon is effectively stopped by a special carbon repellency treatment.

The oxygen molecule adsorbed on the carbon surface is ionized in accordance with the 2-electron transfer process:

$$O_2(ads.) + H_2O + 2e^- \rightarrow HO_2^- + OH^-$$ [10]

Using special peroxide decomposing catalysts, the hydrogen peroxide concentration is reduced beyond the sensitivity of analytical tests to an estimated value of 10^{-10} molar. Suitable catalysts for this purpose are described in the patents by Marko and Kordesch.[14] The low concentration of peroxide corresponds to the open circuit potential of 1.10 to 1.13 volts against the hydrogen electrode. The oxygen formed by decomposition of the H_2O_2 is entirely reused. This fact changes the 2-electron process to an apparent 4-electron mechanism. Only the 0.1 volt differences in the open circuit potential of the oxygen-water electrode reveals that the electrode is <u>not</u> following the equation

$$O_2 + 2H_2O + 4e \rightarrow 4OH^-$$

The hydrogen peroxide mechanism on carbon electrodes was also confirmed by E. Yeager and co-workers.[15] The temperature coefficient of the oxygen electrode open circuit potential is -1 mv/°C (negative). Under a load condition of 10 ma/cm^2 we found a positive coefficient of +0.75 mv/°C, increasing with the load.[12]

In accordance with the theory, the oxygen electrode potential must be dependent on the alkali concentration of the electrolyte. The pH function is shown

in Figure 2. The slope of the oxygen-H_2O_2-electrode curve is about 30 to 32 mv per pH unit, in good agreement with the postulated value of 29 mv for a 2-electron process. In solutions containing less than 0.01N-caustic, the potential values are not reproducible. The non-linearity at higher caustic concentration is a direct measure of the activity coefficient. The abscissa indicates normality of the KOH, determined by titration with 1-N-sulfuric acid.

The potential of the oxygen-carbon electrode follows the Nernst equation. As a result, such electrodes can be used for the determination of oxygen partial pressures. The practical usefulness of such electrodes for oxygen sensing elements is very much increased by the fact that a 1 ma/cm^2 load does not cause marked deviations from this behavior in the range between 0.1 to 10 atmospheres pressure.[16] Total pressure changes give the same indication as partial pressure changes on open circuit measurements but not under heavy load conditions. In the latter case the diffusion through the blocking inert gas causes an additional pressure drop across the carbon electrode wall.

Figure 3 shows typical pressure curves of oxygen carbon electrodes, measured against an HgO reference electrode.

The effect of hydrogen peroxide concentrations in the electrolyte has been studied by E. Yeager and co-workers[15] and recently again by W. Vielstich.[17] The influence of the pH value of the caustic electrolyte on the hydrogen peroxide decomposition with and without catalysts was studied by Hunger[13] and led to the remarkable result that a minimum half life of peroxide is observed around pH-14. Different catalysts change the half lifetime several magnitudes but the minimum stays in the same pH region. In strong caustic solutions only the best catalysts are useful. Under pH-13 no catalyst was found which prevented a rapid increase in H_2O_2 half life to values one hundred and one thousand fold that at pH-14.

2. The Hydrogen Electrode

Hydrogen is not active on untreated carbon electrodes as shown by careful experiments with carbons free of heavy or precious metals. On our hydrogen electrodes we deposit a catalyst on the electrode surface.

The reaction occurring at the catalytically active sites of the hydrogen electrode can be represented by the equation

$$H_2\,(\text{gas}) \rightarrow 2H_{(\text{ads. on catalyst})}$$

$$2H(\text{ads.}) + 2OH^- \rightarrow 2H_2O + 2e^-$$

As with the oxygen electrode, the structure of the hydrogen electrode is important for the best gas diffusion rate. A permanent three phase zone: solid/gas/liquid, has to be established by wetproofing of the carbon material. In addition we had to take precautions against "internal drowning" of the H_2-electrode by the reaction product water. As indicated by the equation above, water forms at the anode and this creates a second current-limiting situation, at least at low temperatures. (Water-removing measures will be discussed in a later paragraph.)

The hydrogen electrode also follows the theoretical pH function very closely as is shown in Figure 2. The good reproducibility of measurements makes the carbon-hydrogen electrode a tool for determination of activity coefficients. Electrode equilibria are reached in minutes instead of many hours as is required with the Pt/Pt black electrode.

It is not easy to poison our carbon hydrogen electrodes. In four years of experimental testing of hydrogen electrodes, no electrode has failed as the result of catalyst poisoning, except for experiments in which large amounts of cyanide were deliberately introduced. Oxygen is detrimental only if mixed into the hydrogen in such quantities that large amounts of water form catalytically. This catalytic recombination feature prevents accumulation of a dangerous gas mixture above the electrolyte. In case of accidental gas leakage, this is important.

The open circuit potential has a small negative temperature coefficient. Under load the voltage increases rapidly with temperature, especially in the range between 20°C and 70°C.

The pressure sensitivity on open circuit follows the Nernst equation. Under heavy load conditions, the pressure effect is magnified because of the faster gas diffusion and higher adsorption values reached under pressure.

3. Removal of Reaction Water

In principle there are four ways of disposing of the reaction water:

a. Operation at a temperature near or above 100°C, in the latter case under higher pressure.

b. Operation at low temperatures under reduced pressure; current densities even at 100 mm Hg are above 20 ma/cm^2 at 0.8 volt.

c. Use of gas circulating principle. Water from the electrolyte evaporates through the porous carbon wall especially if a temperature difference is set up. The water removal speed depends also on gas flow rates and is limited by the saturation value of water vapor. With a cell temperature of 70°C and a condenser temperature of 20°C, 180 g of water is transferred by each cubic meter of gas streaming through the electrodes. Evaporation of water occurs on both electrodes, however, we find more water at the anode if the cell is operating.

d. Operation at low cell temperatures, allowing all the water to enter the electrolyte, with concentration of the electrolyte in a separate thermal or low pressure unit. For low power applications considerable dilution of electrolyte can be tolerated. The cell operates as well in 20 per cent KOH as in 50 per cent KOH. For example, a one ampere cell can be operated for one thousand hours with the production of less than one pound of water.

4. Cell Geometry

Because of the many possible fuel cell constructions, a comparison of different electrode arrangements and cell constructions had to be made. Figure 4 shows five basic arrangements of electrodes used in fuel cell constructions. The two-electrode tube cell (A) is the laboratory test cell model, several hundreds of which have been built to investigate electrode performance. The other constructions show remarkable improvements as can be seen from the table in Figure 4. The current factor given in this comparison represents the lower average polarization achieved by a more uniform potential distribution in the cell. The influence of ohmic resistance variations is eliminated by using the pulse current technique.[19] This method made our comparison insensitive to the distance between the electrodes.

The improvement factor in respect to current output per unit volume or weight is more spectacular than the mentioned polarization drop. Cell D, for

instance, is 10 times more efficient in volume utilization than type A. The internal resistance is a major factor to be considered in high current cells. Construction E is many times better than type C at 100 ma/cm^2 current densities, but the difference is negligible at 10 ma/cm^2. These few examples show how important the engineering of fuel cells for special applications can be, independent of electrode performance.

5. Performance Characteristics

Figures 5 and 6 show the voltage/current curves of hydrogen-oxygen carbon fuel cells under different conditions. The ohmic resistance is again eliminated by means of the pulse current (interrupter) technique.[19] All curves on the graph can be compared on an equal polarization basis. To calculate actual terminal voltages in special cells the following values should be used:

Electrolyte resistance: 1.0 to 2 ohm cm. (depending on temperature and concentration)

Electrode spacing: 0.1 to 0.3 cm.

As an example, the voltage drop due to the ohmic resistance in cell components is about 0.02 volt at 100 ma/cm^2 for a parallel plate battery, the terminal voltage of the cell can then be determined by combining this internal resistance loss with the appropriate polarization value from Figures 5 or 6.

6. Life Expectancy

Low temperature, low pressure cells are not subject to electrode attack by electrolyte or oxidation. The only life limiting factor is wettability of the carbon electrodes.[18] The tendency of the electrode to wet appears to depend on the potential at which the electrode operates rather than the current density at which it operates. We have achieved two years' intermittent service on 10 ma/cm^2 and over one year continuous service on 20 ma/cm^2 at 0.8 volt, with tests still in progress. This at atmospheric pressure, between room temperature and 70°C. In the meantime better repellency treatments and more active catalysts have brought our expectations up to 30 to 50 ma/cm^2 over 0.8 volt for at least the same time period. The use of increased pressure gives us the benefit of very high currents at low temperature, at the price of more need of auxiliary equipment. The operation of completely "wet" carbon electrodes under high pressures might give us the additional advantage of reducing maintenance and control devices very considerably.

7. Special Fuels

Hydrogen is an ideal fuel. One-eighth of one pound produces 1 kwhr in a fuel cell. In liquid state hydrogen can be stored for months, with a container weight approximately that of the hydrogen weight.

For every day purposes, hydrides, decomposed by water, are more convenient choices. One pound LiH is equivalent to 1 kwhr.

A practical, widely used fuel cell must operate on air, must be inexpensive and should use a readily available fuel. Our cells operate with high current densities on air with only a small potential difference to the pure oxygen-hydrogen cell. The use of carbonaceous fuels (liquids or gases) at low temperatures is one goal which we are attempting to accomplish. The need of removing carbonate from

the alkaline electrolyte complicates this system.

Unfortunately, the present oxygen-carbon electrode does not function in acid. The use of a redox-chemical intermediate (e.g., bromine) is necessary, which complicates the system.

All halogens operate on carbon electrodes with high current densities in acid systems. As a result hydrogen chlorine fuel cells can be operated at high power outputs for extended periods. Despite the higher voltages and high current densities which can be achieved in hydrogen chlorine fuel cells, the energy output per pound of combined fuel is less than that of the hydrogen-oxygen cell (because of the low equivalent weight of oxygen).

8. Outlook

It may safely be assumed that the fuel cell will eventually become a major power source, replacing other systems in some applications. The fuel cell-operated flashlight is still a long way in the future. For the immediate present, fuel cell applications will probably be restricted to those in which the excellency of fuel efficiency, silence, freedom from fumes, simplicity of design and operation are important requirements.

REFERENCES

1. W. R. Grove, Phil. Mag.III, 14, 129 (1839)
2. E. Baur, J. Tobler, Z. Elektrochem. 39, 148-180 (1933).
3. G. W. Heise, E. A. Schumacher, Trans. Electrochem. Soc. 62, 383 (1932) ibid., 92, 173 (1947), ibid., 99, 191 (1952).
4. W. G. Berl, Trans. Electrochem. Soc. 83, 253 (1943).
5. Proceedings, Twelfth Annual Battery Research and Development Conference, U. S. Army Signal Research & Development Laboratory, 1958 Symposium on Fuel Cells. Proceedings of Thirteenth Annual Power Sources Conf. of the U. S. A. S. R & D Lab., 1959 (in print)
6. A Review of the State of the Art and Future Trends in Fuel Cell Systems, Office of Naval Research, Cont. Nonr 2391 (00), 1958, by E. Yeager, Western Reserve University, Cleveland, Ohio
7. F. Kornfeil, Survey of Galvanic Fuel Cells, AIEE Conference paper 56-327 (1956), F. Kornfeil, Dissertation, Univ. of Vienna (1952).
8. O. K. Davtyan, Bull. Acad. Sci. USSR, Dept. Sci. Techn. 1, 107 (1946) and 2, 215 (1946).
9. E. Justi and co-workers, Jahrbuch Akad. Wiss. Lit., Mainz (1955) ibid., 1956, No. 1. See alsc: H. Spengler, Angenwandte Chemie 68, 689 (1956).
10. F. T. Bacon, Beama J., 61, 6 (1954).
11. K. Kordesch and A. Marko, Oesterr. Chem. Ztg. 52, 125 (1951).
12. K. Kordesch and F. Martinola, Monatsh. Chemie 84, 1, 39 (1953).
13. H. Hunger and A. Marko, 5th World Power Conference, Vienna 1956, No. 275 (paper K/11), H. Hunger, Dissertation, Univ. of Vienna, (1954).
14. A. Marko and K. Kordesch, U. S. Pat. Nos. 2,615,932 and 2,669,598.
15. R. R. Witherspoon, H. B. Urbach, E. Yeager and F. Hovorka, Tech. Report 4, Western Reserve University, ONR Cont. Nonr 581 (00), 1954
16. K. Kordesch and A. Marko, Microchemica Acta 36/37, 420 (1951), K. Kordesch and E. M. King, BuShips Cont. Nobs 72374 (1958).
17. Wolf Vielstich, Z.f. Physikal. Chemie 15, 409 (1958)
18. H. Hunger, Proceedings, Twelfth Annual Battery Research and Development Conf. U.S.A.S.R. & D Lab., 1958.
19. K. Kordesch, Electrochem. Soc. Meeting, Oct., 1956, paper, Abstract No. 27. U.S. Pat. No. 2,662,211.

Figure 1

CONCENTRIC HYDROGEN-AIR-FUEL CELL

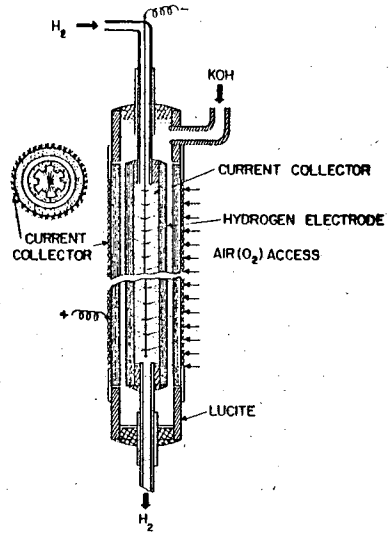

Figure 2

pH-FUNCTION OF THE OXYGEN AND HYDROGEN ELECTRODE

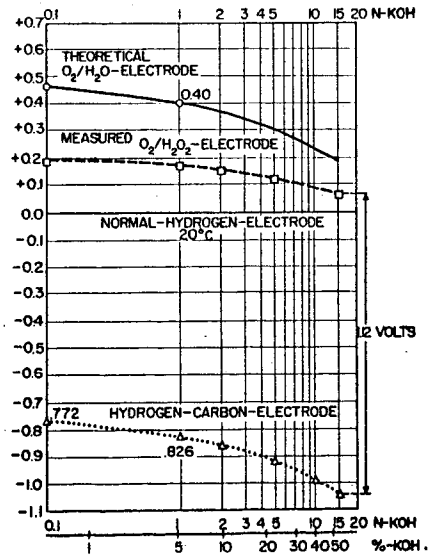

Figure 3

THE POTENTIAL OF THE OXYGEN ELECTRODE
AS A FUNCTION OF PRESSURE

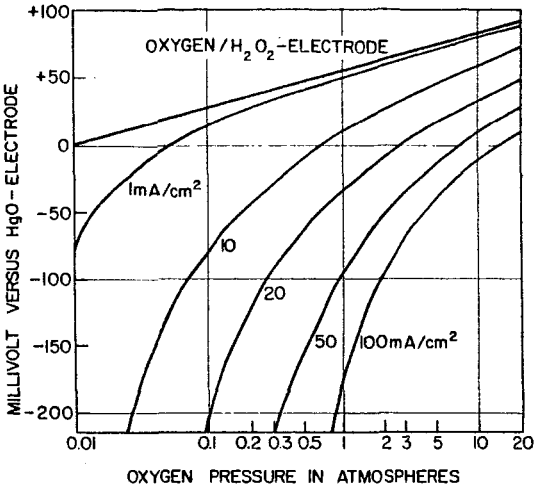

Figure 4

THE EFFECT OF CELL GEOMETRY
ON THE CURRENT OUTPUT OF A CELL

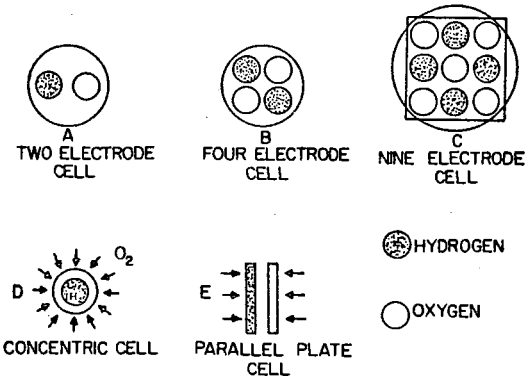

CURRENT DENSITY	CURRENT FACTORS FOR TYPES				
mA/cm²	A	B	C	D	E
10	1	1.4	1.7	1.8	1.8
50	1	1.5	1.8	2.0	2.0
100	1	1.6	2.0	2.5	2.5

Figure 5

PERFORMANCE PARAMETERS
OF NATIONAL CARBON FUEL CELLS

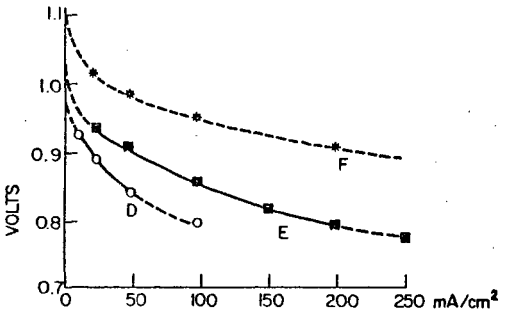

D-CELL AT 60°C O_2/H_2, ATMOSPHERIC PRESSURE(1958)
E-CELL AT 60°C O_2/H_2, 10 ATMOSPHERIC PRESSURE (1958)
F-CELL AT 60°C O_2/H_2, ATMOSPHERIC PRESSURE (1959)
---- DENOTES LACK OF LONG-TIME DATA

Figure 6

PERFORMANCE PARAMETERS
OF NATIONAL CARBON FUEL CELLS

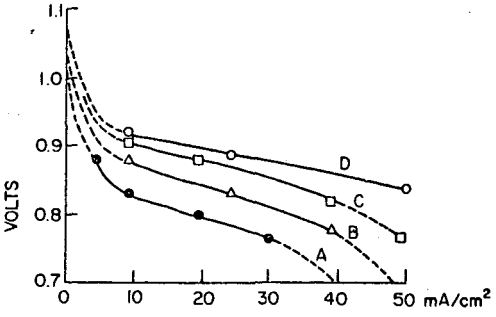

A-CELL AT 50°C O_2/H_2 PRESSURE 100 mm Hg
B-CELL AT 25°C AIR/H_2, 760mm Hg (CONCENTRIC CELL)
C-CELL AT 25°C O_2/H_2, ATMOSPHERIC PRESSURE
D-CELL AT 60°C O_2/H_2, ATMOSPHERIC PRESSURE
---- DENOTES LACK OF LONG-TIME DATA

Not for Publication
Presented Before the Division of Gas and Fuel Chemistry
American Chemical Society
Atlantic City, New Jersey, Meeting, September 13-18, 1959

CATALYSIS OF FUEL CELL ELECTRODE REACTIONS

G. J. Young and R. B. Rozelle
Catalysis Laboratory, Alfred University, Alfred, New York

Research on fuel cells over the past few years has resulted in the development of commercial prototypes of fuel gas cells operating on such gases as hydrogen, carbon monoxide, and hydrocarbons. Several considerations (1,2,3) have dictated the choice of this type of fuel cell (which includes all cells operating directly on fuel gases) over other types. Depending on projected applications and power requirements, fuel gas cells have been designed to operate at low and medium temperatures using aqueous electrolytes (4,5,6) and at higher temperatures using molten salt electrolytes (3,7).

Fuel gas cells, particularly those operating at lower temperatures, are subject to an irreversible free energy process resulting from the interaction of the reactant gases with the electrode surfaces (3,8). The reactant gases are chemisorbed by the electrode catalyst (or the electrode surface, which may act in a similar manner) and the reaction established is between the chemisorbed species and the electrolyte. The potential (free energy) developed by the cell therefore will depend on the equilibrium pressure of the chemisorbed species and has been shown (8) to be inversely proportional to the heat of chemisorption at high coverages. Thus, the catalyst surface can play a dual role in fuel cell electrode reactions - it can enhance the rate of reaction if chemical kinetics are the rate controlling factor, thus playing its usual role as a catalyst, and secondly, it can influence the potential of the cell by minimizing the free energy loss due to chemisorption.

While it is evident that the proper selection of catalysts in the design of fuel cell electrodes is essential for optimum performance, very little systematic work in this area has been published. Our present understanding of catalysis and surface physics, while far from complete, is nevertheless sufficiently comprehensive to enable a general explanation of fuel cell catalysts to be given. The present paper is concerned with a discussion of the activity of a variety of catalysts for both the fuel electrode and oxygen (air) electrode thus giving a guide to the selection of catalysts for specific cell reactions.

FUEL ELECTRODE

The role of the catalyst at the anode in a fuel gas cell is twofold: It must rapidly chemisorb the fuel gas in such a manner as to make it more susceptible to oxidation by the active species of the electrolyte and at the same time it should act to minimize the free energy loss due to chemisorption. Thus, the criteria for an active catalyst generally will be a weak, but rapid chemisorption of the fuel gas. In the selection of a catalyst these conditions must be met in addition to the requirement that the catalyst surface must preferentially

chemisorb the fuel gas species over the reaction products so as to limit self poisoning.

Hydrogen

The chemisorption of hydrogen, particularly on metal surfaces, has been studied more extensively than other fuel gases. At normal temperatures, chemisorption of the type required for high catalytic activity involves a partially covalent surface bond between hydrogen atoms and the d electrons of the metal. Thus, the general requirement for high catalytic activity of a metal in simple gas reactions of hydrogen is that it possesses d band vacancies. This limits the active metal catalysts to the transition elements, although not all of the transition metals are active catalysts even though they chemisorb hydrogen. The early members of the transition series, which have vacancies in both the first and second sub-bands, chemisorb hydrogen strongly and are not particularly good catalysts in hydrogen reactions. The later members of the three transition series, which have vacancies only in the second sub-band, exhibit the lowest heats of chemisorption at the surface coverages involved in heterogeneous reactions, and are recognized as highly active catalysts for hydrogen reactions. Thus, it would appear that the most active metal catalysts for fuel cell electrode reactions where hydrogen is the fuel gas should be selected from those transition metals with d-band vacancies only in the second sub-band- e.g. the group VIII metals.

Confirmation for the views stated above is given by Figure 1 where the open circuit potentials for the hydrogen half-cell are plotted as a function of the approximate number of d-band vacancies of the 5d transition metals and their alloys when used as catalysts at the hydrogen electrode. These data were obtained with a low temperature fuel cell (27°C) employing an aqueous sodium hydroxide electrolyte and porous graphite electrodes which were impregnated with the metal catalysts. In general the catalytic activities of the metals appear to parallel their open circuit potentials e.g. a small free energy loss due to chemisorption generally implies a high catalytic activity. Tungsten and rhenium both have relatively low open circuit potentials and high heats of chemisorption. Tungsten and quite probably rhenium have vacancies in the first d sub-band. The open circuit half cell potential of osmium is intermediate between the latter metals and platinum and iridium. The alloys of platinum-iridium appear to exhibit a maximum in catalytic activity at about one d band vacancy. As the vacancies in the d band of platinum are filled by the s electrons of gold upon alloying, the fuel cell potential decreases sharply until the 60% Au - 40% Pt alloy after which the potential appears to remain relatively constant.

Table I lists the open circuit, hydrogen half-cell potentials for the group VIII transition metals and the neighboring Ib metals. The same trend in catalytic activity is observed in the three transition series, the potential reaching a maximum between the last two transition metals and falling sharply for the following Ib metal. The irreversible free energy loss in chemisorption is larger for the group VIII metals of the first series (Fe, Co, Ni) than for the metals in the second and third series. Also, these metals of the first series are more susceptible to poisoning by impurity gases such as sulfur compounds. Platinum and

Palladium are probably the best catalysts for hydrogen electrodes in fuel gas cells. Although, a maximum in activity is obtained with alloys of certain of these metals the slight increase in potential over the pure metals would probably not justify the difficulties of alloying in commercial practice.

Table I

OPEN CIRCUIT HYDROGEN HALF CELL POTENTIALS FOR GROUP VIII AND Ib METAL CATALYSTS

Fe	Co	Ni	Cu
533	703	693	323
Ru	Rh	Pd	Ag
740	763	743	243
Os	Ir	Pt	Au
603	733	753	263

The results given in Table I for low temperature fuel cells, using aqueous hydroxide electrolyte, in general are paralleled by high temperature cells employing molten salt electrolytes, although the free energy loss on chemisorption often decreases with increasing temperature and consequently is of less importance. For example, palladium and platinum catalysts give higher open circuit potentials with hydrogen as a fuel gas than does nickel, iron, etc. in a variety of molten salt electrolytes. At relatively high temperatures (Ca 500-800°C) the nature of the hydrogen chemisorption changes for several of the group VIII metals. Quite probably, hydrogen forms d s p hybrid bonds with the metal. Indeed, in some cases the catalyst can be poisoned by being heated to a high temperature and then cooled in hydrogen. Presumably, this leaves a strongly bonded form of chemisorbed hydrogen on the surface which is not active in the electrode reaction since the activity of the catalyst can be restored by heating and cooling in helium.

Acetylene and Ethylene

The catalytic activities of the group VIII and Ib metals in the oxidation of ethylene and acetylene in a fuel cell appear to be similar to their activities with hydrogen, i.e. a high catalyst activity is favored by vacancies in the d band of the metal. However, these reaction systems are fundamentally more complex than those of the hydrogen cell. The reactions which occur at the anode are complicated by two factors (i) the nature of the chemisorbed complex, which is in doubt, since either carbon-carbon or carbon-hydrogen bonds may be broken in chemisorption and (ii) the amount of self-hydrogenation at the surface.

The reaction species may be alike in some instances since the fuel cell potentials, for both ethylene and acetylene on certain catalysts, are very similar.

The fuel cell employed for studies of acetylene and ethylene was similar to the cell used for hydrogen except that the electrolyte was a 40% aqueous solution of K_2CO_3. The reactive species in solution may be either the carbonate ion, bicarbonate ion, or the hydroxyl ion. All three ions are present in the solution in reasonable concentrations. Preliminary experiments, however, appear to favor the bicarbonate ion. The products of the reaction at the fuel electrode are in doubt, but first analyses seemed to indicate the presence of aldehydes and carbon dioxide.

The most active catalysts among the metals studied are the group VIII metals of the first transition series along with palladium and iridium as illustrated in Table II.

Table II

Metal	Half Cell Potential (millivolts) Ethylene	Acetylene
Fe	780	790
Co	675	715
Ni	605	595
Cu	410	475
Ru	205	475
Rh	365	535
Pd	710	705
Ag	095	095
W	405	460
Os	425	570
Ir	610	625
Pt	380	570
Au	190	185

The maximum in catalytic activity appears at a different place in each transition series. The group Ib metals, although possessing some activity, are in general poor catalysts for these reactions.

The catalytic activities of these metals in the ethylene and acetylene oxidation reactions at the anode are quite sensitive to the state of the catalyst surface as was the case with hydrogen. This is especially true for the group VIII and Ib metals of the 2nd and 3rd transition series. If, after reduction, these metals are exposed to the atmosphere only momentarily their catalytic activity is decreased

considerably. This is illustrated in Figure 2 where the lower curves represent catalysts with surface oxides. Although the members of the first transition series are susceptible to oxygen poisoning the effect on catalytic activity is much less accentuated.

The most active catalysts are produced by 'in situ' reductions where the surface, after reduction, is not exposed to the atmosphere but remains constantly under hydrogen until the electrode-electrolyte contact is made.

As in the case for hydrogen, a low heat of chemisorption in either ethylene or acetylene will minimize the irreversible free energy loss at the fuel electrode and, hence, produce a higher potential in the fuel cell. There are two factors which determine the heat of chemisorption of ethylene and acetylene: (i) a geometric factor, i.e., interatomic distances in the catalyst lattice, and (ii) an electronic factor. The most favorable interatomic distance, for ethylene hydrogenation, according to Beeck (9), is 3.75 Å as observed in catalyst activity in ethylene hydrogenation reactions. Our results can neither support nor refute this, since the crystal planes exposed are not known and, thus, the more active spacings cannot be predicted. Probably the more important factor is the electronic character of the catalyst. Our results and the results of other investigators support this view (10). Only transition metals or near transition metals catalyze these reactions. Although surface reactions of acetylene have been investigated only to a limited extent, the results of this paper indicate they follow a pattern similar to that of ethylene.

The slight activity shown by the Ib metals in these reactions can be attributed to either their small d-s electron promotion energies (11), which give rise to vacancies in the d band or σ bonding by the metals to these molecules which can be achieved by a rearrangement of the metallic orbital together with the formation of a bond by overlap of the filled d-orbitals with the antibonding orbitals of the adsorbate(12).

Carbon Monoxide

The same type of fuel cell was used for studies on carbon monoxide as with ethylene and acetylene, the electrolyte being a 40% aqueous K_2CO_3 solution.

The catalytic activities of the transition metals investigated in this cell for the anodic oxidation of carbon monoxide are shown in Table III. The variation in the half cell potential among the transition metal catalysts are small with the exception of Palladium which appears to be the most active catalyst for the reaction. The activities of the Ib metals are low as for the fuel gases previously mentioned. This would indicate the necessity of vacancies in the d band of the metal catalysts for a high activity.

The chemisorption of carbon monoxide may take place by a number of different mechanisms. On certain metals, such as palladium and platinum, it chemisorbs with a one site attachment forming a surface layer similar

Table III

HALF CELL POTENTIALS (MILLIVOLTS) FOR CARBON MONOXIDE

Fe	Co	Ni	Cu
-	440	495	190
Ru	Rh	Pd	Ag
475	540	825	225
Os	Ir	Pt	Au
520	510	545	150

in structure to the metal carbonyls, i.e., M = C = O (13). The second mode of chemisorption is a two site sorption with the carbon monoxide complexes covering two surface sites as indicated in the following diagrams (14).

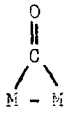

Two site chemisorption probably takes place on rhodium (13) in this manner. The two types of two site mechanisms cannot be differentiated since the lattice geometry required in the metals for chemisorption falls in quite narrow limits, otherwise, the valence angles would be prohibitive. All of the transition metals studied probably expose crystal planes suitable for both mechanisms.

Again the activities of the Ib metals may be due to the small energies required for d-s electron promotion.

OXYGEN (AIR) ELECTRODE

The general requirements of a catalyst at the oxygen electrode of a fuel gas cell are essentially the same as for the fuel electrode catalyst except that negative ion formation is the process under consideration. In cells employing aqueous hydroxide electrolytes, the oxygen must be chemisorbed in such a manner as to lead to the rapid formation of peroxide and hydroxide ions in the presence of water. A further role of the catalyst in this case is to aid in the decomposition of the peroxide.

The most active catalysts, among those investigated, for the electrode reaction of the oxygen half-cell in aqueous hydroxide electrolytes are the oxides of the group Ib metals: copper, silver, and gold. Copper and silver oxides are known to be active oxidation

catalysts (e.g. they must chemisorb oxygen in a state that will readily take part in oxidation reactions) and their presence presumably also promotes decomposition of peroxide ions formed under current drain. Gold films, however, have been reported to be inert toward the chemisorption of oxygen up to 0°C (15). Possibly O_2^- ions are formed on the gold surface as an intermediate step in the reduction of oxygen. Such a species, if present in small amounts, might not be detected in chemisorption experiments since it would be readily removed from the surface on outgassing. The activities of the Ib metal oxides are in the order: copper silver gold.

Cobalt and nickel oxides possess an activity only slightly greater than unactivated graphite which may indicate that these metals are essentially inactive; while iron oxide has a reasonable activity. The open circuit half-cell potentials for the 3d transition oxides and oxides of cobalt-nickel and nickel-copper alloys are shown in Figure 3. As copper is added to nickel, a slight increase in potential starts after the 60% copper- 40% nickel alloy (oxide) is reached and then a rapid increase is observed as pure copper oxide is approached. A similar behavior is found for palladium-silver alloys (oxides) in the 4d transition series.

The activity of oxides as catalysts at the oxygen electrode may be varied considerably by the introduction of a defect structure. It is well known that heterogeneous reactions proceeding by negative ion formation can be profoundly altered by the defect state of the catalyst surface.

ACKNOWLEDGMENT

The authors wish to gratefully acknowledge the financial assistance given by the Office of Naval Research to support this work.

REFERENCES

(1) Liebhafsky, H.A. and Douglas, D.L., Paper 59-SA-22 published by the Am. Soc. of Mechanical Eng. (1959).

(2) Young, G.J. and Rozelle, R.B., J. Chem. Ed. 36, 68 (1959).

(3) Broers, G.H.J., "High Temperature Galvanic Fuel Cells", Ph.D. Thesis, University of Amsterdam, 1958.

(4) Evans, G.E., Proceedings of the Twelth Annual Battery Conference, p. 4 (1958).

(5) Bacon, F.T., Beama, J. 61, 6 (1954).

(6) Bacon, F.T., British Patent 677,298 (1952).

(7) Gorin, E. and Recht, H.L., Paper 58-A-200 published by the Am. Soc. of Mechanical Eng. (1958).

(8) Rozelle, R.B. and Young, G.J., J. Phys. Chem., in press.

(9) Beeck, O., Rev. Mod. Physi. 17, 61 (1945).

(10) Trapnell, B.M.W., "Chemisorption", p. 228 Butterworths Scientific Pub. London, England 1955.

(11) Ibid. p. 74.

(12) Dowdin, D.A. "Chemisorption" p. 9, Butterworths Scientific Pub. 1957.

(13) Trapnell, B.M.W., "Chemisorption", p. 181, Butterworths Scientific Pub. 1957.

(14) Ibid. p. 182.

(15) Ibid. p. 61.

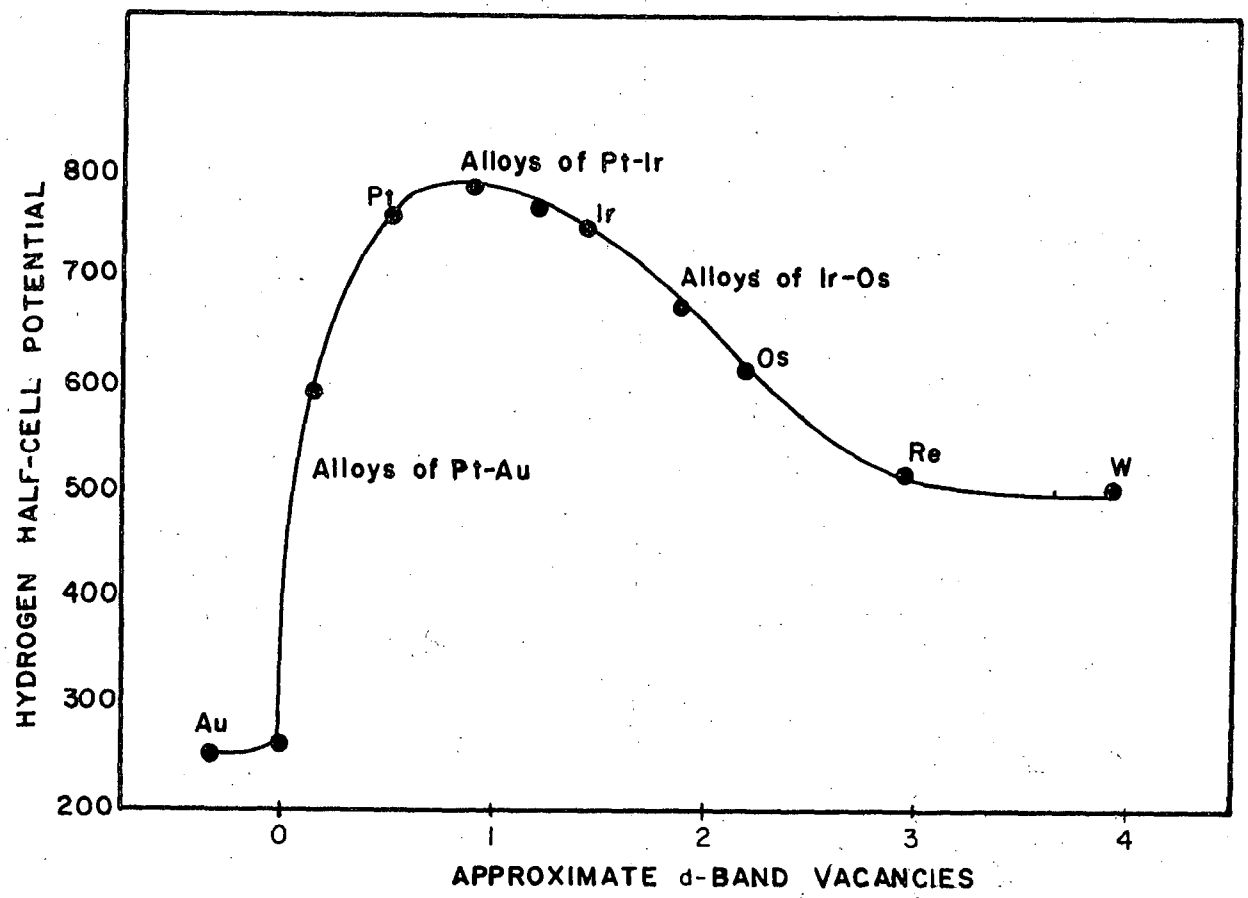

Figure I Hydrogen Half Cell Potentials as a function of d band Vacancies for the 5d Transition

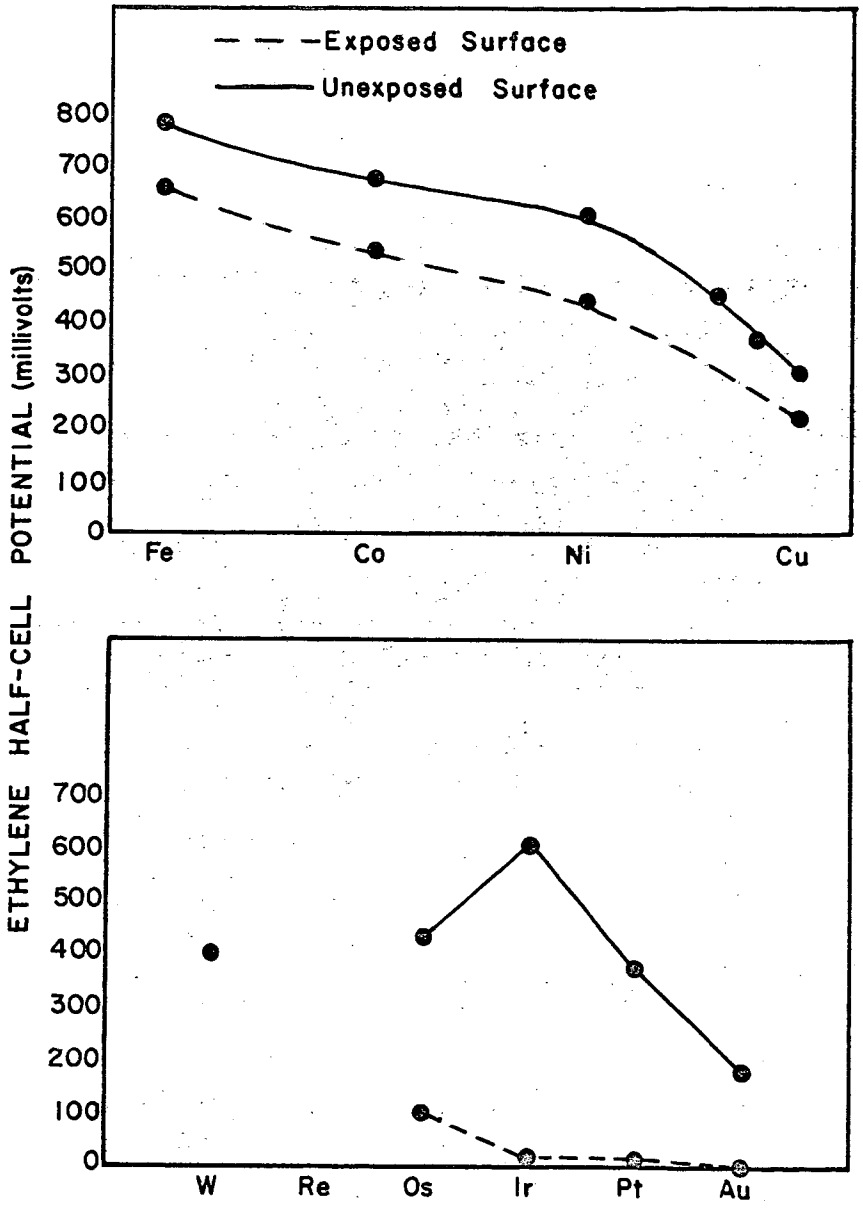

Figure II Ethylene Half Cell Potentials for the 3d and 5d Transition Metals

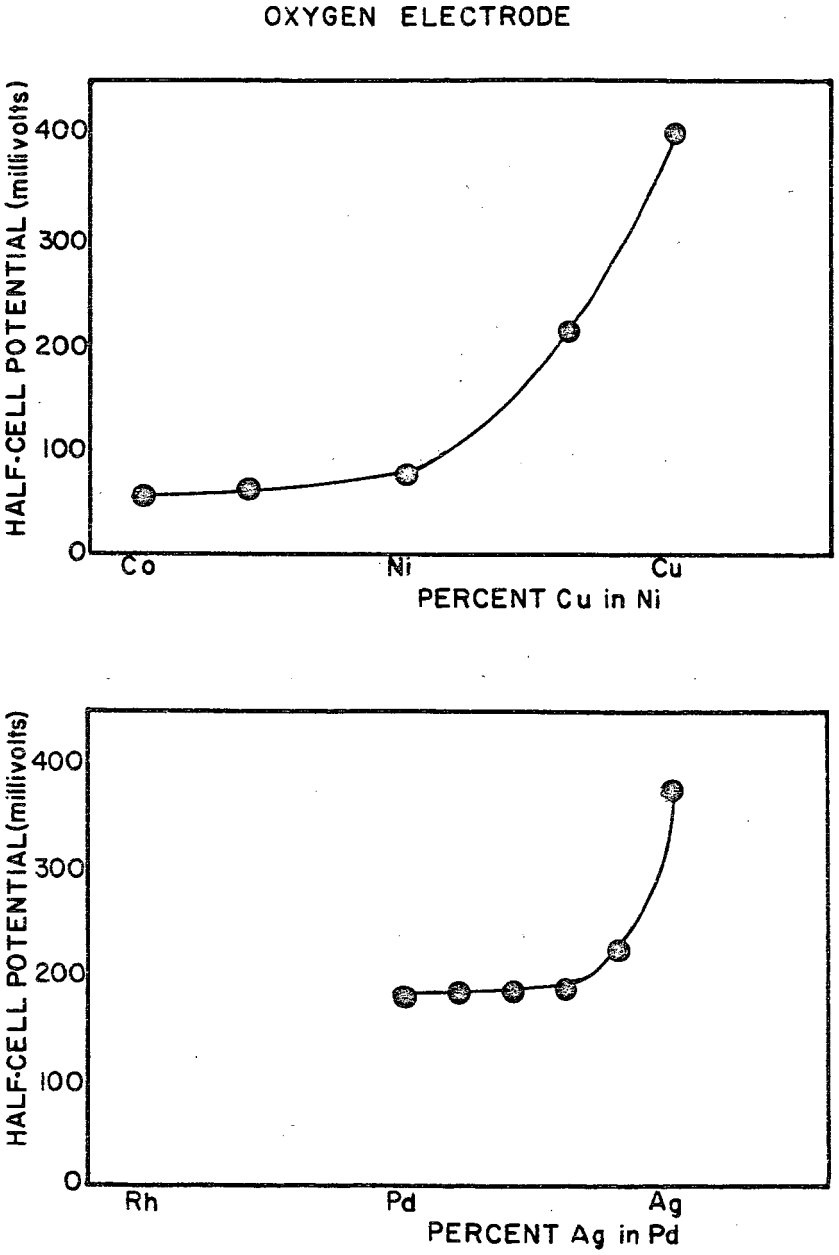

Figure III Oxygen Electrode Half Cell Potentials

Not for Publication

Presented Before the Division of Gas and Fuel Chemistry
American Chemical Society
Atlantic City, New Jersey, Meeting, September 13-18, 1959

The Fundamentals of Electrode Kinetics as They Apply to Low Temperature Hydrogen Oxygen Fuel Cells

L.G. Austin

Fuel Technology Department
The Pennsylvania State University
University Park, Pennsylvania

INTRODUCTION

In a short paper such as this it is impossible to do more than briefly summarize and explain some of the fundamental equations of irreversible electrode kinetics. It is believed, however, that there is a need for such a presentation since many of the workers becoming interested in the field of fuel cells will not be familiar with the terms and concepts involved. The subject is treated with respect to the well known [1] low temperature hydrogen oxygen fuel cell employing porous conducting electrodes.

DISCUSSION

Basic Formulae

The following thermodynamic formulae form the basis of the more specific formulae derived later and are presented for convenience. In any process

$$aA + bB + \cdots\cdots \rightleftharpoons mP + nQ + \cdots\cdots$$

the change in free energy per mole of reaction from left to right is given by

$$\Delta G = -RT \ln K_p + RT \ln \frac{(P)^m (Q)^n \cdots}{(A)^a (B)^b \cdots} \quad (1)$$

a, b, m, n are the number of molecules involved, (A), (B), (P), (Q) are the activities of the reactants and products and K_p is the equilibrium constant of the reaction.

For some arbitrary definition of a standard state where the activities are unity

$$\Delta G_o = -RT \ln K_p \quad (2)$$

where ΔG_o is known as the standard state free energy change. For a substance going from one activity, a_1, to another, a_2, $K_p = 1$, and

$$\Delta G = RT \ln a_2/a_1$$
$$a_2 = a_1 e^{\frac{\Delta G}{RT}} \qquad (3)$$

The rate of an activated chemical reaction in one direction is given by

$$v_1 = k_1 (A)_1^a (B)_1^b ( ) \cdots ( ) e^{\frac{-\Delta G_o^*}{RT}} \qquad (4)$$

where v_1 is the rate of reaction, $(A)_1$, $(B)_1$ are the activities of reactant at the reaction condition, ΔG_o^* is the free energy of activation at the standard state used to define the activities and k_1 is a constant for the reaction.

The electrical potential, E, involved for a change of free energy ΔG is given by

$$\Delta G = -nFE \qquad (5)$$

where F is the Faraday and n is the number of electrons involved in the reaction. A consistent system of units must be used.

Open Circuit Potentials

Hydraulic Analogy

At open circuit, when no current is drawn from the cell, the potential obtained from the cell is equal to the corresponding free energy change in transporting reactant to product under these ideal reversible conditions. Figure 1 shows a hydraulic analogy of a fuel cell at open circuit. Since it is impossible to measure the potential of a single electrode it is necessary to have two electrodes, represented by the two U-tubes of the figure. The difference in levels of the liquid in each arm of a U-tube (h_1 say) represents the free energy change between the reactant and the product for a half cell. For a fuel cell in which reactant is supplied continuously to each electrode and product removed continuously, the hydraulic analogy requires infinite reservoirs at the liquid levels; one of these is shown at A for illustration.

It is impossible to measure the voltage corresponding to h_1 but if the right hand U-tube is considered as a reversible standard state hydrogen half cell, h_2 is arbitrarily taken as zero, and Δ_p corresponds to the half cell potential (with respect to the standard hydrogen half cell) of the left hand electrode. With valve V closed, that is, no flow through the system, $\Delta_p \equiv h_1$, and the open circuit potential, E_r (infinite external resistance is comparable to the valve being closed) is equivalent to ΔG. It is clear from this picture that the potential change <u>through</u> the electrode-electrolyte surface is zero at zero current drain; the potential drop, Δ_p, exists <u>across</u> the external electrode to electrolyte connection. In an electrode process at open circuit, at the instant of electrode immersion ions pass into solution across the

electrode-electrolyte interface. The charge remaining on the electrode produces an attractive electric field holding back further dissolution, while the charge of opposite sign produced in the electrolyte also produces an electric field opposing further dissolution. These forces are equivalent to the p_1 (suction) and p_2 (pressure) in the analogy.

Hydrogen half cell with catalyzed porous carbon electrode and alkaline electrolyte

The half cell reaction can be represented as

$$H_2 + \text{active site} \rightleftharpoons 2[H]_{\text{chemisorbed}} \qquad (6)$$

$$[H] + OH' \rightleftharpoons H_2O + e + \text{active site} \qquad (7)$$

At equilibrium let the fraction of the active sites occupied by chemisorbed hydrogen be θ_e. The fraction of unoccupied sites is then $1-\theta_e$ and the chemisorption equilibrium of reaction (6) can be represented (2) by

$$p(1-\theta_e)^2 i = \theta_e^2 j \qquad (8)$$

where i and j are rate constants and p is the pressure of hydrogen. Thus, from equations (1) and (2), the free energy change on chemisorption is

$$(\Delta G)_c = (\Delta G_o)_c + RT \ln \theta/(1-\theta)p^{\frac{1}{2}} \qquad (9)$$

For reaction (7), the free energy change from the chemisorbed state to product, $(\Delta G)_{C\text{-}H_2O}$, is given by

$$(\Delta G)_{C\text{-}H_2O} = (\Delta G_o)_{C\text{-}H_2O} + RT \ln \frac{(H_2O)(1-\theta)}{(\theta)(OH')} \qquad (10)$$

Substituting for $\theta/1-\theta$ from (9)

$$(\Delta G)_{C\text{-}H_2O} = (\Delta G_o)_{C\text{-}H_2O} + (\Delta G_o)_c - (\Delta G)_c + RT \ln \frac{(H_2O)}{(OH')\,p^{1/2}}$$

Now at equilibrium in the chemisorption process, equation (1) shows that $(\Delta G)_c$ is zero; further $(\Delta G_o)_{C\text{-}H_2O} + (\Delta G_o)_c = (\Delta G_o)_{H_2\text{-}H_2O}$, therefore

$$(\Delta G)_{C\text{-}H_2O} = (\Delta G_o)_{H_2\text{-}H_2O} + RT \ln \frac{(H_2O)}{(OH')\,p^{1/2}} \qquad (11)$$

where $(\Delta G_o)_{H_2\text{-}H_2O}$ is the overall standard state free energy change from hydrogen

to product. From equation (5)

$$nFE_r = nFE_o + RT \ln \frac{(H_2O)}{[OH^-]P^{1/2}} \qquad (12)$$

Thus, at open circuit, the reversible potential E_r should be independent of the chemisorption step and hence independent of the surface or catalyst used. Young and Rozelle [3,4] have presented evidence to show that this is not true, and they ascribe the loss of potential on open circuit as being due to loss of free energy on chemisorption. This immediately raises the question as to why, when hydrogen is allowed to stand in contact with the catalyst surface, a normal adsorption equilibrium fitting a Langmuir or Tempkin isotherm is not reached? Equation (8) can be expressed as

$$\theta = \frac{aP^{1/2}}{1+aP^{1/2}} \qquad (13)$$

where a is a constant at a given temperature. This indicates that the surface is saturated, and hence irreversible, only at infinite pressure. A similar result is obtained by the use of the Tempkin isotherm[5]. The theory of these isotherms states that, providing θ is not continually removed as some other product of reaction, then the gas surface reaction is reversible and will reach an equilibrium state. The modification of the Freundlich adsorption isotherm suggested by Taylor and Halsey[6] gives θ as

$$\theta = (a_o P)^{\frac{RT}{q_m}} \qquad (14)$$

where a_o, q_m are constants. Clearly when $P = 1/a_o$, θ is 1, and hence $1/a_o$ represents a saturation pressure p_s, beyond which further increase in gas pressure (and hence gas free energy) produces no further free energy increase in the surface, and the system is irreversible. The loss of theoretical open circuit voltage, assuming that the Langmuir isotherm (equation 8) has fair numerical agreement with the Freundlich isotherm up to the saturation pressure[7] is approximately

$$E_r - E_{actual} = \frac{RT}{nF} \ln \frac{P}{P_s} \quad , P \not< P_s \qquad (15)$$

Raising the temperature of the cell should bring the cell nearer to reversibility since p_s increases with temperature. Different catalyst surfaces may have different values for p_s.

Young has attempted to correlate the loss of open circuit potential with heats of chemisorption[4]. However, such heats are free energy changes obtained on raising the pressure and consequently have little significance for an equilibrium process. Indeed these heats are often calculated using isotherms derived by assuming that an equilibrium state exists in which the transfer of an infinitesimal quantity of gas to the surface involves no free energy change.

There are other possible explanations for the open circuit voltage loss. It may be that a pseudo equilibrium is reached in which stray currents

are sufficiently large to disturb the equilibrium on a poorly catalyzed surface. Again the attainment of equilibrium may be slow, especially if the activation energy for chemisorption is high and θ_e tends to one. The rate of chemisorption is proportional to $(1-\theta)^2 \exp(-\Delta G_a^*/RT)$.

Under these circumstances it would be expected that the potential of the half cell would increase slowly with time. In general, if such irreversibility exists, it should be difficult to obtain consistent results for open circuit potentials.

Loss of Potential During Current Flow

The polarization or loss of potential during current flow is obviously of prime importance in the design of fuel cells. To obtain good fuel efficiency the cell must be operated at a maximum internal voltage loss of about 20 to 30% of the open circuit voltage. If the current flowing per sq. cm. of electrode area or per pound of cell is small, then the cell will be bulky and uneconomic. The theoretical analysis of polarization is an attempt to show which factors must be varied to obtain optimum conditions.

Activation polarization across the electrode-electrolyte surface

Consider the hydraulic analogy discussed previously. The transfer of ions across the electrode-electrolyte interface, being a chemical reaction, is activated, and the potential energy curve through the surface at open circuit can be visualized as in Figure 2. The energy is composed of the original chemical free energy and the electrical field energies which counterbalance the chemical energy to give zero free energy change across the interface. Stated more precisely, the activities of the reactants and products at the surface change to bring the reaction into dynamic equilibrium. This produces a concentration of electrons in the electrode surface and a concentration of positive ions at the plane of closest approach in the electrolyte; the open circuit potential is due to this double layer. Reducing the external resistance from infinity is comparable to partially opening valve V and allowing flow. Clearly a small flow will increase p_1 slightly and reduce p_2, Δp will decrease, and a pressure gradient is set up across B. In the electrical case this is equivalent to reducing the retaining electric fields and consequently the energy curve on the left in Figure 2 rises and that on the right falls. (See broken curves in Figure 2). The change in free energy through the surface on flow is clearly not available for outside potential and E_r is reduced to E. The rest of the overall free energy change of the reaction is carried through the external circuit by the electrons involved and the reaction can proceed only as fast as the external resistance will allow the current to flow, with Ohm's Law applying.

Let the change in free energy through the surface be $d(\Delta G)$. Then

$$\eta_a = E_r - E = \frac{-d(\Delta G)}{nF} \qquad (16)$$

η_a is called the activation polarization at the given current flow. At short circuit, if there were no other resistances to flow present, then the drop of free energy through the surface would be the total free energy change and $\eta_a = \frac{-\Delta G}{nF} = E_r$ where ΔG is the total free energy change of the reaction.

At open circuit a dynamic equilibrium exists across the interface,

$$[H] + OH' \rightleftharpoons H_2O + e +$$

Let $(a_H)_e$ be the activity of the chemisorbed hydrogen at equilibrium, $(a_{OH})_e$ be that of OH', $(a_{H_2O})_e$ be that of water, and $(a_s)_e$ be activity of active sites. Then from equation (4)

$$\text{forward reaction rate} \quad v_{1e} = k_1 (a_H)_e (a_{OH})_e e^{\frac{-\Delta G_{01}^*}{RT}}$$

$$\text{back reaction rate} \quad v_{2e} = k_2 (a_s)_e (a_{H_2O})_e e^{\frac{-\Delta G_{02}^*}{RT}}$$

The rate may be expressed as amps per sq. cm. of active area, and at equilibrium $v_{1e} = v_{2e} = I'$. Under non-equilibrium conditions, from equation (3)

$$(a_H)(a_{OH}) = (a_H)_e (a_{OH})_e e^{\frac{\Delta G_1}{RT}}$$

where ΔG_1 is the free energy change from equilibrium activities to those considered. A similar expression can be written for the back reaction with a free energy change of ΔG_2. Clearly the free energy changes represent the loss in free energy through the surface due to current flow and

$$-\Delta G_1 + \Delta G_2 = d(\Delta G) = -nF\eta_a$$

Let α be the fraction of η_a aiding the reaction from left to right. Then

$$\Delta G_1 = \alpha n F \eta_a$$

The new reaction rate from left to right is

$$v_1 = k_1 (a_H)(a_{OH}) e^{\frac{-\Delta G_{01}^*}{RT}}$$

$$= k_1 (a_H)_e (a_{OH})_e e^{\frac{-\Delta G_{01}^*}{RT}} e^{\frac{\Delta G_1}{RT}}$$

$$= I' e^{\frac{\alpha n F \eta_a}{RT}} \qquad (17)$$

I' is the equilibrium current corresponding to rate in either direction at equilibrium. Similarly, $\Delta G_2 = -(1-\alpha) nF\eta_a$ where $1-\alpha$ is the fraction of η_a decreasing the reaction from right to left, and

$$v_2 = I' e^{\frac{-(1-\alpha) n F \eta_a}{RT}} \qquad (18)$$

Thus the net current flow from left to right is

$$i' = I' \left(e^{\frac{\alpha n F \eta_a}{RT}} - e^{\frac{-(1-\alpha) n F \eta_a}{RT}} \right) \qquad (19)$$

In general, part of the polarization measured in equation (19) exists through the diffuse part of the double layer [8] extending from the plane of closest approach into the electrolyte. The structure of the double layer can be changed by the presence of salts in the electrolyte, specific adsorption on the electrode surface and electrolyte concentration. Thus I' in equation (19) is changed by these factors. It is easily shown[9] that I' may be represented as

$$I' = (I)_c \, e^{\frac{Fz\psi}{RT}(\alpha n - z)} \qquad (20)$$

where ψ is the potential drop in the double layer and z is the number of electrons involved in transfer through the layer. $(I)_c$ is an equilibrium current which is more nearly characteristic of the reaction, while the term involving ψ can be used to explain the effects of modification of the double layer [10]. For the type of cell considered here the composition of the electrolyte is usually dictated by other considerations and providing specific adsorption is avoided the factor involving ψ is predetermined.

In equation (19), the value of i' was derived per sq. cm. of active site area. Normally, current is expressed per sq. cm. of geometric electrode area and

$$i = (\text{constant}) \quad N_s A_e i' \qquad (21)$$

where N_s is the number of sites per unit effective area and A_e is the effective area per unit geometric electrode area. Then

$$\begin{aligned} i &= k N_s A_e I' \left(e^{\frac{\alpha n F \eta_a}{RT}} - e^{\frac{-(1-\alpha) n F \eta_a}{RT}} \right) \\ &= I \left(e^{\frac{\alpha n F \eta_a}{RT}} - e^{\frac{-(1-\alpha) n F \eta_a}{RT}} \right) \end{aligned} \qquad (22)$$

I is called the exchange current density as it is the equilibrium forward and reverse currents flowing at open circuit. This term is sometimes reserved for the equilibrium current for standard state conditions, I_o, but it is easy to convert from one to the other knowing the cell pressures and concentrations.

As η_a becomes large in equation (22) (and if α does not alter in value) then the reverse reaction becomes negligible and

$$i = I \, e^{\frac{\alpha n F \eta_a}{RT}} \qquad (23)$$

or

$$\begin{aligned} \eta_a &= \frac{2.3RT}{\alpha n F} \log i - \frac{2.3RT}{\alpha n F} \log I \\ &= a + b \log i \end{aligned} \qquad (24)$$

where

$$a = \frac{2.3RT}{\alpha n F} \log \frac{1}{I}$$

$$b = \frac{2.3RT}{\alpha n F}$$

This is known as the Tafel equation. It applies when the polarization is greater than about 100 millivolts. For a required current the polarization is small as I is large. Neglecting double layer effect

$$I = k N_S A_e e^{\frac{-\Delta G^*_{01}}{RT}} \quad \text{(terms in equilibrium activities)} \qquad (25)$$

To obtain low polarization it is desirable to have as much effective surface per unit geometrical area as possible. This is accomplished by having a system of small pores with a high surface roughness in contact with the electrolyte. Thus when using porous carbon electrodes it is sometimes necessary to "activate" the carbon by reaction with air or steam. This burns open pores which were closed and increases the surface roughness. Again, since the reaction takes place at an area of contact of gas, solid and liquid, saturation of the surface with electrolyte will greatly increase polarization.

The function of the catalyst impregnated on the surface is to decrease the activation energy ΔG^*_{01} of the reaction. The standard state free energy change during the reaction is illustrated in Figure 3. Considering the chemisorption step,

$$\Delta G^*_{cf} = \Delta H^*_{cf} - T\Delta S^*$$

The desorption step gives

$$\Delta G^*_{cb} = \Delta H^*_{cb} - T\Delta S^*$$

Therefore

$$\Delta G^*_{cb} - \Delta G^*_{cf} = \Delta H^*_{cb} - \Delta H^*_{cf} = q$$

where q is the exothermic standard state heat of chemisorption[11]. When comparing catalysts, the catalyst with the smaller q should have a smaller ΔG^*_{01} and hence less activation polarization at a given current.

Increase in temperature increases I, but it also reduces the other term in equation (22). Normally the polarization is markedly decreased by increase in temperature. The effect of the quantity of catalyst is governed by N_S. As the quantity is increased from zero the polarization is decreased, but a saturation state is reached when the surface is completely covered with the optimum quantity of catalyst.

Increasing the gas pressure on the cell increases the equilibrium activities and should thus decrease polarization.

Activation polarization of chemisorption.

Equation (22) was derived specifically for the reaction

$$[H] + OH' \rightleftharpoons H_2O + e + \text{active site}$$

However, it is possible that the preceding chemisorption of hydrogen is slow during current flow. If this is true, the electrochemical reaction comes into balance with the chemisorption and an additional polarization is introduced, due to free energy changes on chemisorption. Considering the reaction

$$H_2 + \text{active site} \rightleftharpoons 2[H]$$

the activities may be represented as p, $(1-\theta)^2$ and θ^2. In a similar manner to the derivation of equation (22)

$$i = k N_S A_e p (1-\theta_e)^2 e^{\frac{-\Delta G_c^*}{RT}} \left(e^{\frac{\alpha n F \eta_a}{RT}} - e^{\frac{-(1-\alpha) n F \eta_a}{RT}} \right)$$

$$= I \left(e^{\frac{\alpha n F \eta_a}{RT}} - e^{\frac{-(1-\alpha) n F \eta_a}{RT}} \right)$$

where the rate constant, value of activation energy and exchange current are for the chemisorption process. When the cell is supplying current, θ must decrease to allow more chemisorption. If θ is near 1, a small decrease in θ produces much extra chemisorption but virtually no change in the back reaction; therefore the polarization completely aids the reaction from left to right and $\alpha = 1$. Since $n = 2$, the slope b of the Tafel line under these circumstances is

$$b = \frac{2.303RT}{2F} \simeq 0.03 \text{ volts, at room temperature.}$$

If the chemisorption is fast compared to the electrochemical step the value of θ does not change much and the value of (θ_H) in equation (17) can be considered constant; α is about 1/2, n is 1 and the slope of the Tafel equation is about 0.12 volts[12]. Thus the slope of the Tafel equation gives a means of determining whether the chemisorption step or the electrochemical step is predominantly rate controlling. For chemisorption rate controlling, the function of the catalyst is to lower the activation energy of chemisorption. Activation and chemisorption activation polarization are considered in more detail by Parsons[13].

At sufficiently large current flows, θ tends to zero, α tends to zero and η_a tends to infinity. This expresses the fact that the reaction cannot proceed faster than chemisorption on to an almost bare surface. Thus the complete polarization versus current curve is as illustrated in Figure 4. If θ is not near 1 at open circuit, the curve will start at E_T but its shape will be that of the right hand portion of Figure 4.

Concentration Polarization

Concentration polarization is the loss of potential during current flow due to mass transport limitations in the cell. During current flow reactant has to be transported to the reaction site and energy is thus used in overcoming the resistance to flow which is always present.

Gas transport polarization

Gas transport through a porous carbon electrode is illustrated in Figure 5. If the reversible potential of the cell is for a pressure of p_1, then as the reaction proceeds and p_2 becomes less than p_1, the cell e.m.f. will fall.

If the fall is η_c at a current of i

$$\eta_c nF = RT \ln \frac{P_1}{P_2} \qquad (26)$$

Assuming the carbon has an effective diffusion coefficient D_{eff}, independent of pressure [14] and that the electrode is in the form of a slab

$$\text{Rate} = D_{eff} \frac{(P_1 - P_2)}{\Delta L} \quad \text{per sq. cm.} \qquad (27)$$

ΔL is the thickness of the electrode. Equation (27) may be expressed as

$$i = B (P_1 - P_2)$$

where B includes a conversion factor. Then

$$\eta_c = \frac{RT}{nF} \ln \frac{P_1 B}{P_1 B - i}$$

Since the maximum value of $P_1 - P_2$ is P_1, BP_1 represents a limiting current, I_ℓ say, and

$$\eta_c = \frac{RT}{nF} \ln \frac{I_\ell}{I_\ell - i} \qquad (28)$$

When i is small compared to I_ℓ, η_c is linearly dependent on i, and as i approaches I_ℓ, polarization becomes very great. Thus it is desirable for I_ℓ to be large. The thickness of the electrode cannot in practice be reduced beyond a certain limit. Due to the inhomogeneous nature of the pore system, reducing the thickness tends to give either gas leakage from the surface or flooding of the pore system by the electrolyte. Thus it is desirable to have an electrode which has a high diffusion coefficient, high internal area or roughness factor and which is as homogenous in pore structure as possible. In operation, since p_2 has to be maintained sufficiently high to prevent electrolyte flooding, p_1 would have to be raised as concentration polarization becomes appreciable.

Electrolyte concentration polarization

In a similar manner to that above the concentration polarization due to mass transfer of ions is

$$\eta_c = \frac{RT}{nF} \ln \frac{i_\ell}{i_\ell - i}$$

where the limiting current i_ℓ is given by

$$i_\ell = \frac{D_i z F a_1}{(1 - t_i)\delta} \qquad (29)$$

D_i , a_i, t_i are respectively the diffusion coefficient, bulk activity and transport number of the ion and δ is the effective thickness of the diffusion layer adjacent to the electrode surface. This type of polarization is well described by Kortüm and Bockris [15].

The effect of concentration polarization can be introduced into equation (22) by writing

$$\alpha_1 \eta_o = \alpha \eta_a + \eta_c$$

where η_o is the overall polarization and η_c is the concentration polarization in the same direction as $\alpha\eta_a$. Considering just this direction

$$\begin{aligned} i &= I\, e^{\frac{\alpha n F \eta_a}{RT}} \\ &= I\, e^{\frac{\alpha_1 n F \eta_o}{RT}} e^{\frac{-nF\eta_c}{RT}} \\ &= I\, \frac{C_r}{C_{ro}}\, e^{\frac{\alpha_1 nF\eta_o}{RT}} \end{aligned} \qquad (30)$$

where C_r is the effective activity and C_{ro} is the original bulk activity of the reactants. $C_r/C_{ro} = I_e - i/I_l$ thus i appears on both sides of equation (3). The general form of the equation is similar to that in Figure 4. The introduction of concentration polarization in equation (22) must be made for all of the steps in the reaction which give appreciable concentration polarization.

Ohmic Resistance

In addition to the polarization already described an internal loss of potential, η_r , occurs due to the electrical resistance of the electrolyte. By Ohm's Law

$$\eta_r = i r$$

r is low for high concentration of ions in the electrolyte. It is of interest to note that if penetration of electrolyte into the pore system occurs, then the effective conductivity for ionic conduction is [16]

$$C_{eff} = \frac{\epsilon}{q} C_{free} \qquad (31)$$

where ϵ is the porosity of the carbon and q is a tortuosity factor. For porous carbon electrodes ϵ is of the order of 1/3. q may be very high[17] but is often[18] about 2 to 3 Thus a penetration of 1 mm will usually give as high an electrical resistance as about 1 cm of the free electrolyte between the electrodes.

The Oxygen Alkali Half Cell

If the oxygen half cell reaction were

$$\tfrac{1}{2} O_2 \rightleftharpoons [O] \quad , \quad [O] + H_2O + 2e \rightleftharpoons 2\,OH'$$

then the standard state potential of an hydrogen oxygen fuel cell should be about 1.23 volts at room temperature. However, it has been shown[19,20] that the half cell reaction is

$$[O_2] + H_2O + 2e \rightleftharpoons HO_2' + OH'$$

Since the normal cell is not standard with respect to peroxide concentration the open circuit potential is usually not 1.23 volts. It is easily shown that if the peroxide ion is rapidly decomposed to its equilibrium value with respect to oxygen (in the electrode) and hydroxyl then the cell voltage would again be 1.23 volts. Even if peroxide decomposing catalysts are employed it appears that, at room temperatures, the decomposition is not sufficiently rapid for this equilibrium to be reached near the electrode surface and a loss of ideal potential occurs[21].

CONCLUSION

In studying the polarization of the type of fuel cells considered here it is important to determine the contribution of each type of polarization to each half cell. If such determinations are made, they will indicate what can be done to improve the performance of the cell. The various techniques for determining each polarization are described in the literature[12,15,22]. However, even if optimum conditions for minimum polarization are obtained, there are still many mechanical and technological difficulties to overcome in the construction of operating fuel cells.

REFERENCES

1. Evans, G.E., Proceedings, Twelfth Annual Battery Research and Development Conference, U.S. Army Signal Research and Development Laboratory, 1958 Symposium on Fuel Cells.
2. Trapnell, B.M.W., "Chemisorption", Butterworth's Scientific Publications, London (1955), p.111.
3. Young, G.J. and Rozelle, R.B., Journal of Chem. Education, 36 (1959) 68.
4. Young, G.J. and Rozelle, R.B., Private Communication (1959).
5. Trapnell, B.M.W., "Chemisorption", Butterworth's Scientific Publications, London (1955), p.126.
6. Halsey, G. and Taylor, H.S., J. Chem. Phys. 15 (1947) 624.
7. Trapnell, B.M.W., "Chemisorption", Butterworth's Scientific Publications, London (1955), p.118.
8. Frumkin, A.N., Bagotskii, V.S., Iofa, Z.A., and Kabanov, B.N., "Kinetics of Electrode Processes", Moscow University Press, Moscow (1952), 177.
9. Berzius, T. and Delahay, P., J. Am. Chem. Soc. 77 (1955) 6448.
10. Frumkin, A.N., Trans. Faraday Soc. (London) 55 (1959), 156.
11. Trapnell, B.M.W., "Chemisorption", Butterworth's Scientific Publications, London (1955), p.209.
12. Potter, E.C., "Electrochemistry", Cleaver-Hume Press Ltd., London (1956), p.133.
13. Parsons, R., Trans. Faraday Soc. (London) 54 (1958), 1053.
14. Walker, P.L. Jr., Rusinko, F. and Austin, L.G., "Advances in Catalysis", Vol. XI, Chapter on Gas Reactions of Carbon, Academic Press Inc., New York, 1959, in press.
15. Kortüm, G. and Bockris, J. O'M., "Textbook of Electrochemistry", Vol. II, Elsevier Pub. Co., New York (1951), p.400.
16. Carman, P.C., "Flow of Gases Through Porous Media", Academic Press Inc., New York (1956), p.46.
17. Dutcheon, J.M., Longstaff, E. and Warner, R.K., Preprints of Conference on Industrial Carbon and Graphite (London), 1957, "Flow of Gases Through Fine-Pore Graphite".
18. Wiggs, P.K.C., Preprints of Conference on Industrial Carbon and Graphite (London), 1957, "Gas Permeability and Pore Size Distribution".
19. Berl, W.G., Trans. Electrochem. Soc., 83, (1943) 253.
20. Witherspoon, R.R., Urbach, H., Yeager, E. and Hovorka, F., Technical Report No. 4, Electrochemistry Research Laboratory, Western Reserve University (1954).
21. Kordesch, K., and Marko, A., Oesterr. Chem. Ztg. 52 (1951) 125.
22. Broers, G.H.J., Ph.D. Thesis, University of Amsterdam (1958).

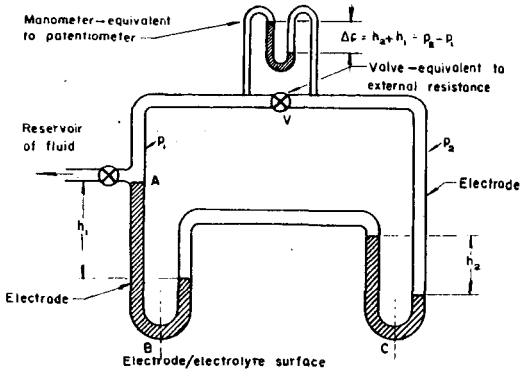

FIG. 1 Hydraulic analogy of a hydrogen–oxygen porous electrode fuel cell.

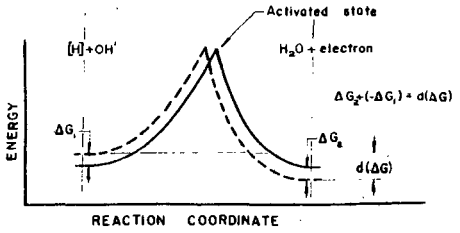

FIG. 2 Representation of energy state of reaction across electrode – electrolyte interface

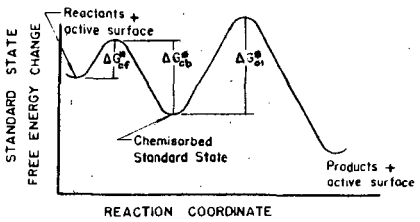

FIG. 3 Illustration of standard state free energy changes during reaction.

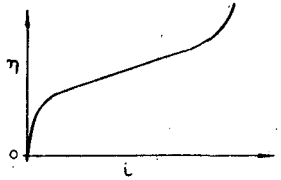

FIG. 4 Illustration of variation of chemisorption polarisation with current flow.

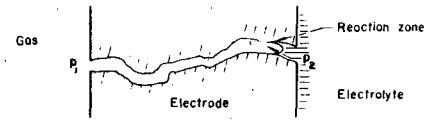

FIG. 5 Illustration of gas transport process in a porous electrode.

Not for Publication

Presented before the Division of Gas and Fuel Chemistry
American Chemical Society
Atlantic City, New Jersey, Meeting, September 13-18, 1959

THE HIGH PRESSURE HYDROGEN/OXYGEN FUEL CELL

F. T. Bacon, M.A., A.M.I.Mech.E.
Marshalls' Flying School, Ltd.
Cambridge, England

1. Introduction.

The hydrogen/oxygen cell is particularly attractive, when compared with other types of fuel cell, for a number of reasons; it has always appeared likely that a practical unit could be developed working at low or medium temperatures, and it raises the interesting possibility that it could be used as a kind of electrical storage battery, the two gases having been previously generated by the electrolysis of water, using power produced on a large scale.

Moreover, when the author first became interested in fuel cells in 1932, a search through the available literature soon showed that the most promising results had in fact been obtained with this type of cell. The cell was first described by Sir William Grove in 1839(i), and in 1889, particularly good results were recorded by the great chemist Ludwig Mond and his associate Charles Langer (ii), they achieved a current density of 6A/ft.^{2}(6.5m A/cm^2) at 0.73 V., using either oxygen or air, and they also showed that the best results were obtained when the platinized platinum electrodes were kept substantially dry on the gas side. Further progress was prevented largely because of the high cost of the platinum electrodes.

Since the end of the second World War, a great deal of interesting work has been done in many countries on the hydrogen/oxygen cell, and this need not be referred to in detail here. Particular reference, however, should be made to the work of Davtyan(iii) and Kordesch(iv) and his associates.

2. Types of Cell Investigated.

In 1938 a small cell similar to Grove's original gas battery was constructed, and fair results obtained; but when activated nickel gauze electrodes were used, in conjunction with an alkaline electrolyte of potassium hydroxide, the results were poor, even when the temperature was raised to the boiling point of the liquid.

It was next decided that the problem would have to be attacked essentially from an engineering point of view, and that with this type of cell operation under pressure could not be avoided if high current densities were to be obtained, in conjunction with comparatively cheap materials of construction such as nickel. So in 1939 a cell was designed which would stand a pressure of 3000 p.s.i. and any reasonable temperature (Fig.1).

The electrolyte was a 27% solution of potassium hydroxide and the cylindrical electrodes were of nickel gauze, activated by alternate oxidation in air and reduction in hydrogen; they were separated by a diaphragm of asbestos cloth. Other metals, such as platinum, palladium, silver and copper were tried, but were discarded in favour of nickel, partly because of cost and corrosion difficulties, but mainly because of the superior performance shown by nickel under these circumstances. The cell was tested by alternately charging it from an external source of direct current and discharging it through an ammeter and variable resistance at a constant current. It was found finally that a current density of 12.2 A/ft.^{2} (13.1m A/cm^2) of the external surface of the inner electrode could be maintained for 48 minutes at about 0.89 V., with a temperature of 100°C; many thicknesses of gauze and fairly high pressures were used to get these results. Curiously enough, no advantage was obtained by using higher temperatures than 100°C., and this was tentatively ascribed to the irreversible anodic oxidation of the oxygen electrode during the charging period.

The next stage was to construct two cells, one acting as an electrolyser for generating the two gases and the other being the current-producing cell (Fig.2). The gases produced in the electrolyser were carried separately up into the cell in solution in the electrolyte, the liquid returning to the electrolyser through separate pipes. Activated nickel gauze electrodes and asbestos diaphragms were again used, but this time in the form of flat discs.

It was found that the performances of this cell improved continuously with increasing temperatures and pressures up to 240°C. and 1075 p.s.i., the highest tried. The highest current density obtained at 240°C. was 75A/ft.^{2} (81m A/cm^2) at 0.65 V. with six gauze electrodes on each side of the cell. The current density appeared to be limited by the rate at which fresh gas could be brought up to each electrode in solution in the electrolyte. The materials and methods of construction used proved to be reasonably satisfactory.

3. The Present Cell with Diffusion Electrodes.

At this stage it was still considered that the performance was not good enough for any practical application, bearing in mind that high pressures inevitably lead to higher container weights than would be necessary with a fuel cell working at atmospheric pressure. So it was decided that a new apparatus should be built with the gases confined to the backs of porous nickel electrodes; this design has been used with very little change ever since.

The details of the construction of the cell have often been described before (v), but it is probably best to recapitulate them briefly here.

A single cell is illustrated diagrammatically in Fig.3. The electrodes are made of porous sintered nickel, and the main cell parts are of nickel-plated steel or pure nickel; the electrolyte is strong potassium hydroxide solution, between 37 and 50% concentration. The normal operating conditions are 200°C. and 300-600 p.s.i.. At the present time a pressure of 400 p.s.i. is normally being used. The porous nickel electrodes, which are about one sixteenth of an inch thick, have a pore size of about 30 microns or more, on the gas side, with a thin layer of much smaller pores on the liquid side; a small pressure difference is

set up in the apparatus across each electrode, so that the liquid is expelled from the large pores on the gas side, but the gas cannot bubble through the smaller pores on the liquid side owing to the surface tension of the liquid. The interior of the 30 micron pores, which are wetted throughout with electrolyte, presents a large surface for absorption of gas. The oxygen electrodes are subjected to a pre-oxidation treatment at a high temperature in air, and this protects them from corrosion by the high pressure oxygen and electrolyte. Lithium atoms are incorporated into the crystal lattice of the nickel oxide, thus converting the ordinary green nickel oxide, which is an insulator, into a black double oxide of nickel and lithium, which is a good semi-conductor.

With this arrangement, the gases are of course supplied from cylinders in the normal way; other advantages over previous designs are that the gas sides of the electrodes are coated with only a very thin layer of electrolyte, giving a very short diffusion path for the gases in solution before reaching the active surface of the electrodes, the useful surface area of the electrodes is greatly increased, and the asbestos diaphragm is eliminated.

4. Electrode Design.

A good electrode design is of course of the utmost importance, and several different designs have been tried. The largest electrodes made so far are 10 in. effective diameter, though this does not by any means represent the limit in size; they are sintered directly onto a flat circular perforated sheet of nickel or nickel-plated steel, about one sixteenth of an inch thick; this provides adequate strength, and serves also to conduct away the current generated. Electrodes up to 5 in. diameter were previously made without a backing plate of solid metal, but it was considered unlikely that larger ones would be satisfactory, without adequate support. Separators, in the form of narrow vertical strips of p.t.f.e., have to be used with 10 in. diameter electrodes, to prevent internal short-circuits when the pressure difference is applied.

An alternative from of electrode which has been employed comprises a bipolar structure with recesses machined on either side of a solid metal plate, each recess then being filled with porous sintered nickel for a hydrogen and oxygen electrode respectively. A thin dimpled perforated plate is first sintered into each recess, and this leaves a narrow space for leading the gas from ports in the rim to all parts of the porous metal. When bipolar electrodes of this type are assembled in series, with gaskets of insulating material between each, they form a series of cells which do not require any external current connection except at each end of the battery. This electrode construction is attractive in many ways, and leads to a very compact battery, but it has temporarily been abandoned in favour of the simple unipolar design, mainly owing to difficulties in manufacture.

The coarse pore layers of hydrogen electrodes are made from Grade B carbonyl nickel powder (average particle size 2-3 microns) mixed with about 20% by weight of 100-240 mesh ammonium bicarbonate which acts as a spacing agent during sintering; it is pressed lightly in a rubber press, and then sintered for about $\frac{1}{2}$ hour at 850°C. in a reducing atmosphere. The fine pore layer is then applied as a suspension of Grade A carbonyl nickel powder (average particle size 4-5 microns) in alcohol; this is sintered for $\frac{1}{2}$ hour at 800°C., any leaks being repaired by further thin applications of A nickel as before.

The coarse pore layers of oxygen electrodes are now usually made from Grade D carbonyl nickel powder (average particle size 7-9 microns) mixed with 15-20% of 100-240 mesh ammonium bicarbonate; it is pressed lightly and sintered for $\frac{1}{2}$ to 1 hour at 1000°-1150°C. in a reducing atmosphere. The fine pore layer is again of Grade A nickel, sintered for $\frac{1}{2}$ to 1 hour at 950-1000°C. Alternatively, the coarse pore layers of the oxygen electrodes may be made from a coarse nickel powder, about 200-250 mesh, without a spacing agent; but in this case a higher compressing pressure and a higher sintering temperature (1150°C. as a minimum) are required to get a really strong compact.

Finally the oxygen electrodes are pre-oxidised after impregnation with a dilute solution of lithium hydroxide and drying; air is used for oxidation, and a satisfactory thickness of oxide is formed in $\frac{1}{4}$ to 1 hour at 700°-800°C.

Hydrogen electrodes are activated by impregnation with a strong solution of nickel nitrate, followed by a roasting treatment in air at 400°C. and finally reduction in hydrogen at about the same temperature. Work is proceeding on the activation of oxygen electrodes, but a standard treatment has not yet been arrived at.

Typical microsections of hydrogen and oxygen electrodes are shown in Figs. 4 and 5.

5. Prevention of Corrosion of Oxygen Electrodes.

When porous nickel electrodes were first put into use, serious trouble arose with the gradual corrosion of oxygen electrodes, leading first to a drop in output and finally to complete breakdown. This trouble has now been largely overcome by the pre-oxidation treatment already described. It was first found that samples of nickel pre-oxidised in air at about 800°C. were extremely resistant to corrosion when subsequently exposed to strong KOH solution and oxygen under similar conditions to those in the cell. But the green oxide layer produced during pre-oxidation is an electrical insulator, so an electrode protected in this way would be useless in the cell. However, it was ascertained that if lithium atoms are incorporated into the crystal lattice of the nickel oxide, a black double oxide of nickel and lithium is produced, which is a good semiconductor(6); and the corrosion resistance is unimpaired, or even enhanced. Using this technique, oxygen electrodes have been in operation in the cell for periods up to 1500 hours at 200°C. without failure, and with only a very small drop in performance. Specimens of pre-oxidised nickel have been exposed to oxygen under pressure and potassium hydroxide solution at 200°C. for more than 10,000 hours without visible deterioration; and accelerated corrosion tests at a higher temperature have shown that considerable improvement on this figure should be possible. It should be mentioned here that before the pre-oxidation treatment had been introduced, experiments were made with various corrosion inhibitors which were dissolved in the electrolyte; potassium silicate and potassium aluminate were particularly successful in arresting corrosion of oxygen electrodes, but they also reduced the performance of the cell to a serious extent. It is believed that this provides the explanation for the curious fact that no corrosion of oxygen electrodes was observed when using the previous cells with nickel gauze electrodes; these earlier cells all had diaphragms of asbestos cloth, and it is to be expected that the electrolyte would therefore become somewhat contaminated with potassium silicate or aluminate. It is interesting also that a small amount of copper, added to the KOH in the form of copper oxide, was also effective as a corrosion inhibitor and in all cases led to the formation of a black oxide on the nickel.

The results of some accelerated corrosion tests on samples of nickel pre-oxidised in the presence of lithium hydroxide, and exposed to 65% KOH and oxygen at 300°C. and 800 p.s.i. total pressure, are shown graphically in Fig.6. The samples were placed in oxidized nickel crucibles, which were set up in autoclaves; the samples were half in and half out of the KOH solution. The gas space was filled with oxygen under pressure, and readings of temperature and pressure were recorded periodically. The autoclaves were opened at intervals and the samples washed in distilled water, dried and weighed; the extent of corrosion was indicated by the weight change. Fresh KOH solution was used in each run. These curves emphasize the importance of a sufficiently thick oxide layer, in order to obtain really good durability. It is estimated that an oxide layer about 3 microns thick can be obtained by coating the nickel with 2 g. of lithium hydroxide per square metre of surface and oxidising in air at 800°C. for 16 minutes.

In Fig. 7 some results of tests at 200°C, 260°C. and 300°C. have been plotted together. These samples are not exactly comparable due to differences in the initial thickness of the oxide coating and in the conditions under which the corrosion tests were carried out. It is possible to say, however, that similar samples corrode at 200°C. much more slowly than at 260°C.. Also a further considerable increase in corrosion rate is produced if the temperature is raised to 300°C.. By pre-oxidising the samples to produce an increase in weight of 5g/metre^2 instead of 2-3g/metre^2, the rate of corrosion at 300°C was reduced considerably as shown in Fig.6. It seems reasonable to suppose that if the samples oxidized, with lithium present, to give an increase in weight of 5g/metre^2 were tested at 200°C., they would give a life many times longer than those already tested at this temperature (Fig.7). Even if it were to prove impossible to produce such a thick oxide layer on the oxygen electrode, a thinner layer of 2g/metre^2 will protect an electrode for more than 10,000 hours at 200°C.

6. Jointing Material.

There must be at least one electrically insulating gasket per cell, and at the present time, using unipolar electrodes, four gaskets must be used per cell..

Many different materials have been tried, but at the present time nothing has been found which is superior in all respects to ordinary compressed asbestos fibre jointing, which is mainly composed of asbestos fibre and rubber (generally neoprene). This has a number of disadvantages, the principal one being that the rubber content is gradually oxidised where exposed to the high pressure oxygen; this finally leads to loss of strength and leakage to atmosphere. However, runs as long as 800 hours have been achieved without failure, and runs greatly exceeding this should be possible with a superior design. One other fault is that substances given off when the rubber decomposes on heating, poison the hydrogen electrode and tend to reduce the output of the cell.

The most attractive alternative to CAF jointing would appear to be p.t.f.e. loaded with asbestos fibre, or possibly loaded with powdered glass, but these materials are only now in process of development in England; and the metal surfaces would certainly have to be specially roughened to prevent slip. End pressure on the gaskets could no doubt be reduced by the use of a pressure cylinder or tank, in which the whole cell pack is contained under pressure, but this line of development is not being pursued at present in England, owing to the extra complication involved.

7. Cell Performance.

The performance of the cell improves with both temperature and pressure, but in order to attain a long life it will probably prove desirable to limit the working temperature to 200°C or slightly higher. The best performance obtained so far with a 10" dia: cell at 200°C and 400 p.s.i. is shown in the table, and plotted as a voltage-current density characteristic in Fig.8; the diameter of the sinter is somewhat less than 10", and is approximately 9⅞", but it is felt that it is more precise to base the figures for current density on the internal diameter of the body of the cell.

TABLE.

Current Density	A/ft.^{2}	0	10	50	100	200	300	440
	mA/cm^2	0	11	54	107.6	215	323	473
Voltage, V		1.04	1.005	0.93	0.885	0.82	0.755	0.68

These figures were taken from one cell in a 10-cell battery, and using 37% KOH as electrolyte; both these factors contribute to the rather low open-circuit voltage obtained. Under the above conditions of 0.68 V. and 440 A/ft^2 (or 240A), the power output per unit of internal volumn corresponds to 8.2 kW/ft^3.

The current efficiency has been measured over a period of some hundreds of hours in a 5 in diameter unit with two cells in series, and works out at 98%. This means that the energy efficiency, based on the free energy of the reaction, will approximate at any useful current density to the voltage efficiency; e.g. at 0.9V and 200°C and 600 p.s.i. the energy efficiency will be $\frac{0.9}{1.20} \times 100 = 75\%$; at 0.8V. it will be 66%, and at 0.6V. it will be 50%.

When the cell is on load, the losses which appear in the form of heat, are mainly due to the irreversibility of the electrode reactions, or what may be called activation polarization; a smaller proportion of the losses are due to resistance and concentration polarization. On open circuit, and at low current densities, there will in addition be a 'lost current' due to diffusion of the two gases in solution through the electrolyte, followed by combination on the opposite electrode.

A graph showing the relative proportions of polarization due to each electrode and to the electrolyte is shown in Fig.9. Ordinary C&F jointing was used, so the hydrogen electrode was somewhat "poisoned". Assuming that activation of the hydrogen electrode can easily reduce polarization from this source to a negligible amount, while electrolyte resistance and oxygen electrode polarization are less easily improved, then a curve showing the best easily obtained performance to be expected from a cell can be drawn (see Fig.9). This shows that 223A/ft.^{2} (240 mA/cm^2) at 0.8 V. and 650 A/ft.^{2} (700 mA/cm^2) at 0.6V can reasonably be expected at 200°C. and 620 p.s.i..

The experimental method has been improved by the measurement of purely resistive polarization in the cell circuit using a commutator technique in conjunction with a cathode ray oscilloscope, so that individual electrode performance can be studied precisely. This is particularly important in the case of the hydrogen electrode, where both resistance and activation polarization have the same linear dependence on the current passing. The use of a reference electrode, in the form of a small resting (i.e. unloaded) hydrogen electrode of porous nickel, situated in the electrolyte space, about halfway between the main hydrogen and oxygen electrodes, has made it possible to study the polarization in each electrode separately; a reference electrode of this kind is used fairly regularly in cell operation, even when the commutator technique is not being employed. This has shown that the polarization of the hydrogen electrode at 200°C., when plotted against current density, gives approximately a straight line; at lower temperatures, the behaviour becomes logarithmic (see Fig.10). In the case of the oxygen electrode, however, the behaviour is logarithmic even up to the highest temperature yet tried the shape of the curve which it gives at 200°C, can be seen in Fig.9. The difference in the shape of the polarization curves shown by hydrogen and oxygen electrodes at 200°C. can be explained by the fact that the exchange current is much less in the latter case, or in other words the oxygen electrode is much less reversible than the hydrogen one; in addition to this, the surface area of the oxygen electrode is much less than that of the hydrogen one. But even an oxygen electrode of large surface, made from Grade B nickel, will polarize more than a hydrogen one made from the same powder and having the same surface area. To improve the performance of oxygen electrodes, a very large increase in surface area will be required; this can probably best be obtained by some form of activation.

Since electrodes have been made with a backing plate, it has been possible to test hydrogen and oxygen electrodes as thin as 1/32 in. The performance of these thin electrodes is within 20% of that of the previous electrodes which were $\frac{1}{8}$" - 5/32" thick. If the electrodes are made 1/16 inch thick, there does not appear to be any sacrifice in performance. A number of other hydrogen and oxygen electrodes of varying structures have been tested, but so far none has shown a striking improvement in performance when compared with the standard types.

8. The Effect of Cell Conditions on Performance.

(8.1). Pressure.

The effect of temperature and pressure on the reversible voltage of the hydrogen/oxygen cell can be seen in Fig.11. Measurements of electrode and cell performance at varying pressures of gas (the electrolyte vapour pressure having been measured, see Fig. 12) show that small variations in pressure have only a small effect. A tenfold change in gas pressure from 30 atmospheres to 3 atmospheres (441 to 44 p.s.i.) approximately halves the cell performance at normal operating voltages (see Fig. 13). A theoretical analysis done fairly recently shows that for a given power output, and assuming that the gases are both stored in high tensile steel cylinders at 3,000 p.s.i., the overall weight of the battery and storage cylinders would not be increased if the operating pressure were reduced from 600 to 300 p.s.i.; the efficiency would be slightly reduced, however; this calculation allows for the "dead" fuel left in the cylinders when the battery is discharged, and also for the reduction in weight of the battery itself.

(8.2). Temperature.-

The maximum cell temperature is limited by the materials used in it's construction. Thus, p.t.f.e. is found to corrode relatively quickly at 250°C. undercell conditions, where in contact with porous nickel; and the nickel-lithium oxide of the oxygen electrode breaks down fairly quickly at 300°C.. Between 100° and 250°C. the cell output at normal operating voltage increases rapidly with rise in temperature, as the hydrogen electrode changes from logarithmic behavious at 100°C. to linear behaviour. After 200°C. the output does not increase as rapidly as it does between 100° and 200°C.. Taking 100°C. as unit performance, that at 150°C. is roughly 4, at 200°C. it is 10, and at 250°C. it is 15. The actual maximum power available (at a low efficiency) rises increasingly steeply with increasing temperature, and is roughly doubled with each 50°C. rise in temperature.

(8.3). Electrolyte Concentration.

The effect of the vapour pressure of the electrolyte on the reversible voltage of the hydrogen/oxygen cell at a temperature of 200°C. is shown in Fig.14. This assumes that the total pressure is kept constant at 600 p.s.i.. It has been necessary to plot the vapour pressure of the electrolyte, rather than the concentration, as the relationship between concentration and vapour pressure of very strong KOH solutions has not been measured, as far as is known.

It has been assumed that the disposable energy in the formation of water vapour at a constant pressure of one atmosphere is 219.4 kilo-joules per gramme formula weight, at 200°C. At other values of pressure the disposable energy is increased by an amount

$$\frac{0.5\ R\ T \log_n (P_{H_2}{}^2 . P_{O_2})}{P_{H_2O}{}^2}$$

the pressures being measured in atmospheres.

The theoretical voltage is obtained by dividing the disposable energy by 2F, where F is the Faraday, 96,500 coulombs.

Increasing the concentration of the potassium hydroxide electrolyte to 35% by weight, increases the cell output progressively, but further increase from 35% to 45% has a smaller effect. Operation at higher concentrations than 45% leads to practical difficulties with the KOH electrolyte going solid on cooling down. Long continuous operation of cells on load for periods of 50-100 hours has shown that the very high concentrations of KOH lead to build-up of concentration polarization (absence of water in the oxygen electrode is the most probable cause), so that a concentration of about 35% KOH seems likely to be the optimum at present. If later it proves feasible to condense out twice the water formed from the hydrogen electrodes, and then return one half of this, in the form of steam mixed with the oxygen, to the oxygen electrodes, this difficulty should disappear and stronger concentrations could be contemplated.

The values obtained for specific conductivities of a range of electrolytes at various temperatures are shown in Fig.15; these have been obtained by measuring cell resistance with two different inter-electrode distances using the commutator technique mentioned previously; they are only approximate. Results for 36% KOH are particularly erratic, and the measurement of conductivity using an a.c. bridge and high temperature conductivity cell should provide accurate results.

The values predicted by T.M. Fry[7] are also plotted; these were obtained by using the relationship between conductivity and viscosity, and using an estimated value of viscosity; also values quoted for KOH by C.E. Bowen[8] (deduced from work by Kohlrausch in 1898); a general agreement is observed.

The contribution of electrolyte resistances to cell operation will be approximately 0.25 ohm/cm^2 of apparent electrode surface, for $\frac{1}{8}$ in. electrode spacing using electrodes of the types described. For a current density of 250 mA/cm^2, this would give a polarization of 0.0625 V., i.e. a voltage drop corresponding to about 5% of the total free energy available.

(8.4). Shunt currents in Multi-cell Packs.

A six cell pack of 5 in. diameter electrodes was constructed in 1954 and fair results were obtained.

Measurements of the shunt currents along the common eletrolyte ports, and a theoretical treatment, suggest that the magnitude of the shunt currents will depend largely on the dimensions of the axial electrolyte ports through the pack.

If V = the open circuit voltage of one cell
n = the number of cells in the pack
R = the resistance of one pair of axial ports in one cell, and
r = the resistance of one pair of radial ports in one cell,
then the shunt current = $\frac{(n-1)\ V}{2r + (n-1)\ R}$

For large packs, where distribution of liquid may be important, it might be better to have a number of axial ports serving groups of cells, rather than one large port serving all the cells.

9. Use of Other Gases.

It has often been suggested that a cell of this type could be used as a genuine fuel cell for generating power on a large scale, using hydrogen produced from coal by ordinary chemical methods, and oxygen from the air. This is, of course, a very ambitious project and cannot honestly be envisaged at present, owing to the high cost of pure hydrogen produced in this way; pure oxygen is also expensive.

Nevertheless, it is obvious that the scope of the whole project could be greatly widened if it were found to be possible to make use of a liquid fuel which could be converted into some gas which is electrochemically active in the cell; in this way it would become possible to compete on rather more level terms with the internal combustion engine.

A number of experiments have been carried out using other gases, and with mixtures of gases, and the conclusions can be summarized as follows :-

1. No other fuel gas, apart from hydrogen, has been found to be electrochemically active on a nickel electrode at temperatures which it would be practicable to use in a cell of this type. Carbon monoxide, methane and methanol were tried and were all unsuccessful.

2. Both carbon monoxide and carbon dioxide are soluble in caustic potash and would lead to the eventual carbonation of the electrolyte.

3. Complete carbonation of the electrolyte would lead to a serious loss in performance, amounting to a reduction to one quarter of the normal performance; this is partly due to loss in oxygen electrode performance and partly to increased cell resistance.

4. Hydrogen containing inert diluents, such as nitrogen or methane, can be used with a high volume percentage of inert gas, as long as provision is made for exhausting the residue; some hydrogen would no doubt be wasted in the exhaust, but the amount lost is not likely to be serious.

5. Possibly because of its solubility in hot caustic potash solution, carbon monoxide does not poison the fuel electrode, but it may attack the nickel pipe-work leading gas into the cell. No poisoning was observed with other gases used.

6. Experiments using nitrogen-oxygen mixtures showed that air could be used in place of oxygen, as long as the nitrogen left over was continuously removed, and the carbon dioxide extracted before entry into the cell.

The above conclusions show that the presence of any gases, apart from hydrogen and oxygen, may lead to rather awkward problems which it would probably be wise to avoid at present. On the other hand, small percentages of inert gases would do no harm to the cell, provided adequate means were worked out for exhausting them to atmosphere from time to time, before they had built up to large proportions inside the electrodes. A small purification plant could no doubt be designed for continuously purifying a slightly carbonated electrolyte.

The additional polarization at the oxygen electrode, caused by using air instead of pure oxygen, can be seen in Fig.16; this also shows the effect of oxygen pressure on polarization. Fig.17 shows the effect of various fuel gases on the polarization at the fuel electrode; the curve for technical hydrogen, and also for the mixture of 90% hydrogen plus 10% carbon monoxide is identical with that for pure hydrogen, over short periods of time. The "technical hydrogen" is the gas which is produced as a by-product in oil refineries, from the "platforming process".

10. Present Design.

In 1957, the National Research Development Corporation of Great Britain agreed to finance the development and construction of a unit developing 5-10 kW., complete with all automatic controls, and a contract for this work was placed with Marshall of Cambridge, England.

It was decided that a 10 in. diameter cell should be constructed, and this has been in operation since March 1958. The present electrode design has already been described; axial ports for the admission of the two gases and the electrolyte are drilled in the rim, as shown in Fig.18; when these electrodes are bolted up together in the correct order, with rings to provide space for the electrolyte and with flat discs of metal to separate the hydrogen from the oxygen in the adjacent cell, they form a battery, the voltage of which depends upon the number of cells connected in series. Radial ports for admitting gas or electrolyte from the axial ports to each cell are provided simply by slotting the gaskets. A distributor plate for leading the gases and electrolyte into and out of the battery is provided either at one end, or else in the centre of the cell-pack. The whole assembly is bolted up between two ribbed end plates, with powerful bolts, with electrical insulation between the ends of the pack and the end plates. Electrical connections are silver-soldered onto each electrode, and the inter cell connections are made externally; the main connections are of course made to the electrodes at each end of the pack.

Up to 30 cells in series have been operated so far (see Fig.19), and no special difficulties have been encountered with, for example, sealing of the joints, excessive shunt currents between cells, excessive electrolysis in the electrolyte ports, etc. But more experience will have to be obtained with large multi-cell packs before reliable results can be quoted.

11. Development of Control Gear.

Control of gas admission has always been a problem, as a very delicate pressure balance has to be maintained between the two gases in the battery. A system has now been worked out whereby as a basis the pressure of the oxygen remains constant under all conditions of load; this is achieved with a standard two-stage reducing valve. The hydrogen then has to be admitted at precisely the correct rate, so that the two gas pressures are balanced to within a few inches water gauge; this is done by fitting an accurate differential pressure meter, which actuates a power-operated valve admitting the hydrogen, the valve-opening being controlled by a servo mechanism operating with compressed air. A fair amount of experience has been obtained with this gear which works extremely well. Figure 20 shows various items which made up this control gear, mounted on the front of the protective framework enclosing the cell pack.

Much thought has also been given to the problem of the removal of water, at the same rate at which it is formed. Previously this has been achieved by circulating the hydrogen steam mixture by thermosyphonic action, the steam being condensed out in a small vessel outside the lagging. In order to do this in a large battery, very large hydrogen circulating pipes and ports would be needed, so it was decided that a small hydrogen blower would be used; it was considered that a glandless form of drive would be necessary, in view of the difficulty of preventing hydrogen leakage with a standard type of gland. A magnetically driven pump using a sealing shroud of thin non-magnetic metal has been successfully employed for some time; it can be seen mounted underneath the battery in Fig.19. The rate at which the condensate is removed from the system is controlled by switching the blower on and off at intervals, the switch being controlled by a second differential pressure meter which operates on the pressure difference between the hydrogen in the system and the electrolyte. In this way, the removal of water is controlled by the total volume of electrolyte which should of course be kept approximately constant. The condensate collects in a small vessel, from which it is released periodically by a level-sensing device such as a capacitor probe. The main parts of this gear, which can be also seen in Fig.20, have been in operation and appear to work perfectly well.

Until more experience with this gear is obtained, the main level gauges will be retained in use, but eventually it should be possible to remove them.

The initial heating of the battery is accomplished by electrical heaters mounted on the end plates and round the main body of the battery inside the lagging. Various plans have been suggested for maintaining the battery at a constant temperature when on load, but the simplest is undoubtedly to allow cold air to circulate round the battery, inside the lagging, the amount of cold air introduced depending on the temperature of the cell pack.

Lastly, there is the problem of removing gas from the electrolyte system; it is difficult to prevent entirely some generation of hydrogen and oxygen by electrolysis in the common electrolyte ports, although insulation with p.t.f.e. helps considerably in this respect. Moreover, there is always the possibility that an electrode may start leaking, thus allowing gas to get into the electrolyte system. This is taken care of by a level-sensing device, which will release any gas which may collect at the top of the electrolyte system, by means of a solenoid operated valve.

All these controls may seem somewhat complicated and expensive, but there is no doubt that they can be made to work, and with a larger battery they should not be any more complex and would then represent only a small proportion of the cost of the whole plant.

12. Advantages and Applications.

From what has been said, it will be seen that it is unlikely that this kind of battery could be competitive with existing types of accumulator in small sizes, owing to the high cost of the control gear in comparison with the overall cost of the plant. And in very small sizes it would be difficult to keep the cells up to the working temperature unless they were on load continuously and unless very efficient heat insulation were employed. It is difficult to quote exact figures for minimum sizes until more experience is obtained, but a power output as small as 100 watts is believed to be feasable with really good lagging.

One other factor that must be appreciated is that it could not compete with say lead accumulators on a weight basis unless the length of time of discharge is greater than about 1 hour; however, for longer times than this, the saving in weight should become increasingly important, as shown in Fig.21. The figures for conventional accumulators are a few years out-of-date, but the general picture to-day is undoubtedly roughly the same. It is on a weight basis that the hydrogen-oxygen battery should be able to show it's principal advantage over conventional accumulators. A curve for a Diesel engine with fuel is also included, and this serves to show that it will always be difficult to compete on a weight basis with a power generator which can draw it's oxygen from the atmosphere. However, it is as well to bear in mind that both accumulators and internal combustion engines have a great many years of careful development behind them, whereas the fuel cell is still in its infancy.

The fuel cell weight of 50 lb./kW shown in Fig.21 was worked out for a large battery developing about 44 kW.; this weight to power ratio will not be achieved in the small experimental unit now being built, and it would be unwise to hazard a guess about this until it is completed. The first requirement has been that it should work, rather than that it should have minimum weight or volume.

As regards power per unit volume, the figure of 8.2 kW/ft.^{3} of internal cell volume has already been quoted for a cell voltage of 0.68; a figure of 3kW/ft.^{3} for the whole battery without control gear, was quoted by an independent body some years ago, for a cell voltage of 0.8.

It has always been hoped that some specialised application will arise first, an application for which a fuel cell is particularly suited. In this connection, the possible use of fuel cells in satellites and space vehicles is of great interest. Then, when further experience has been obtained, it should be possible to enter the commercial field in competition with storage batteries which have already been developed to a high pitch.

It would seem that fuel cells of this type are most suitable for traction purposes, both road and rail; the combination of battery and direct current series wound motor provides an ideal propulsion unit for many types of vehicle, the limiting factor so far being the weight of the battery. The gases would probably be generated by electrolysis of water, and in this connection the development of an efficient high pressure electrolyser in Germany is of great interest. It is well known that the cost of electrical power from the National grid is considerably less than that of power produced in a petrol engine, and this is of special importance where the vehicle is subject to repeated starts and stops.

Further, if finally most of the power is generated on a large scale from nuclear energy, the cost of the electricity will be mainly due to the capital cost of the plant rather than to the cost of the nuclear fuel; and the need for some kind of large scale storage will become increasingly important, as little will be saved by shutting down the plants during times of light load.

Other advantages of this kind of fuel cell are that it is able to take large overloads at reduced efficiency without damage, it is silent and free from vibration in operation, it has very few moving parts and the "exhaust" is only water; moreover, the "charging" process would merely consist of refilling with the two gases, a very rapid process.

With the advent of new methods of storing hydrogen and oxygen, either in liquid form, or else in the former case as a compressed gas at a very low temperature, it would seem conceivable that vehicles could be propelled over really long distances with fuel cells; and in view of the rapid depletion of the world's oil supplies, the development of a practical fuel cell should, in the author's opinion, be given a high priority.

The author would like to thank his colleagues who have given invaluable help in the preparation of this paper; and in particular Dr. R.G.H. Watson, now at the Admiralty Materials Laboratory, Holton Heath, England.

He would also like to thank the Electrical Research Association and the Ministry of Power for valuable financial assistance over many years of research; also Messrs. Marshall of Cambridge, who are now providing facilities for the development work and who have given all possible advice and help; and specially the National Research Development Corporation who are now financing the development work, and who have kindly given permission for the publication of this paper.

REFERENCES.

(1) Grove. W.R., PhilMag. (3), 1839, 14, 139.

(2) Mond. L. and Langer. C., Proc.Roy.Soc.Lond., 1889, 46. 296-308.

(3) Davtyan. O.K., Direct Conversion of Chemical Energy of Fuel into Electrical Energy (in Russian), Academy of Sciences, Moscow. 1947; E.R.A. Translation Ref. Trans./IB.884(1949).

(4) Kordesch. K. and Marko. A., Osterreichische Chemiker - Zeitung, July 1951, 52, 125-131, etc.

(5) Bacon. F.T., B.E.A.M.A. Journal, 1954, 61, 6.
" " and Forrest, J.S., Trans. Fifth World Power Conference (Vienna), Div. 3, Section K, paper 119K/4.
Watson, R.G.H., Research, 1954, 7, 34.

(6) Verwey, E.J.W., Semi-Conducting Materials, Butterworths Scientific Publications Ltd., 1951, 151-161.

(7) Fry. T.M., private communication.

(8) Bowen, C.E., J.I.E.E.Eng., 1943, 90, 473.

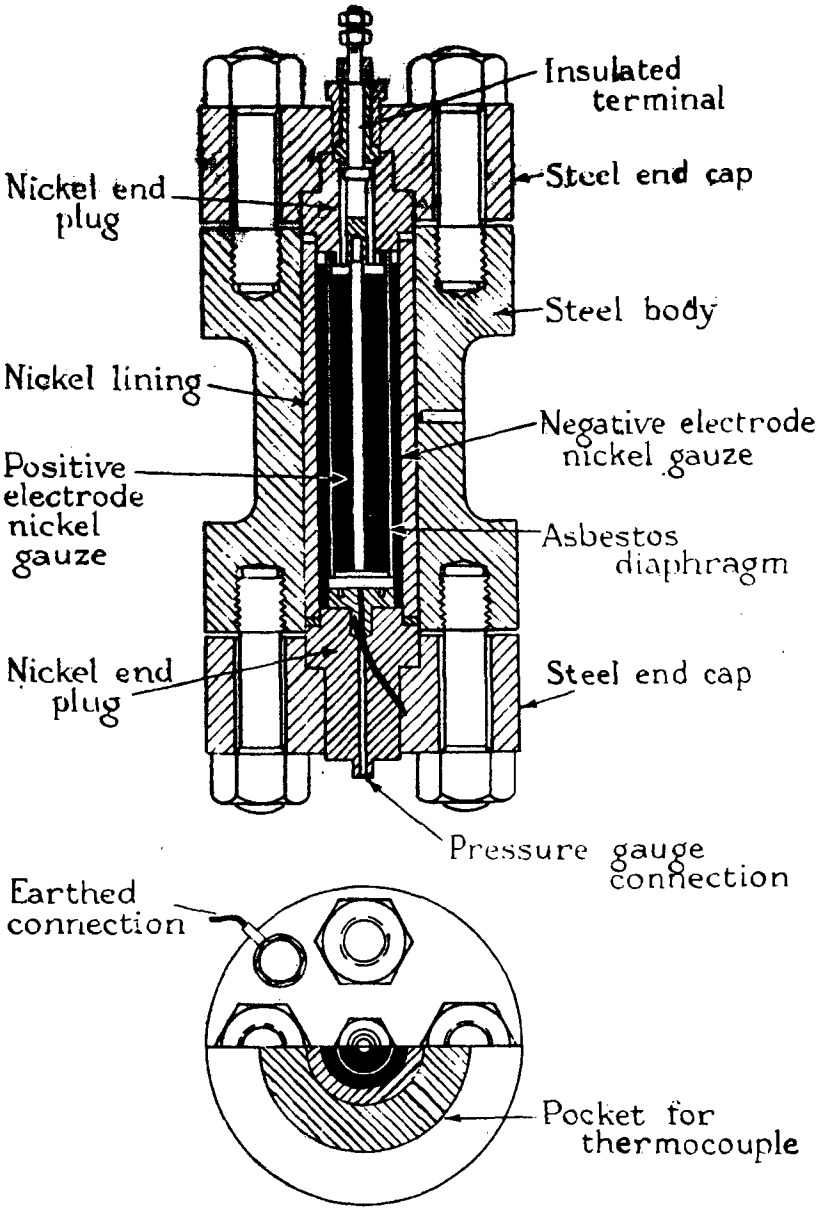

FIG. 1. APPARATUS FOR USING COILS OF GAUZE AS ELECTRODES. GAS SUPPLY BY INITIAL ELECTROLYSIS

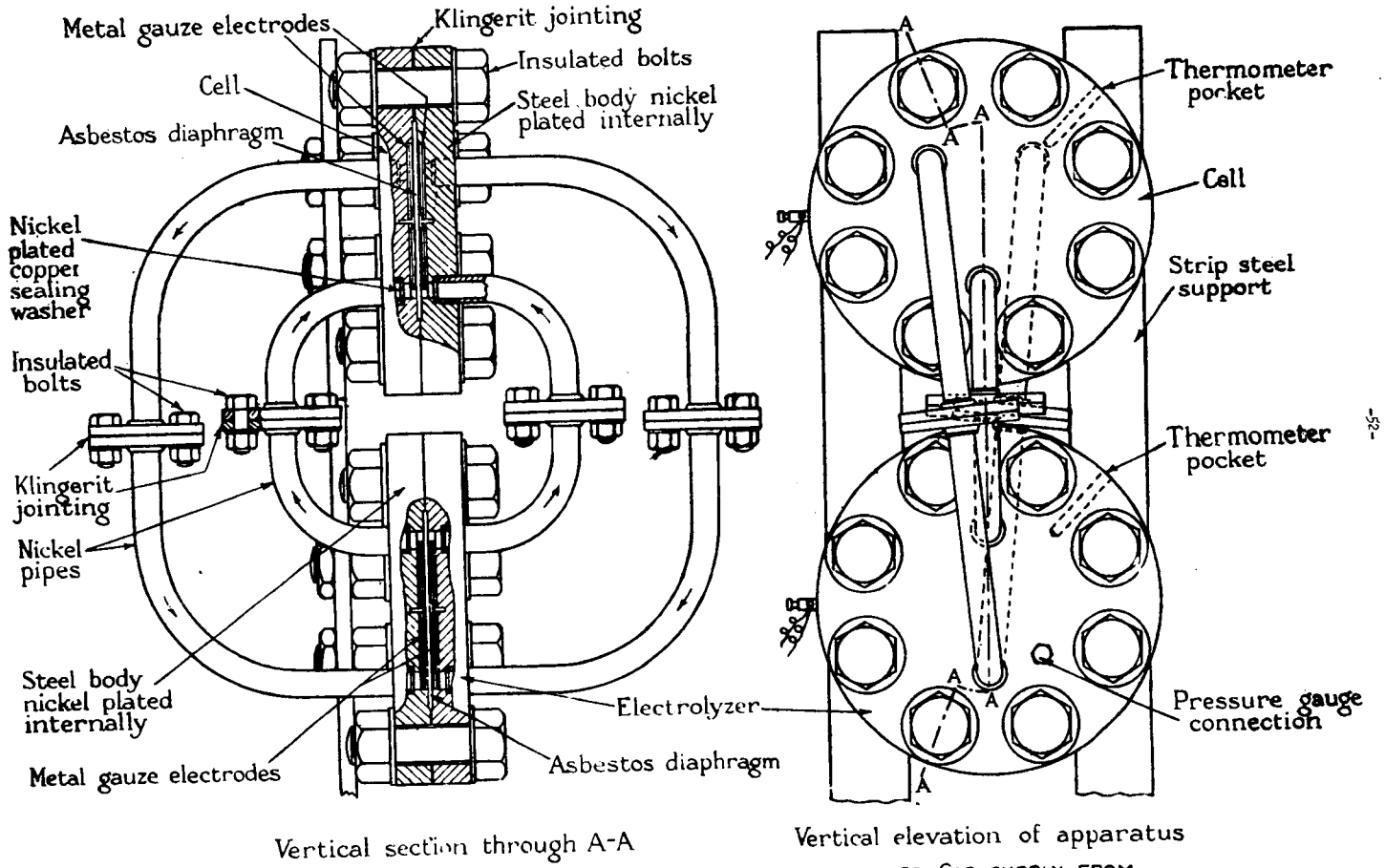

Vertical section through A-A

Vertical elevation of apparatus

FIG. 2. APPARATUS USING FLAT DISCS OF GAUZE AS ELECTRODES. GAS SUPPLY FROM SEPARATE ELECTROLYZER.

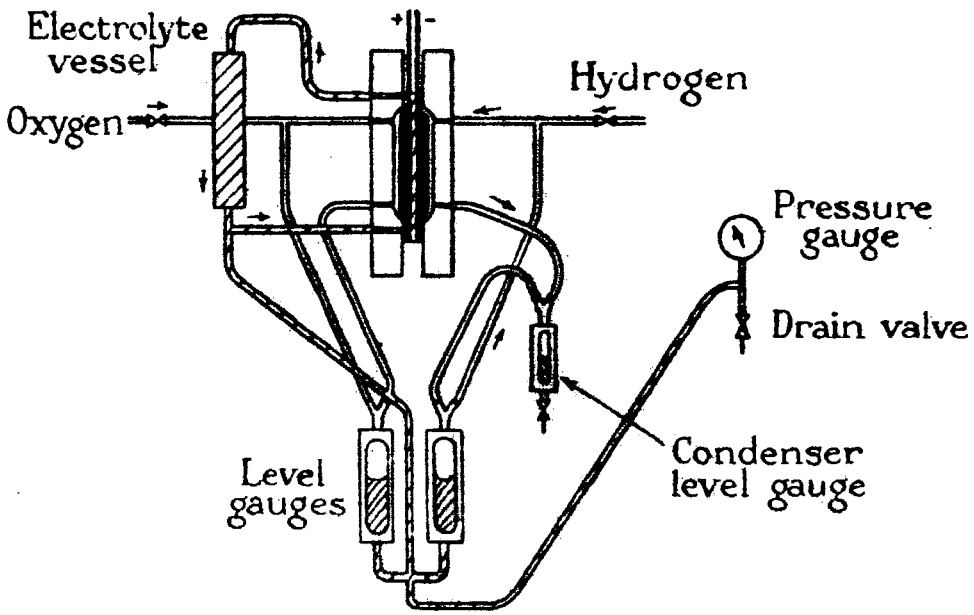

FIG. 3 APPARATUS EMBODYING CELL WITH POROUS DIFFUSION ELECTRODES.

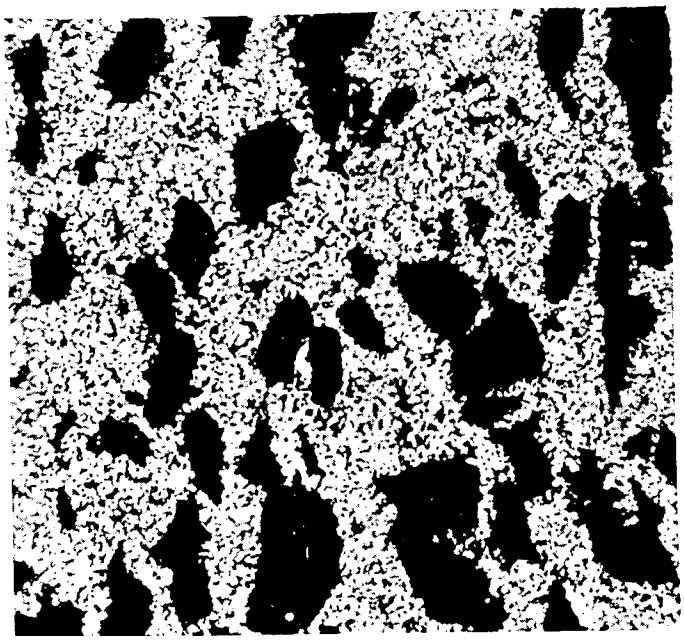

FIG. 4. MICROSECTION SHOWING COARSE PORE SIDE OF HYDROGEN ELECTRODE (x 150)

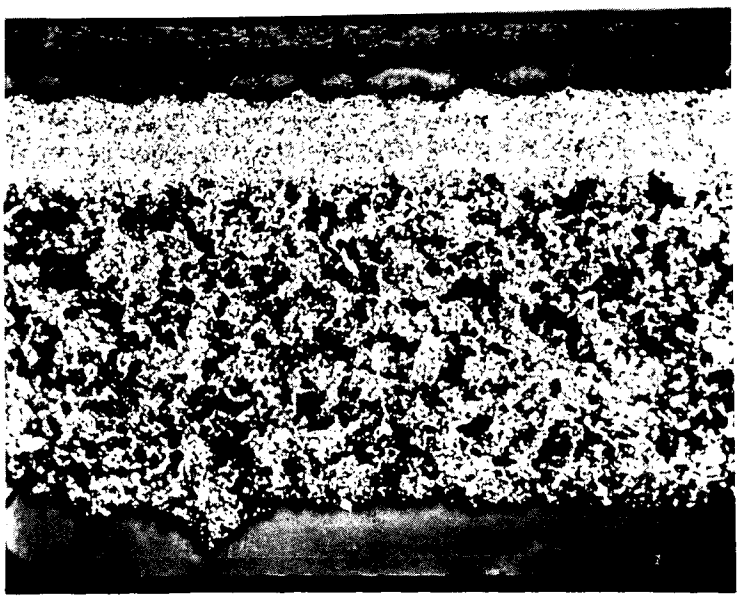

FIG. 5. MICROSECTION SHOWING COARSE AND FINE PORE LAYERS OF OXYGEN ELECTRODE (x 38)

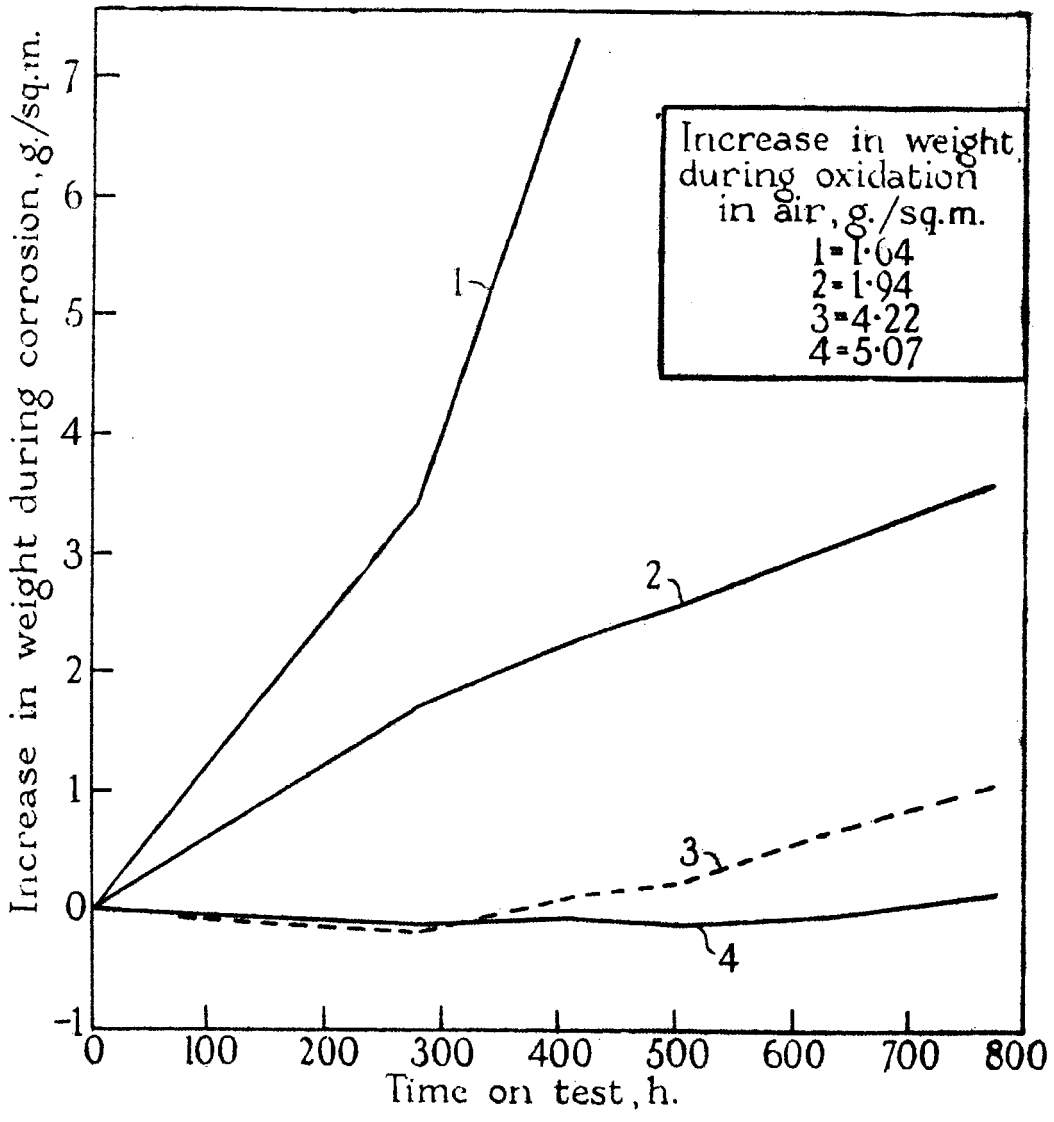

FIG. 6 CORROSION OF SAMPLES OF NICKEL PREOXIDIZED IN THE PRESENCE OF LITHIUM HYDROXIDE AND EXPOSED TO 65 % KOH AND OXYGEN AT 300°C. AND 800 lb./sq. in. TOTAL PRESSURE.

Each curve represents a pair of samples.

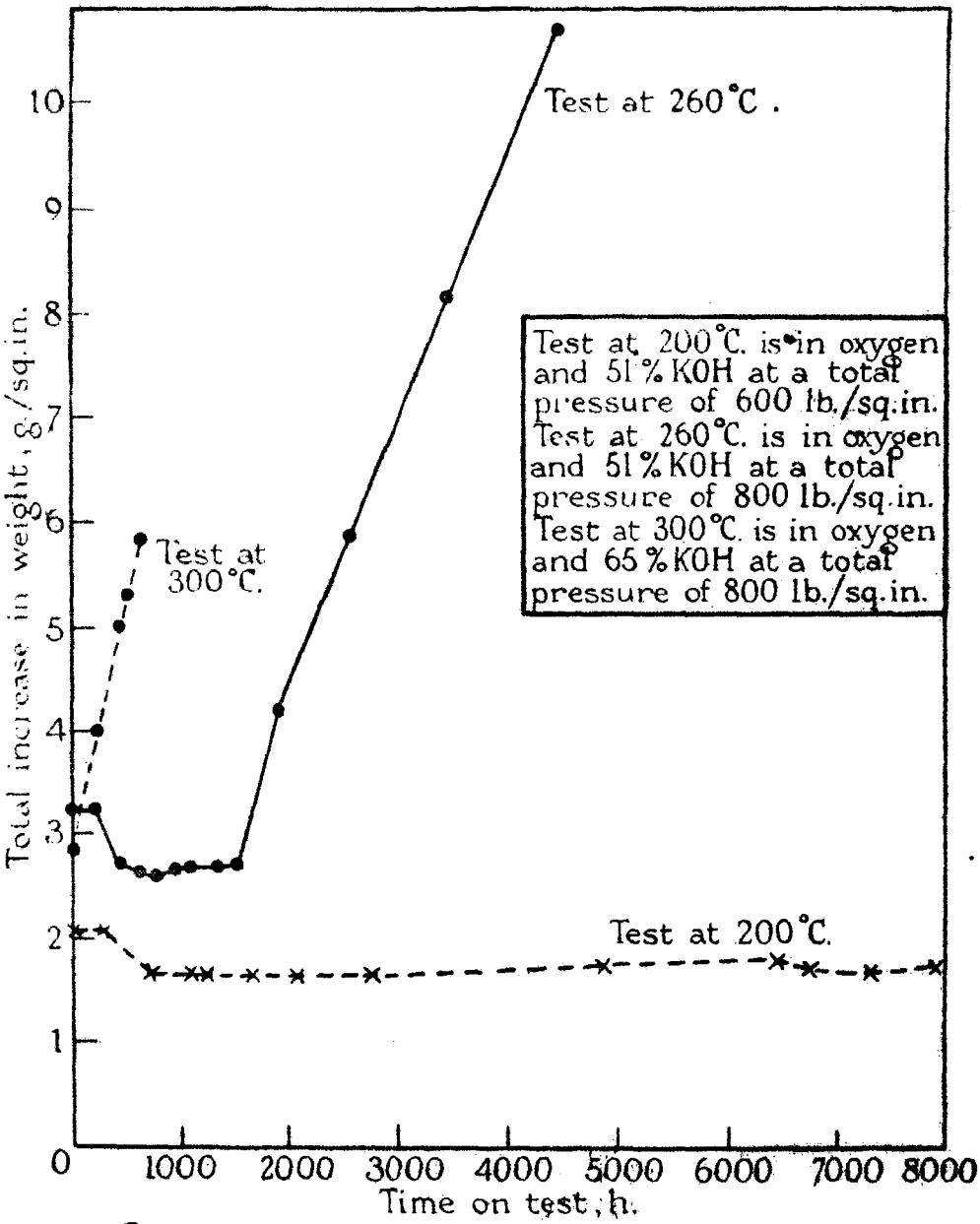

FIG. 7 CURVES SHOWING THE EFFECT OF TEMPERATURE ON CORROSION RATE

Values plotted are averaged from a series of samples coated with a protective oxide containing lithium, the oxide layers being of similar thickness.

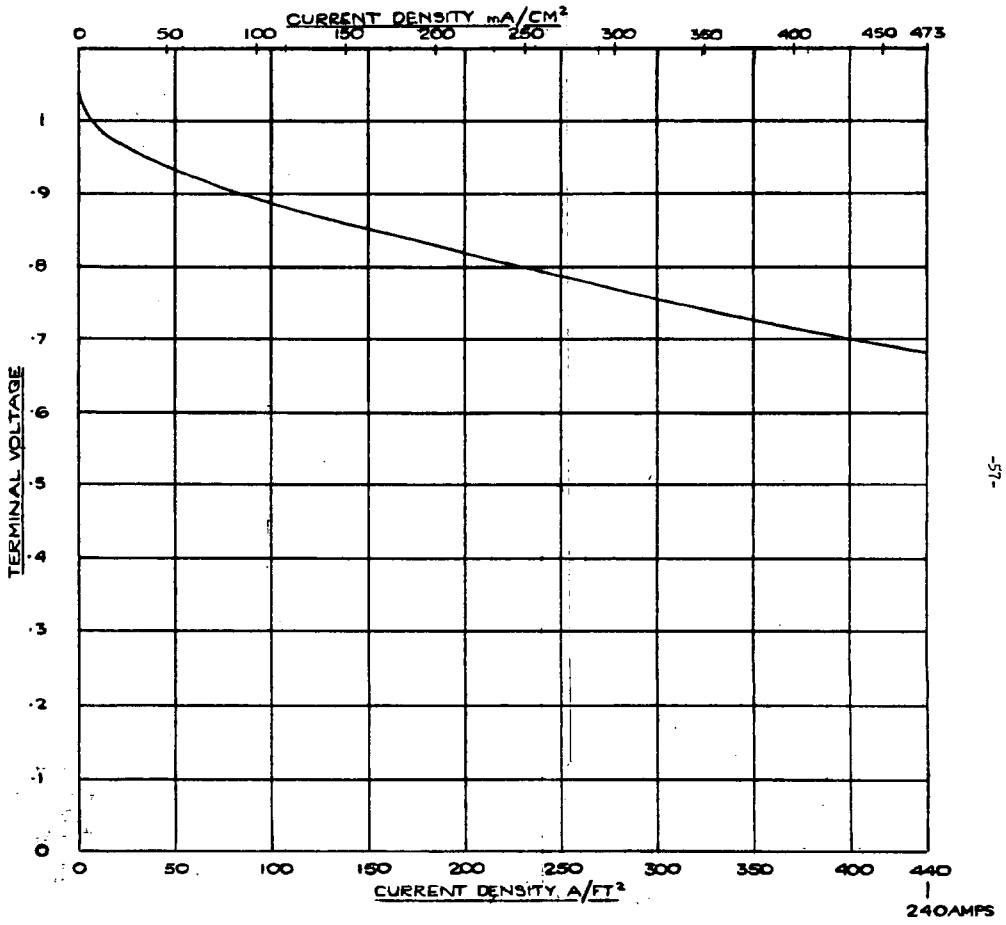

FIG.8 BEST PERFORMANCE OBTAINED SO FAR WITH 10" DIA CELL (MULTI-CELL PACK.)
(200°C; 400 P.S.I; 37% KOH)

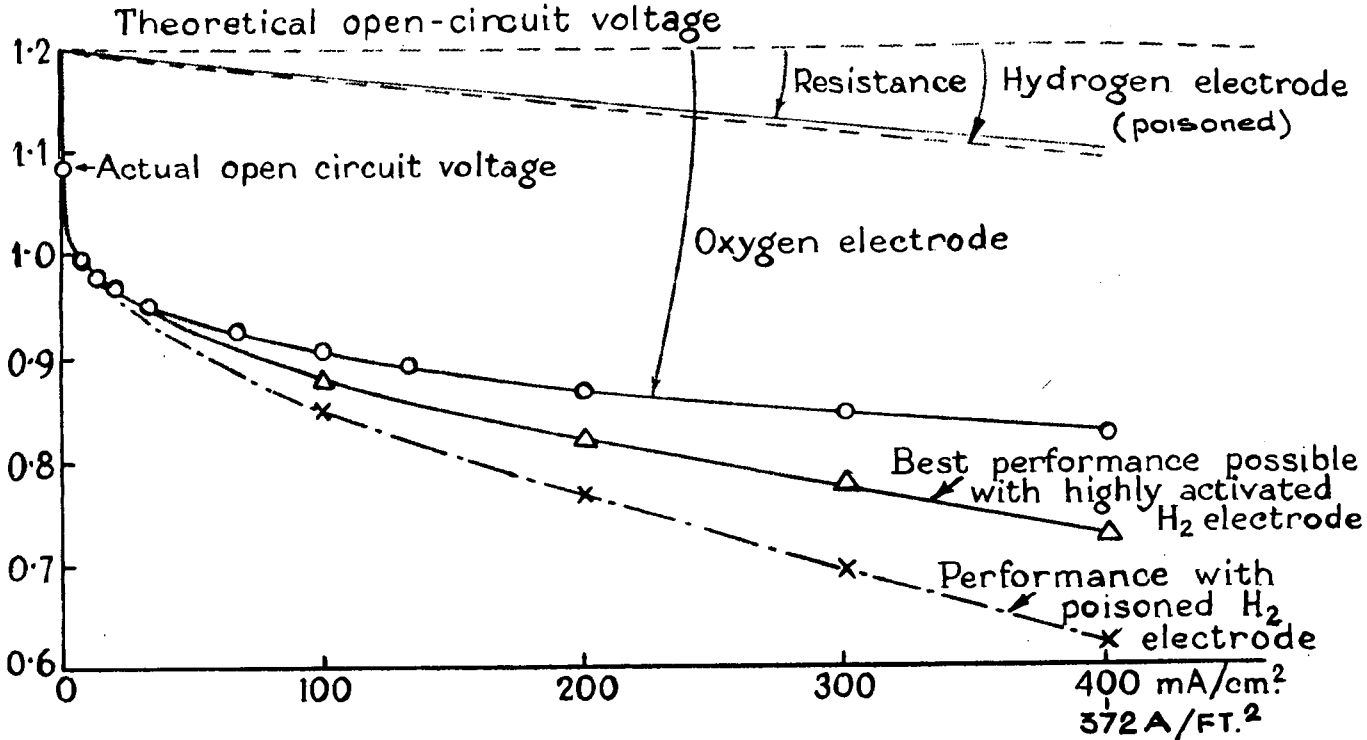

FIG. 9. PERFORMANCE OF CELL IN TERMS OF EACH ELECTRODE AND RESISTANCE 40% KOH ; 200°C ; 620 lb./sq. in.

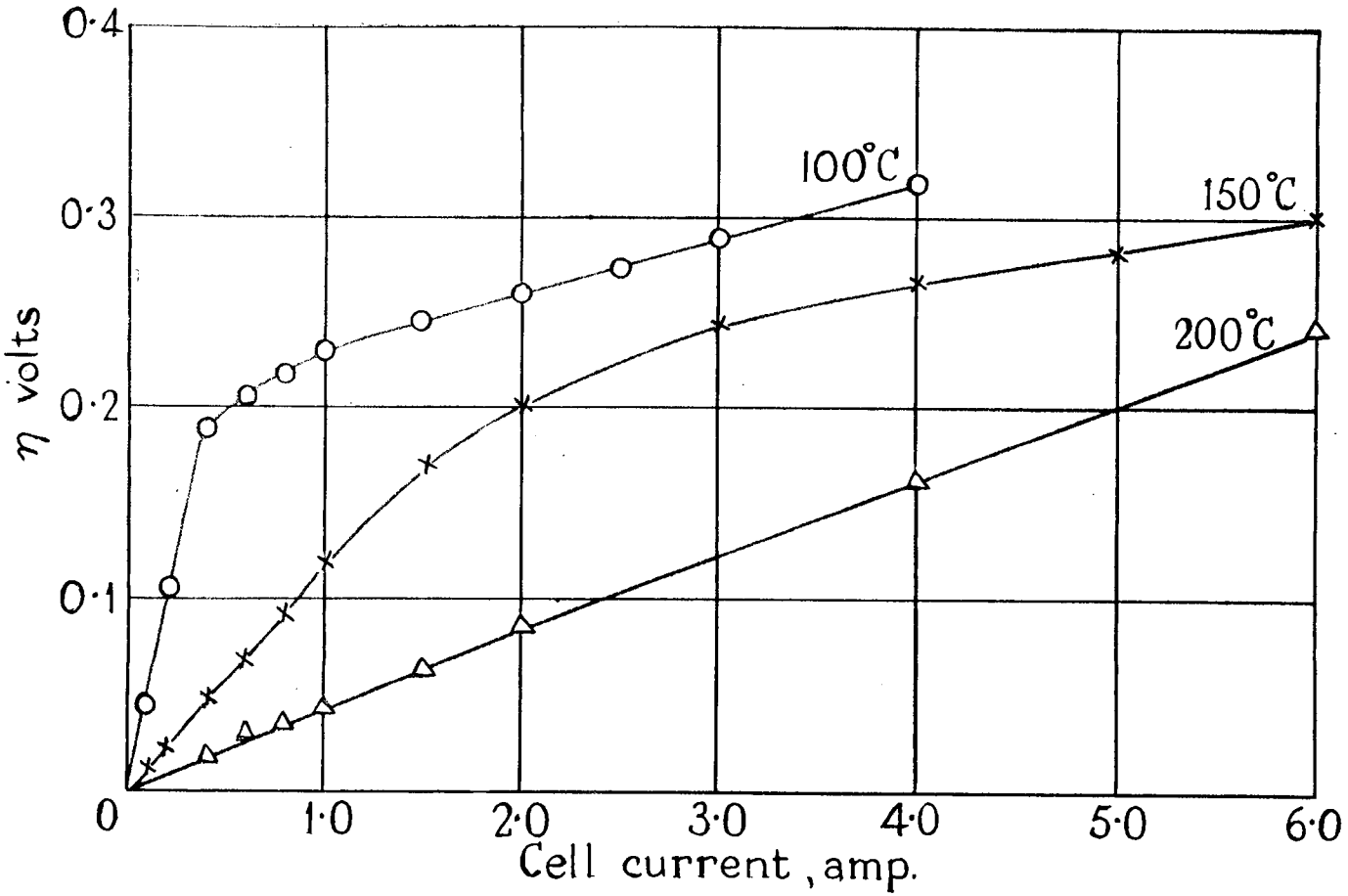

FIG. 10. POLARIZATION OF HYDROGEN ELECTRODE AT VARYING TEMPERATURE IN 5 N, KOH SOLUTION.

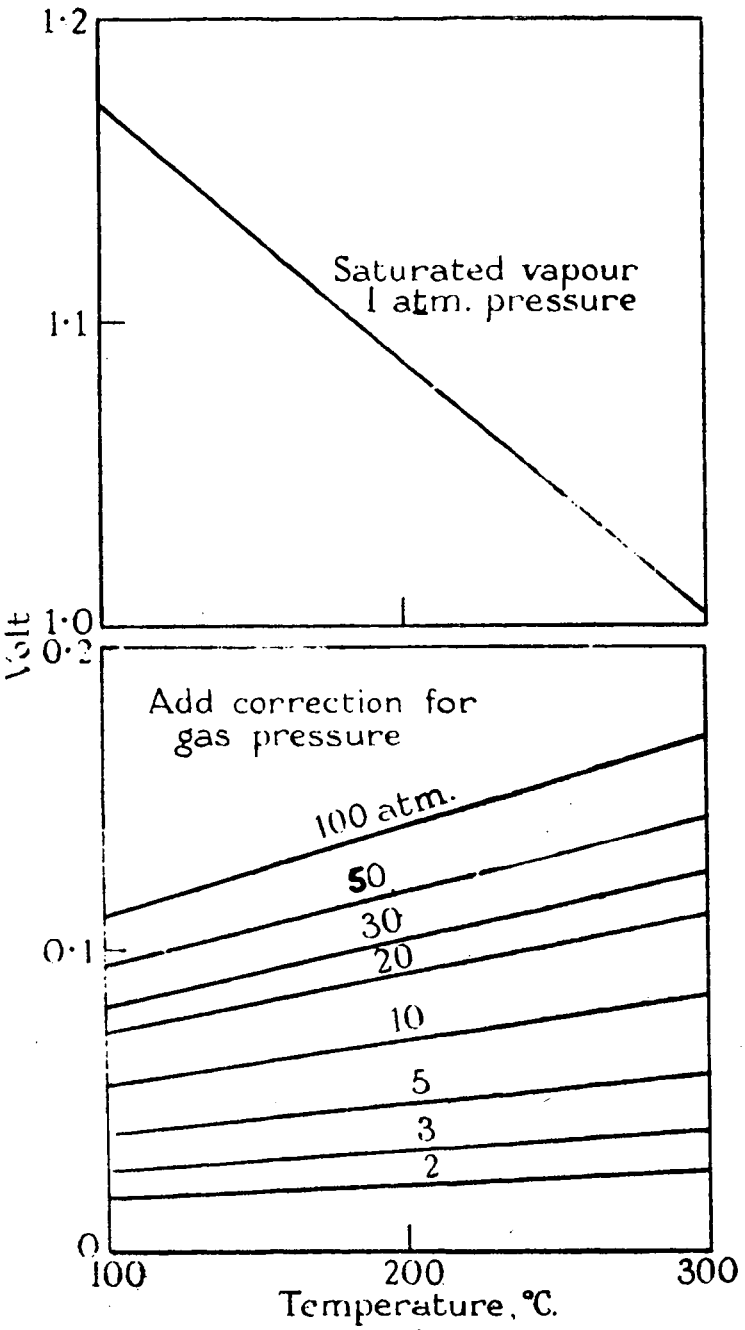

FIG. 11. REVERSIBLE VOLTAGE OF HYDROGEN-OXYGEN CELL

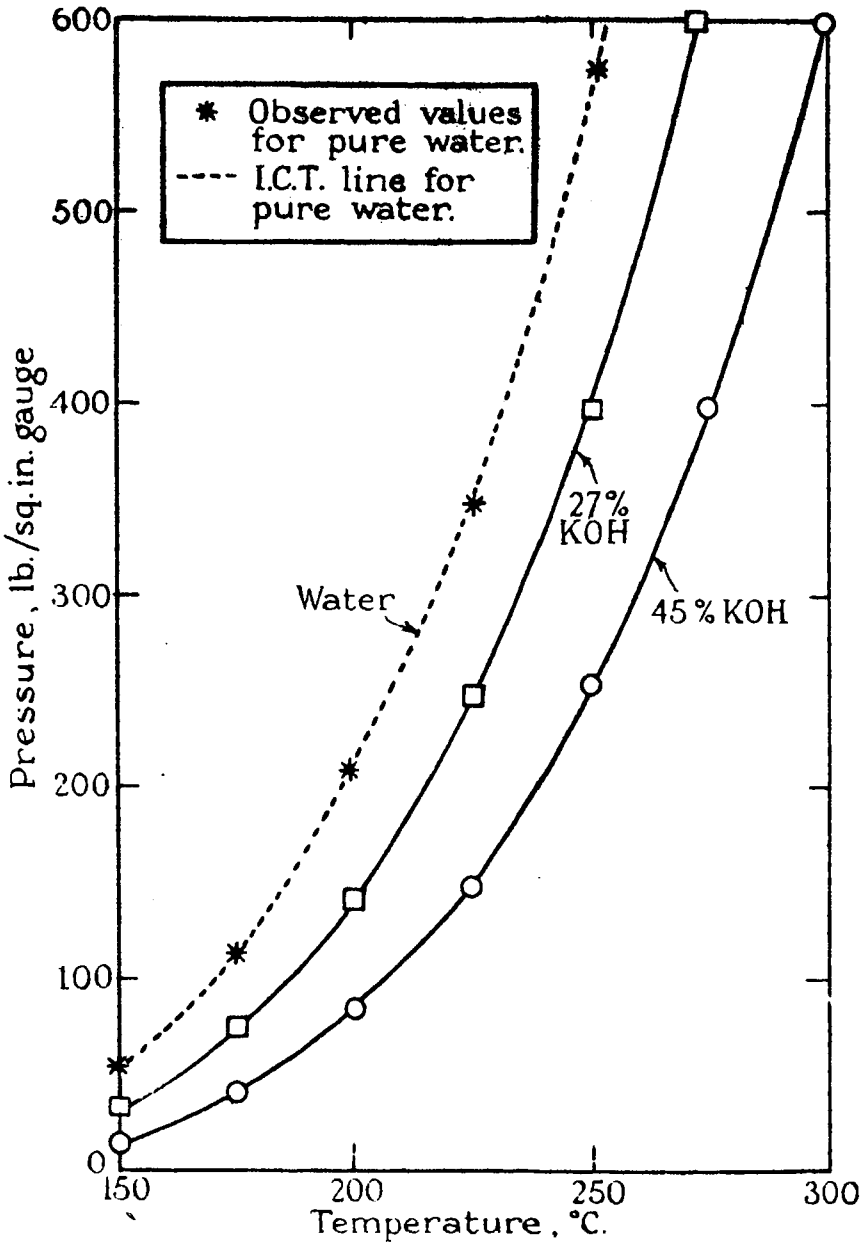

FIG. 12. VAPOUR PRESSURE OF ELECTROLYTES.

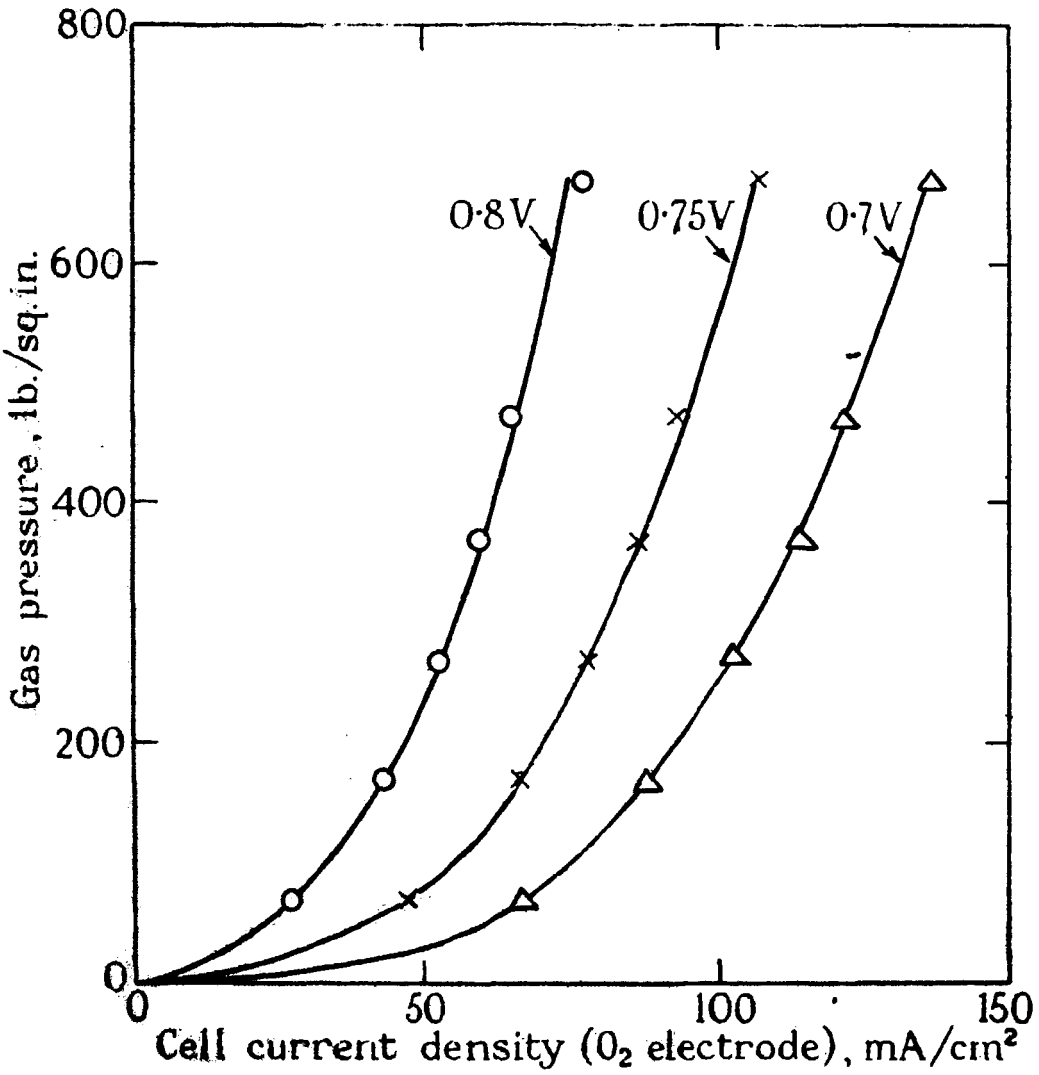

FIG. 13. VARIATION OF CELL OUTPUT WITH GAS PRESSURE FOR VARIOUS VOLTAGES.

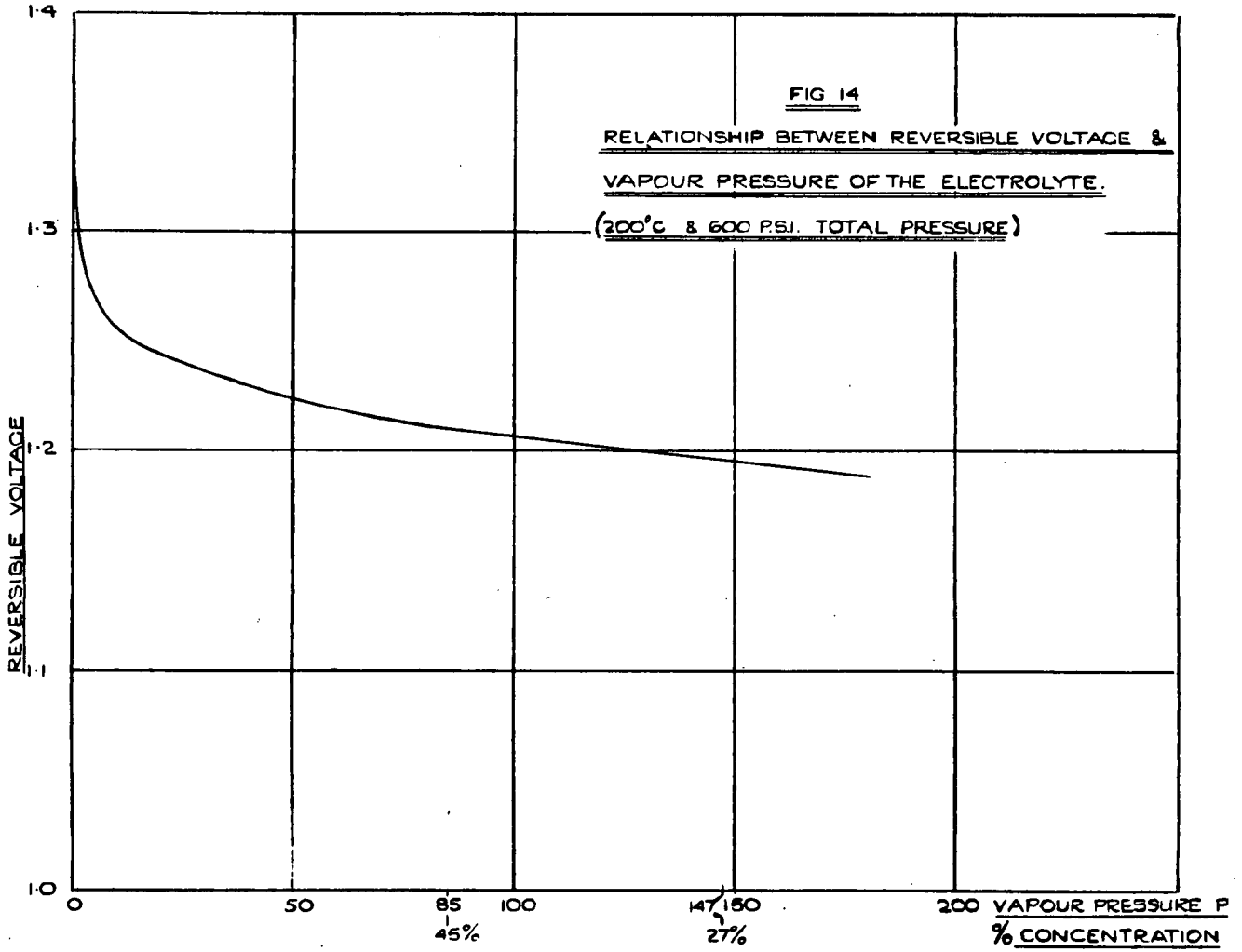

FIG 14

RELATIONSHIP BETWEEN REVERSIBLE VOLTAGE & VAPOUR PRESSURE OF THE ELECTROLYTE.

(200°C & 600 P.S.I. TOTAL PRESSURE)

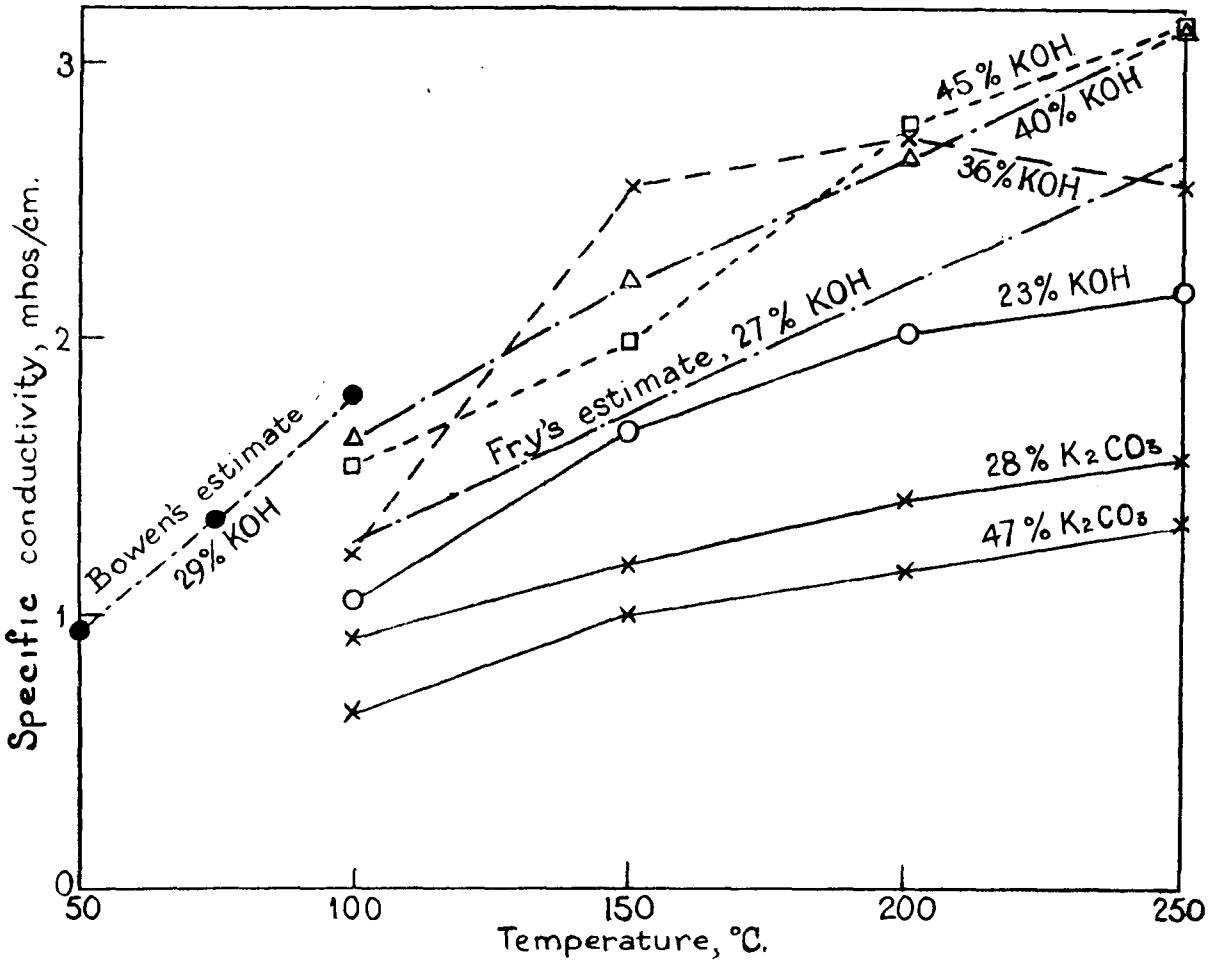

FIG. 15. VARIATION OF ELECTROLYTE CONDUCTIVITY WITH CONCENTRATION AND TEMPERATURE.

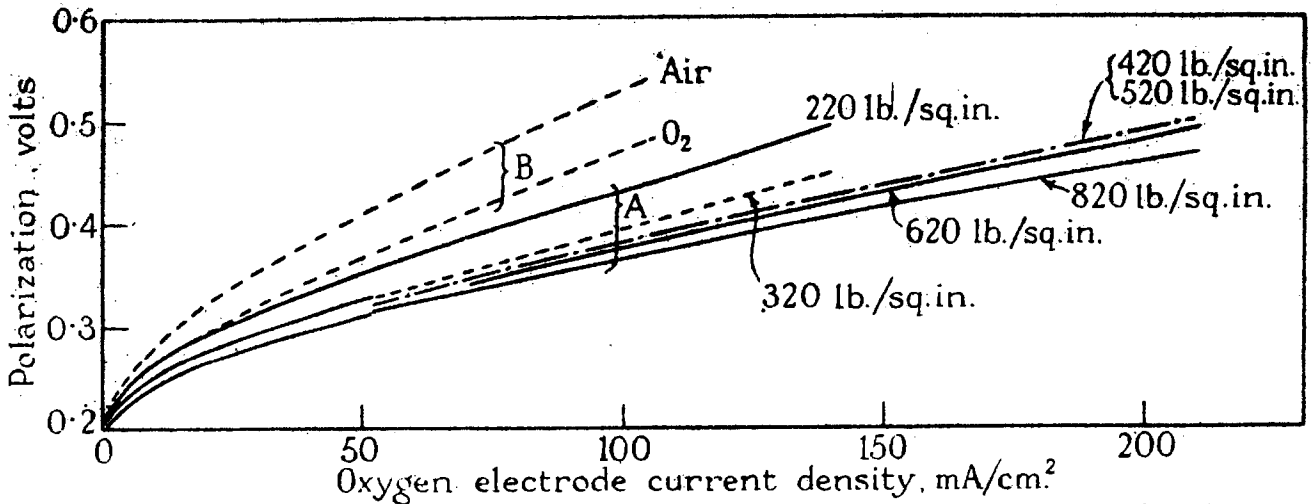

FIG. 16 THE EFFECT OF PRESSURE ON POLARIZATION AT THE OXYGEN ELECTRODE (A) 5 N. KOH, 200°C. G.31. (B) 5 N. KOH 200°C. E.183

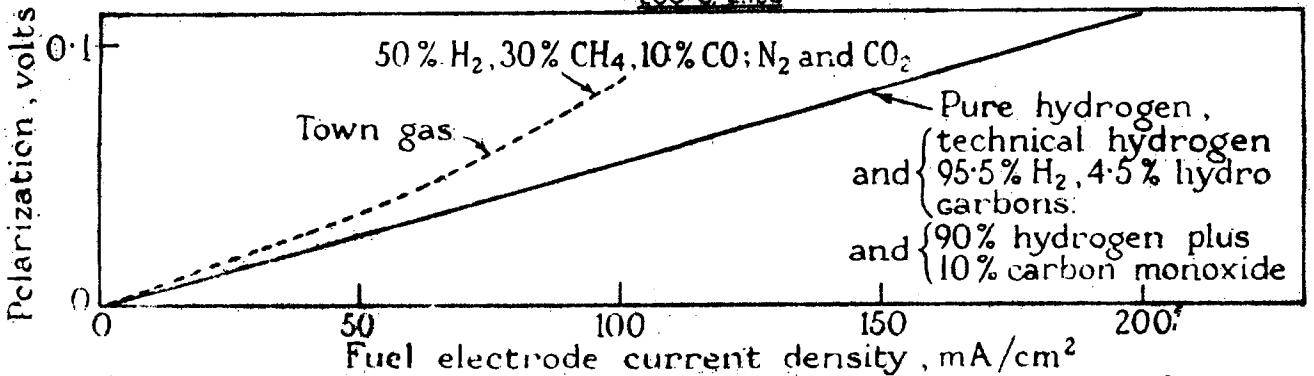

FIG 17 THE EFFECT OF VARIOUS FUEL GASES ON THE POLARIZATION AT THE FUEL ELECTRODE, 200°C. 5 N. KOH. 620 lb/sq.in.

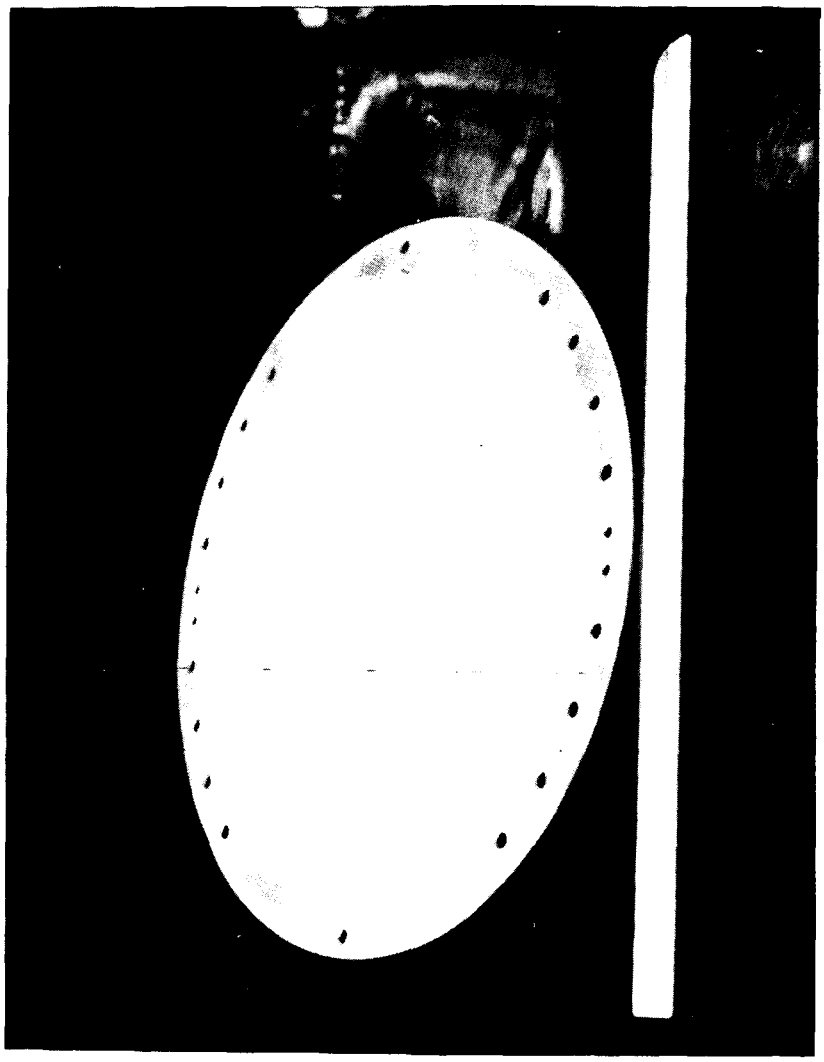

FIG. 18. ELECTROLYTE SIDE OF 10-INCH DIAMETER ELECTRODE

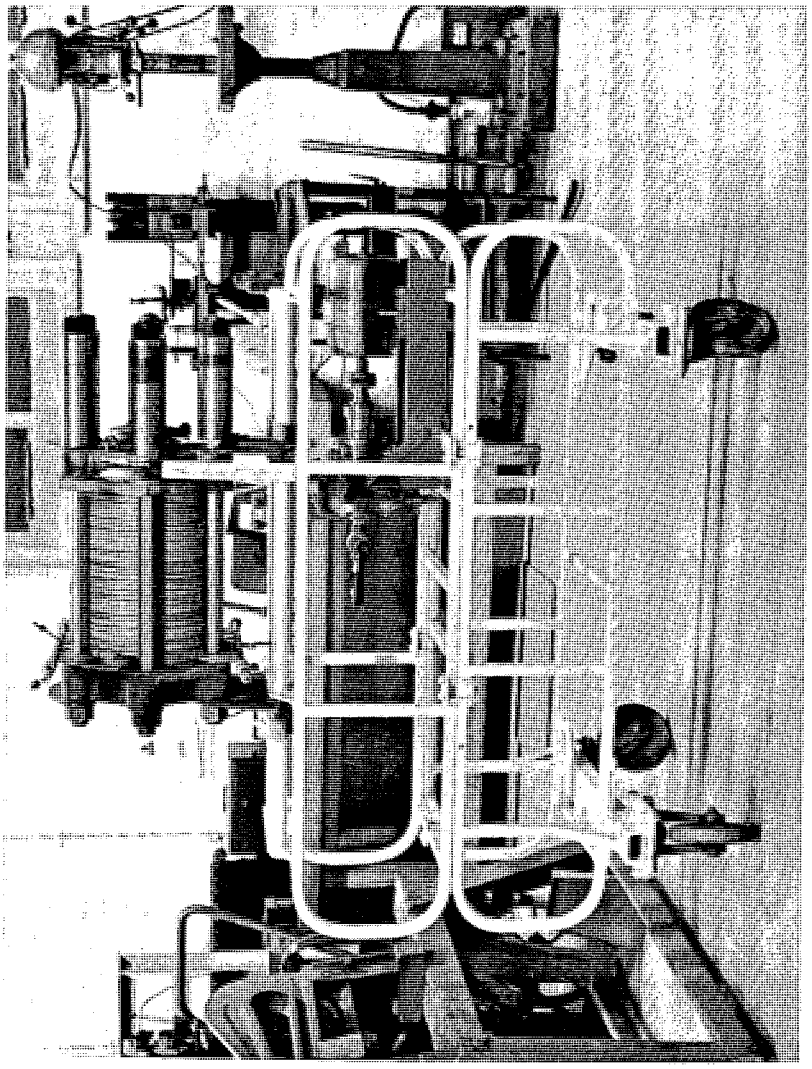

FIG. 19. 30-CELL BATTERY MOUNTED ON TROLLEY; HYDROGEN BLOWER MOUNTED UNDERNEATH

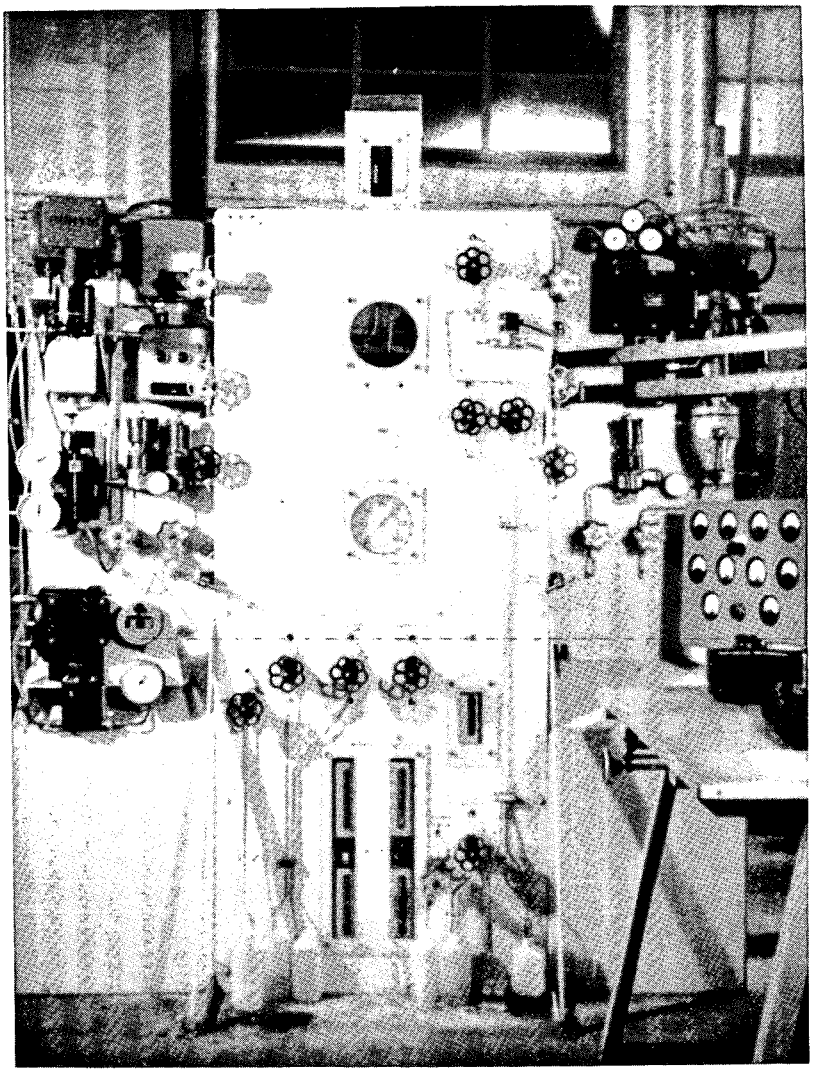

FIG. 20. CONTROL GEAR MOUNTED ON FRONT
OF PROTECTIVE FRAMEWORK

HYDROGEN/OXYGEN CELL (FIG 21)

RELATIONSHIP BETWEEN WEIGHT & ENDURANCE FOR 44 KW CELL

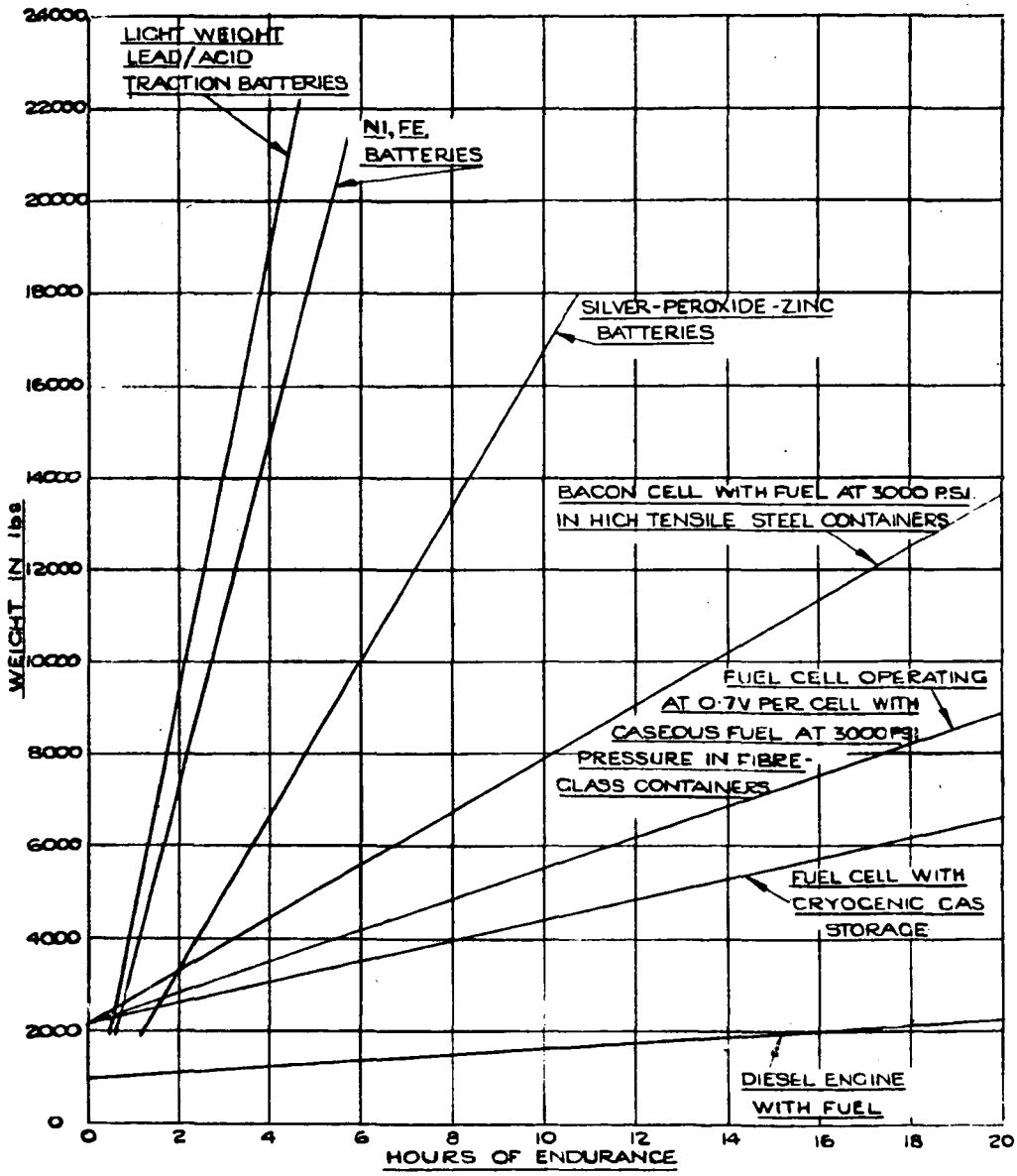

HIGH TEMPERATURE GALVANIC FUEL CELLS*

by

G.H.J. Broers
Central Technical Institute, The Hague, Netherlands

ABSTRACT

Stability of electrolytes for high temperature fuel cells will be discussed. Of all electrolytes investigated, only fused carbonates appear to be stable. The development of laboratory model magnesium oxide - carbonate cells and interpretation of their characteristics will be described. Performance results with regard to electrode gases and stability are surveyed.

* Manuscript not received in time for preprinting.

Not For Publication
Presented Before the Division of Gas anf Fuel Chemistry
American Chemical Society
Atlantic City, New Jersey, Meeting, September, 1959

The High Temperature Fuel Cell And the Nature of the Electrode Process

E. Gorin and H. L. Recht

CONSOLIDATION COAL COMPANY
Research and Development Division
Library, Pennsylvania

INTRODUCTION

Considerable activity has been generated in recent years on fuel cell research. The work has encompassed many different types of cells. The major portion of the work, however, has been concentrated on the low[1] and medium temperature[2] hydrogen oxygen cells and on the so-called high temperature gas cell.

No attempt will be made to review the rather voluminous literature in this field since many excellent review papers are available[3].

The high temperature cell may arbitrarily be defined as a gas cell which operates at atmospheric pressure and at temperatures in the general range of 500-900° C. It operates either with hydrogen or mixtures of hydrogen and carbon monoxide as fuel gas and usually with air as the oxidant. This is the type of cell which has excited most interest as a potential source of Central Station power.

Work on the high temperature fuel cell is now underway at quite a few laboratories throughout the world. The most extensive and probably the most successful work has been carried out at the University of Amsterdam under the direction of J. A. A. Ketelaar[4]. Broers[5] in particular has recently published an extensive account of the work carried out at Amsterdam.

Work has been conducted until recently on the high temperature cell at the laboratories of the Consolidation Coal Company. Recent publications[6] have described some of the experimental results as well as methods that could be employed for effecting the integration of the cell operation with the gas manufacturing process. Such integration is essential to realize the potential advantage of the fuel cell in achieving a high efficiency for power generation.

The high temperature cell[7] utilized in this work has been similar in most respects to that used by Broers[5]. The electrolyte used was mixed alkali carbonates disposed on a specially prepared pure porous magnesia matrix. In addition to the metal gauzes used by Broers, porous sintered metals have been used as the fuel electrode and a semi-conducting lithiated nickel oxide refractory as air[8] electrode. Likewise, metal gauzes, and in particular nickel and silver have been found to operate satisfactorily without the powdered metal activators used by Broers.

The basic problems that remain to be resolved before the fuel cell can attain commercial stature are the attainment of a system of acceptable life and power output. The resolution of these problems could be considerably expedited if a better understanding of the manner in which the cell functions were available.

The purpose of this paper is to present some thoughts with regard to the mechanism of the cell action. The experimental work carried out to date has not been sufficiently extensive to provide positive confirmation of the theories presented. The mechanism is put forth, therefore, without adequate experimental proof, in the hope that it may prove useful to other workers in the field.

EXPERIMENTAL METHOD AND RESULTS

The construction of the fuel cell, the method of fabrication of the components and the operating procedure have been described previously and will not be repeated here[7]. Likewise, some of the experimental results[6,7] have been presented before although in somewhat different form.

The data presented here serve as a basis for discussion of the mechanism of cell action. Most of the data given here revolve about the use of hydrogen as fuel gas. Considerable data have been accumulated also on carbon monoxide-carbon dioxide mixtures as fuel gas. The power outputs achieved are, in general, considerably lower than with hydrogen. These data are not included since the discussion revolves largely about the mechanism of the hydrogen and air electrodes only.

It is felt that the utilization of hydrogen will be the determining factor in any potential practical fuel cell system. All fuel gases that would be utilized in practice would be rich in hydrogen. Due to the relatively poor performance of the carbon monoxide electrode, the major portion of the carbon monoxide would likely be utilized indirectly through conversion in situ to hydrogen by means of the water gas shift reaction. The major distinction in practice between the low temperature and high temperature cells would be the ability of the latter to utilize the carbon monoxide even if it is only indirectly as discussed above.

Operating data obtained with the carbonate type cell are summarized in Tables IA and IB.

The electrolyte employed in the work reported here was an equimolar mixture of sodium and lithium carbonates throughout. Carbon dioxide was always added to the air stream as a depolarizer. The amount used is specified in Table IA.

The results given in the table are, except for individual cases noted, smoothed results. The method of least squares was used for this purpose based on the assumption of a linear drop in cell voltage with current drain. In order to apply this method it was necessary to correct for the decrease in open circuit voltage due to change in gas composition as a result of accumulation of reaction products with current drain. The theoretical voltage was calculated by the application of the Nernst equation. This figure is listed in Column 4) of Table IB. It is noted that the theoretical voltage with no current drain could not be calculated since it is effected by the very small but unknown amount of carbon dioxide in the hydrogen fuel gas.

The application of the statistical method to the treatment of the results is illustrated in Figures 1 and 2. The dotted lines present the field in which the experimental data should fall within a confidence limit of 95 percent.

The fit suggests that the cell operates without substantial electrode polarization at 700-750° C with porous nickel fuel electrode and either silver gauze or lithiated nickel oxide as the air electrode.

The above statement must be qualified, however, by the area as shown for the confidence limits. A polarization of up to .06 volts is permitted at 750° C and of up to .08 volts at 700° C.

Another check for polarization is the agreement between the cell resistance as measured directly by an A. C. bridge and that determined by the least squares analysis. The agreement is excellent for Run Ag2b at 750° C. Broers[5], likewise, reports excellent agreement between calculated and measured resistance even at lower temperatures. In the 700° C runs, however, the calculated resistance is definitely higher than measured. This does not necessarily indicate polarization, however, as will be shown later.

No realistic comparison could be made between measured and calculated resistance in many of the runs shown. This is because the open circuit voltage falls in some cases below the theoretical value. This is attributed to limited mixing of the fuel gas and air through microscopic cracks in the electrolyte matrix. Such cracks were observed after the runs were completed.

A few other interesting observations can be made. Silver is seen to be a fair hydrogen electrode although not nearly as good as nickel. It is practically worthless, however, as a carbon monoxide electrode.

Iron does not appear to be as good a hydrogen electrode as nickel. The data presented are not conclusive on this point. Numerous other data not presented here all point, however, to the same conclusions.

The above discussion is generally in accord with the findings of Broers[5].

Internal Resistance of the Cell

The high internal resistance of the cell during operation is noteworthy. Separate conductivity measurements were made to determine whether this could be attributed to some peculiar property of the electrolyte matrix. Measurements were made with the matrix loaded with an excess of the mixed carbonate melt. Two flat silver gaskets were used as electrodes. An average value of the resistance/cm^2 of 0.7 ohm was found in the temperature range of 700-800° C. The expected value from the thickness and porosity of the matrix, 0.2 cm and 28% respectively, and the specific conductivity of the melt 2.9 ohm^{-1} cm is only 0.25 ohm. Even so, the measured value is smaller by a factor of 7-10 than that observed during cell operation. Broers also found a similar high resistance during cell operation.

The high ratio between the resistance measured during cell operation and the inherent resistivity of the electrolyte matrix can be taken to have

the following significance. The melt inventory must be adjusted until a small area of contact is maintained between the electrode and the electrolyte. This may be required to maintain proper access of the gas to the electrode surface, and greatly increases the effective resistance of the electrolyte if the contact area is sufficiently small.

Consider, for example, an idealized model where the electrode maintains symmetrical square areas of contact having individual areas Δ^2 and a spacing between contact area d as shown in Figure 3.

The effective resistance of a cell containing two such identical infinite plane square mesh electrodes separated by an electrolyte of thickness ℓ may be calculated by a solution of Lapluces equation which relates the potential V to the position in the electrolyte

$$\nabla^2 V = 0$$

The calculation desired is the potential drop across such an electrode system as a function of the current density $\bar{I}$ and the specific resistance $\bar{R}$. This can then be compared with the potential drop across plane flat electrodes. The appropriate boundary conditions and solution of the above partial differential equation for this particular case was given previously[ab] and is omitted here for the sake of brevity. The solution is shown graphically in Figure 4 where the ratio R_{eff}/R is plotted as a function of ℓ/d with Δ/d as a parameter. R_{eff}/R is the ratio of the effective resistance to the resistance obtaining in the case where one has plane flat electrodes.

It is noted, for example, that the experimentally observed ratio R_{eff}/R of about 8.0 could be explained if the spacing d is about 3.2×10^{-2} cm and $\Delta/d = 1.8 \times 10^{-2}$. The above corresponds to an ℓ/d ratio of 6.3 which is in accord with the electrolyte thickness of 2 mm used in our work. It is interesting to note that such a situation corresponds to confining the electrode reaction to only 3.2×10^{-4} cm^2 per square centimeter of electrolyte surface.

The effective resistance ratio is very much a function of the spacing between contact areas. It is clear from Figure 4 that the resistance drops markedly for constant fractional active area as the spacing decreases. The importance of this factor in optimizing cell design is obvious.

Another way of illustrating this point is to repeat the same calculation with a different geometrical pattern. This was done with a parallel wire type electrode as shown in Figure 5. Such a system would correspond to the "hypothetical" case of a wire gauze electrode where none of the cross wires made contact.

Laplaces equation for this case was solved with the following pertinent boundary conditions:

$$\frac{\partial V}{\partial x} = \frac{\bar{I}\bar{R}}{\Delta/d} \qquad \text{for } x = -\Delta/2 \text{ to } +\Delta/2$$

$$= 0 \qquad \text{for } x = -d/2 \text{ to } -\Delta/2 \text{ and } x = \Delta/2 \text{ to } d/2$$

It was assumed again for simplicity that both electrodes were identical. The solution is

$$V = V_0 + \frac{i\bar{R}l}{2} + \sum_{n=1}^{\infty} \frac{i\bar{R}d}{\pi^2 n^2 r} \sin(n\pi r) \tanh\left(\frac{n\pi l}{d}\right) \quad \text{at } z = l/2 \tag{1}$$

$$\frac{R_{eff}}{R} = \frac{V_{z=l_2} - V_{z=l_2}}{i\bar{R}l} = 1 + \frac{2}{\pi^2 \left(\frac{l}{d}\right) r} \sum_{n=1}^{\infty} \frac{\sin n\pi r}{n^2} \tanh\left(\frac{n\pi l}{d}\right) \tag{2}$$

where $r = \Delta/d$ and $\bar{R}$ is the specific resistance.

The fractional area covered in this case is Δ/d as against $(\Delta/d)^2$ for the square mesh electrode. The points therefore were plotted with this in mind such that $(\Delta/d)^{1/2}$ for the parallel wire type electrode corresponded to Δ/d for the square mesh type.

It is readily seen that the parallel wire type electrode can tolerate a much smaller contact area without a large increase in cell resistance. Again the desirability of maintaining close spacing between contact points in cell design is emphasized.

Since the actual area of contact during operation of our cell was unknown one cannot state definitely that this is the major cause of the high resistance observed. Rather it seems likely that the low melt inventory itself may be partly responsible by causing part of the electrolytic conduction to be effected through small zones of extremely thin layers of melt.

As will be shown later, however, it is possible in principle to have a relatively low resistance as measured with an A. C. bridge and an effectively high resistance during cell operation as a result of the electrode reaction being concentrated in a very small area.

Maximum Rate of Electrode Reaction

The electrode reaction as mentioned above must be concentrated in a very small area due to the difficulty of providing acess of the gas through the three phase limit where electrode, electrolyte and gas meet. The minimum area required may be estimated as follows. The electrode reaction can certainly not take place, in the limit, any faster than gas molecules striking the metal surface can be adsorbed. Fortunately, Eyring[9] has provided us with a method of estimating this rate using his theory of absolute reaction rates. For the case where gas molecules strike a surface to form an immobile dissociated adsorbed film, Eyring gives the equation

$$V_1 = \frac{1}{2} \alpha C_g \bar{C}_a \frac{\sigma}{\sigma_\ddagger} \frac{h^4}{8\pi^2 I (2\pi m k T)^{1/2}} e^{-E_1/RT} \tag{3}$$

where V_1 is that rate of adsorption in molecules/cm^2 sec and E_1 is the activation

energy of adsorption. If we use $\lambda = 4$ and $C_s = 10^{15}$ sites/cm^2 as suggested by Eyring one calculates the adsorption rate for hydrogen as

$$v_i = 2.29 \times 10^{-5} T^{3/2} p_{H_2} e^{-E_1/RT} \text{ mols/cm}^2\text{sec.} \qquad (4)$$

Thus, if E_1 is small, i.e., equal to 3000 cal/mol, the endothermic heat of solution in nickel, the rate can be as large as 130 mol/cm^2 sec at 750°C. The above rate is sufficiently large such that a current density of 100 ma/cm^2 could be achieved on a surface as small as 4.0×10^{-9} cm^2/cm^2 of electrolyte area. Such a concentration of the electrode reaction, however, would , in view of the preceding considerations, cause a very considerable increase in the effective resistance of the cell.

In the case of the air electrode, under comparable assumptions, the maximum rate of the electrode reaction would be somewhat smaller due to the lower partial pressure and the higher molecular weight and moment of inertia of oxygen. Even so a rate of the order of 1 mol/cm^2 sec is possible in this case.

The Three Phase Limit

It is obvious that some mechanism must be in force for broadening of the three phase limit. Otherwise two deleterious factors come strongly into play, i.e., activation polarization as a result of concentrating the electrode reaction on a very small area and the concomitant high effective resistance discussed above.

Three mechanisms may be cited, diffusion of the gas through a thin film in the neighborhood of the interface, permeation of gas through the bulk electrode metal and finally surface diffusion across the electrode surface.

The first seems unlikely even though data on the permeation of gases through salt melts at high temperatures is unavailable.

Some data are available, however, on the diffusion and permeability rates of hydrogen and oxygen through aqueous solutions of electrolytes. For example, the diffusion constant of hydrogen through 20% NaOH solution[10] is reported as about 10^{-5} cm^2/sec at 25°C. The solubility C_o is of the order of 2×10^{-7} mols/cc at atmospheric pressure. The rate of transport of hydrogen to the electrode surface per unit area through an electrolyte film of thickness d is thus

$$\frac{D (C_o - C_1)}{d} = \frac{i}{2 \times 96500}$$

where C_1 is the concentration at the electrode interface. The exposure of as much as 1 cm^2 of surface to a thin film of electrolyte per cm^2 of electrolyte area seems rather unlikely with electrodes of the type used in this work. Even so one calculates in the above case that the average thickness of electrolyte film would have to be less than 6×10^{-6} cm to maintain a current density of 100 ma/cm^2.

Corresponding data are absent of course under conditions where the high temperature cell operates but it is not likely that the permeability of

gases through salt melts would be any higher due to a probably very low solubility of gases in melts. It would be interesting of course to obtain such data.

Data are available, however, from which the rate of permeation of gases through metals can be calculated. Probably the best data on the solubility of hydrogen in nickel and iron are those of Armbruster[11]. Edwards[12] gives corresponding data on the diffusion constant of hydrogen in nickel. Combining the two sets of data, one finds the permeation rate of hydrogen through nickel at atmospheric pressure $P = DC_o = 1.46 \times 10^{-6} \; e^{-\frac{13100}{RT}}$ mols/cm^7 sec. The permeation rate at 750° C is thus 2.37×10^{-9} mols/cm^2 sec/cm or greater by a factor of 10^3 than the permeation of hydrogen through electrolyte solutions at room temperature.

The rest of this paper is concerned with an examination of the permeation of gases through the metal electrodes as a mechanism for broadening the three phase limit. Some consideration is given also for the last mechanism.

Permeable Metal Gas Electrodes

A simplified model can be set up of the metal electrolyte contact such that the problem of a permeable metal electrode reaction can be treated mathematically. Such an idealized model is represented graphically in Figure 6. Here a cross section of the contact between the electrode and electrolyte matrix is represented. The cross section represents either a spherical metal granule of radius r, of the porous metal electrode or of a cylindrical wire of the same radius for the case where a wire gauze electrode is used. The angle ψ, represents the portion of the cross section where contact is maintained between the electrolyte and the metal electrode surface.

It is now necessary to make assumptions relative to the rate controlling processes. These must be made primarily on a basis of "reasonableness". It is assumed, therefore, that the rate of solution of gas into the metal is controlled by the rate of penetration of the gas from an adsorbed layer of dissociated atoms. Similarly the rate of dissolution is controlled by the rate at which the gas penetrates the metal surface to form the same adsorbed layer.

Experimentally it is known the rate of solution and dissolution of gas in metals is very rapid relative to the rate of permeation through the metal bulk[12]. No information is available, therefore, on the rate determining step for adsorption and desorption. The experimental facts are also consistent with the hypothesis that the dissolved gases are present in dissociated form when dissolved in metals. The adsorbed layer may therefore also be considered as being present in dissociated form.

Two further assumptions are now required, namely, that the rate of adsorption is very rapid relative to the rate of solution such that the concentration in the adsorbed layer is in equilibrium with gas phase. Similarly, it is assumed that the electrode reaction involves the adsorbed layer and again this is very rapid relative to the rate of desorption from the metal bulk. Thus again, the equilibrium electrode potential is maintained as determined by the concentration in the adsorbed layer.

Since the electrode must be at constant potential, it follows that the concentration of the adsorbed layer must be constant at all points within the electrolyte. This concentration C_1 may be considered to be equivalent to that in equilibrium with gas at a pressure P_1 in atmosphere, i.e., $C_1 = C_0 \sqrt{P_1}$. Similarly, the concentration of the adsorbed layer in the area outside of the electrolyte Cg, must be constant and in equilibrium with pressure of gas existing in the gas phase, i.e., $Cg = C_0 \sqrt{Pg}$. C_0 is the concentration in equilibrium with 1 atmosphere of gas.

The rate of permeation of the gas through the electrode may be obtained by solution of Ficks diffusion equation. For steady flow this reduces to

$$D \nabla^2 C = 0 \tag{5}$$

The boundary conditions for solution of the above equation based on the above assumptions are:

$$D\left(\frac{\partial C}{\partial r}\right)_{r=r_1} = -k(C - C_1) \qquad \psi = 0 \text{ to } \psi_1$$

$$D\left(\frac{\partial C}{\partial r}\right)_{r=r_1} = +k(C_g - C) \qquad \psi = \psi_1 \text{ to } \pi$$

where k is the rate of desorption of the gas from solution in the metal and C is the concentration of gas in the metal.

We obtain two solutions for the two cases considered:

a) Spherical Electrode Contact

$$C = \frac{(C_g + C_1) + (C_g - C_1)h}{2} - \left(\frac{k}{2D}\right)(C_g - C_1) \sum_{m=1}^{\infty} \frac{r^m \left[P_{m-1}(h) - P_{m+1}(h)\right] P_m(x)}{r_1^{m-1}\left(m + \frac{k r_1}{D}\right)} \tag{6}$$

where $x = \cos\psi$ and $h = \cos\psi_1$

and $P_m(x)$ are the Legendre polynomials of the first kind.

$$F = \pi r_1 D (C_g - C_1) X_1 \tag{7}$$

where

$$X_1 = \left(\frac{h_1}{D}\right) \sum_{m=1}^{\infty} \frac{m \left[P_{m-1}(h) - P_{m+1}(h_1)\right]^2}{(2m+1)\left(m + \frac{h_1}{D}\right)} \tag{8}$$

The flux F above is the total flow of gas through the metal electrode surface and is obtained by the integration

$$F = -2\pi r_1^2 D \int_{\psi_1}^{\pi} \left(\frac{\partial C}{\partial r}\right)_{r=r_1} \sin\psi \, d\psi \tag{9}$$

Now the flux F must equal the current flow so that we obtain

$$N\pi h_1 P \sqrt{P_g} \left(1 - \sqrt{\frac{P_1}{P_g}}\right) \bar{X}_1 = \frac{\bar{\imath}}{96500n} \tag{10}$$

where $\bar{\imath}$ is the current density in amps/cm^2, N is the number of spheres making contact/cm^2 area, n is the number of electrons involved in the electrode process (2 in the case of hydrogen) and $P = DC_0$ is the permeability of the gas through the metal. The above equation may be used to calculate the extent of electrode polarization ΔE as determined by the slow permeation through the electrode

$$\Delta E = \frac{RT}{nF} \ln\left(\frac{P_1}{P_g}\right) \tag{11}$$

The maximum current that may be drawn is determined by the value of $\bar{\imath}$ in equation (10) when $p_1 = 0$.

The basic assumption in the above derivation is that activation polarization is absent, i.e., the electrode reaction is very rapid. It will be seen in what follows that a rapid electrode reaction is a necessity in order to obtain adequate permeation rates in any case.

An interesting feature of equation (10) is that the permeation rate decreases only as the square root of the pressure. This tends to favor this

mechanism of broadening of the three phase limit in the low pressure range. The extent of polarization is thus proportional to permeation rate of the electrode P and is, as will be seen later, relatively insensitive to the rate of the electrode process.

b) Cylindrical Wire Electrode Contact

The solutions of equation (5) are obtained in this case in exactly the same fashion as before. They are given below

$$C = C_g - \frac{\psi_1}{\pi}(c_g - c_1) - \frac{2}{\pi}\left(\frac{k}{D}\right)(c_g - c_1)\sum_{n=1}^{\infty} \frac{r^n \sin\psi_1 \cos n\psi}{r_1^{n-1} n\left(n + \frac{k r_1}{D}\right)} \tag{12}$$

$$F = D(c_g - c_1)\left(\frac{k r_1}{D}\right)\left(\frac{4}{\pi}\right)\sum_{n=1}^{\infty} \frac{\sin^2\psi_1}{n\left(n + k r_1/D\right)} \tag{13}$$

$$NP\sqrt{p_g}\left(1 - \sqrt{\frac{p_1}{p_g}}\right)\bar{X}_2 = \frac{\bar{i}}{96500\,n} \tag{14}$$

$$\bar{X}_2 = \frac{4}{\pi}\left(\frac{k r_1}{D}\right)\sum_{n=1}^{\infty} \frac{\sin^2\psi_1}{n\left(n + \frac{k r_1}{D}\right)} \tag{15}$$

The form of the above equations is very similar to the spherical case. N in this case is defined as the number of cylindrical wires of unit length in contact with 1 cm^2 of electrolyte surface.

It is noted that in all cases the flux factor X in the above equations is determined only by the term ($\frac{k r_1}{D}$). The rate constant for the electrode reaction k is unknown.

However, it is possible to make some deductions from the experimental data as to the permissible range of this rate. It is implicit in the above derivation that the rate of the electrode process k (C_g - C_1) must be less than the rate of adsorption from the gas phase.

Consider now porous nickel as a hydrogen electrode. It was shown previously that a maximum value for the adsorption rate at 750°C is of the order of 130 mols/cm^2 sec. For hydrogen in nickel D = 6 x 10^{-5} cm^2 sec^{-1} and C_o = 3 x 10^{-5} mols/cc at 750°C. Thus for a particle of 65 microns diameter mean particle size of the metal granules in the electrode used

$$k(c_o) < 130 \qquad \frac{k r_1}{D} < 2 \times 10^8$$

It is therefore clear that for the present very large values of ($\frac{k r_1}{D}$) are not ruled out. Computations of the flux factor X, however, become very laborous for values of ($\frac{k r_1}{D}$) > 500. Computed values of the flux factor as a function of the contact angle ψ_1 and the flux factor are shown in Figure 7. It may be shown from the behavior of equation (8) that as $\frac{k r_1}{D}$ increases indefinitely so does the flux factor. It is seen from Figure 7 that X may be extrapolated to higher values of ($\frac{k r_1}{D}$) by use of the empirical relationship

$$X_1 = A \left(\frac{k r_1}{D} \right)^n$$

The polarization curves calculated in this way for several assigned values of ($\frac{k r_1}{D}$) and for several immersion angles are illustrated in Figure 8. The cases shown correspond to perfect contact between the electrode and electrolyte, i.e., every granule in a close-packed array makes contact.

It may be noted that the polarization curves are readily translated to different values of P, N, r, and X. Thus, the current density at which an equivalent polarization is obtained is proportional to P, N and X. For close-packed array of contacts it is also proportional to r_1. For the same number of contacts/cm^2 it is inversely proportional to r_1.

The experimental results with the hydrogen nickel electrode showed that the polarization voltage was less than .08 volts at temperatures above 700°C. It is seen from Figure 8 that such a result can reasonably be achieved with the permeation mechanism cited although the case is far from proven.

The permeation rate, as noted above, goes down with temperature. Thus at 600°C it is lower by a factor of 3 and consequently only 1/3 as much current could be drawn before an equivalent amount of polarization sets in. The earlier onset of polarization at lower operating temperatures has been noted in our work and by others.

The polarization curves shown in Figure 8 correspond to rather perfect contact between electrode and electrolyte. The effective resistance ratio may be estimated as discussed above. Take for example, the case shown for $\psi = 5°$, the values of Δ/d, and ℓ/d in this case are .02 and 30 respectively. Referring to Figure 4 the calculated $R_{eff}/R = 2.5$ which is considerably smaller than the observed value of 7. In actuality, less than perfect contact may be anticipated. The case is also illustrated in Figure 8 where only one in two particles at the electrode surface actually make contact. The predicted polarization in this case is in accord with that observed while R_{eff}/R rises according to Figure 4 to 3.5 which is closer to the observed ratio.

One must make one important qualification, however, since it can be shown that for high values of (k_1/D) the current is concentrated over a relatively small fraction of the total contact area. Thus the effective resistance ratio would actually be greater than the value estimated above.

As a matter of fact, a peculiar feature of this treatment of the electrode process is that an extremely rapid electrode reaction causes it to be concentrated in a small area and thus increases the effective internal resistance of the cell.

The iron electrode may be evaluated in a similar fashion. The permeability of hydrogen through iron from the data of Smithells and Ramsley[13] may be described by the following equation

$$P_o = 2.01 \times 10^{-7} \; e^{\frac{-9800}{RT}} \quad \text{mols/cm}^2 \text{ sec/cm.}$$ Thus,

P_o at 750°C is equal to 1.8×10^{-9} which is very close to the value for the permeability of nickel. On this basis its performance as a hydrogen electrode should be very similar to nickel which is in accord with the facts.

The relatively poor performance of carbon monoxide electrode may be ascribed to its low permeability through the metal electrodes.

We will now turn our attention to a discussion of the silver electrode. This electrode was used both as a hydrogen and air electrode in the form of wire gauze. We therefore use equation (15) to discuss this case. The variation of the flux factor X with $(\frac{k_1}{D})$ using the contact angle as parameter is shown in Figure 8. Again the flux factor may be extrapolated to higher values of $(\frac{k_1}{D})$ by means of the empirical equation

$$X_2 = A \left(\frac{k_1}{D} \right)^n$$

The justification again is the behavior of equation (15) which shows that X increases indefinitely as $(\frac{k_1}{D})$ increases. As a matter of fact it may be shown that equation (15) takes the form

$$X_2 = \frac{4}{\pi} \sum_{n=1}^{\infty} \frac{\sin^2 n\psi}{n} \qquad (16)$$

as $\left(\frac{kr_i}{D}\right) \rightarrow \infty$. The above series diverges and thus X_3 becomes infinite. Likewise it may be shown the current is concentrated in an infinitely small area.

The permeability of oxygen through silver was measured by Johnson and LaRose. Their results may be expressed by the equation

$$P_o = 6.2 \times 10^{-6} e^{-\frac{22600}{RT}}$$

and shows a value for P_o of 9.3×10^{-11} mols/cm^2 sec at 750° C. The diffusion coefficient may be obtained by combining the solubility data of Steacie and Johnson[15] with the above permeability data. Thus the value of D at 750° C is 9.5×10^{-6} cm^2 sec^{-1}. By the same argument as was developed previously for nickel we find than the maximum possible value of $\frac{kr_i}{D} \cong 7 \times 10^7$. The maximum current that can be drawn in air under the assumption that all wires contact the electrolyte matrix throughout their length can now be computed for various assigned values of $\left(\frac{kr_i}{D}\right)$. These figures are shown in the table below:

Short Circuit Current For
30 Mesh Silver Wire Gauze Electrode $r_1 = 7 \times 10^{-3}$ cm

Contact Angle	$\frac{kr_i}{D}$	Short Circuit Current ma/cm^2
12.8°	2000	5.0
1.28°	2000	2.8
1.28°	7×10^7	42.0

It is now seen that permeation through a silver air electrode is nowhere sufficiently fast to explain its performance.

Similar considerations may be made with regard to the silver hydrogen electrode. Accurate data are not available for the permeation rate of hydrogen through silver. The indications again are, however, that it would be insufficient to explain its performance as a hydrogen electrode.

To resolve these discrepancies, it is necessary to assume that the permeation rate through a thin surface layer of the metal is much greater than through the metal in bulk. Equations may be derived for this case in a similar manner to the bulk permeation case treated above. The result, for example, for rapid permeation through a thin surface spherical shell of thickness Δ is given below

$$F = \pi r_1 D (c_g - c_1) X_3 \tag{17}$$

$$X_3 = \left(\frac{kr_1}{D}\right) \sum_{m=1}^{\infty} \frac{m\left[P_{m-1}(k) - P_{m+1}(k)\right]^2}{(2m+1)\left(m + \frac{kr_1^2}{\Delta D(m+1)}\right)} \tag{18}$$

Thus, the form of the equation is identical to that for bulk diffusion with the only change being in the flux factor X_3. The dependence of the polarization voltage on the system variables is thus identical.

In conclusion, the performance of the nickel and iron electrodes can be explained on the basis of the bulk permeation rate through the metal. The silver electrode performance required the introduction of the concept of accelerated surface diffusion. Further experimental data are required to determine whether variation of cell performance with system variables such as gas concentration behaves in the predicted fashion.

Literature Cited

1 G. E. Evans

Proceedings of the 12th Annual Battery Research and Development Conference (U.S. Army Signal Corps Research and Development Laboratories Publication) May 1958.

2 F. T. Bacon

The Beama Journal, 61, 2-8 (1954).

3 J. H. McKee

The Production of Electricity From Coal, British Coal Utilization Research Association Bulletin 9, No. 7 193-200 (1945).

A. M. Adams

Fuel Cells II Low Temperature Cells, Future Development, Chemical and Process Engineering, 35, 238-240, 1954.

4 J. A. A. Ketelaar

Die Ingenieur 66, 34 E 88-91 (August 20, 1954).

5 G. H. J. Broers

"High Temperature Galvanic Cells" Thesis, University of Amsterdam, 1958.

6 E. Gorin and H. L. Recht

A. Mechanical Engineering, 81, No. 3, 63 (1959).

B. Chemical Engineering Progress in Press. 55, 51-8 Aug 1959

7 E. Gorin and H. L. Recht

Proceedings of the Tenth Annual Battery Conference, May, 1956.

Proceedings of the Twelfth Annual Battery Conference, May, 1958.

Quarterly Reports 1 - 17 to the
Signal Corps Engineering Laboratories
Fort Monmouth, New Jersey, 1954-1958

8 E. Gorin and H. L. Recht

U. S. Patent Application Pending.

9 H. Eyring, S. Glasstone and K. J. Laidler

Theory of Rate Process - McGraw-Hill, 1941.

10 V. Ipatieff and V. I. Tikhomirov

J. Gen. Chem. USSR 7, 736-9 (1931).

11 M. Armbruster

J. Am. Chem. Soc., 65, 1050 (1943).

12 A. G. Edwards

Brit. Jour. of Applied Physics, 8, 406 (1957).

13 C. J. Smithells and C. B. Ramsley

Proc. Roy. Soc. London A, 157, 292 (1936).

14 F. Johnson and P. LaRose

J. Am. Chem. Soc., 46, 1377 (1924).

15 Steacie and Johnson

Proc. Roy. Soc. A, 112, 542 (1926).

Table I

Summary Fuel Cell Performance Data

A. CONDITIONS OF RUNS

Run No.	Temp., °C	Fuel Electrode	Air Electrode	Fuel Gas Comp.	% CO_2 in Air
Ag-2a	700	"D" Porosity Porous Nickel	80 Mesh Silver Gauze	97% H_2-3% H_2O	16.6
Ag-2b	750	"	"	"	11.1
Ag-2c	800	"	"	"	18.2
Ag-12	750	"	"	"	11.1
Ag-13	800	Fe Powder on "D" Porosity Stainless Steel	"	"	11.1
N-6	700	"D" Porosity Porous Nickel	Lithiated Nickel Oxide	"	11.1
N-16	750	"D" Porosity Porous Nickel	Lithiated Nickel Oxide	"	11.1
Ag-7B	825	80 Mesh Silver Gauze	80 Mesh Silver Gauze	"	16.6
Ag-7C	825	"	"	2 CO - 1 CO_2	16.6

Table I

Summary Fuel Cell Performance Data

B. CURRENT DRAIN BEHAVIOR

Run No.	Current Density ma/cm²	Voltage		Specific Resist. ohm cm	
		Measured	Calc. Open Circuit	Measured	Calculated
Ag-2a	0	1.216	-	6.4	9.1
	30	0.918	1.191	↓	↓
	65	0.578	1.170	↓	↓
Ag-2b	0	1.250	-	5.2	5.3
	30	1.012	1.180	↓	↓
	65	0.781	1.128	↓	↓
	100	0.572	1.100	↓	↓
	127	0.426	1.076	↓	↓
Ag-2c	0	1.170	-	7.6	-
	65	0.625	1.191	↓	-
	100	0.418	1.160	↓	-
Ag-12	0	1.180	-	7.4	-
	35	.923	1.184	↓	-
	65	.680	1.145	↓	-
Ag-13	0	1.143	-	4.2	-
	32*	0.832	1.206	↓	-
Ag-7B	0	0.181	0.931	-	-
	10*	0.140		-	-
N-6	0	1.230	-	7.3	11.1
	30	0.872	1.212	↓	
	65	0.440	1.165	↓	
	100	0.030	1.138	↓	

* Actual experimental points.

Figure 1

Cell Performance at 750°C

Porous Nickel — Fuel Electrode
Silver — Air Electrode
H_2 — Fuel Gas

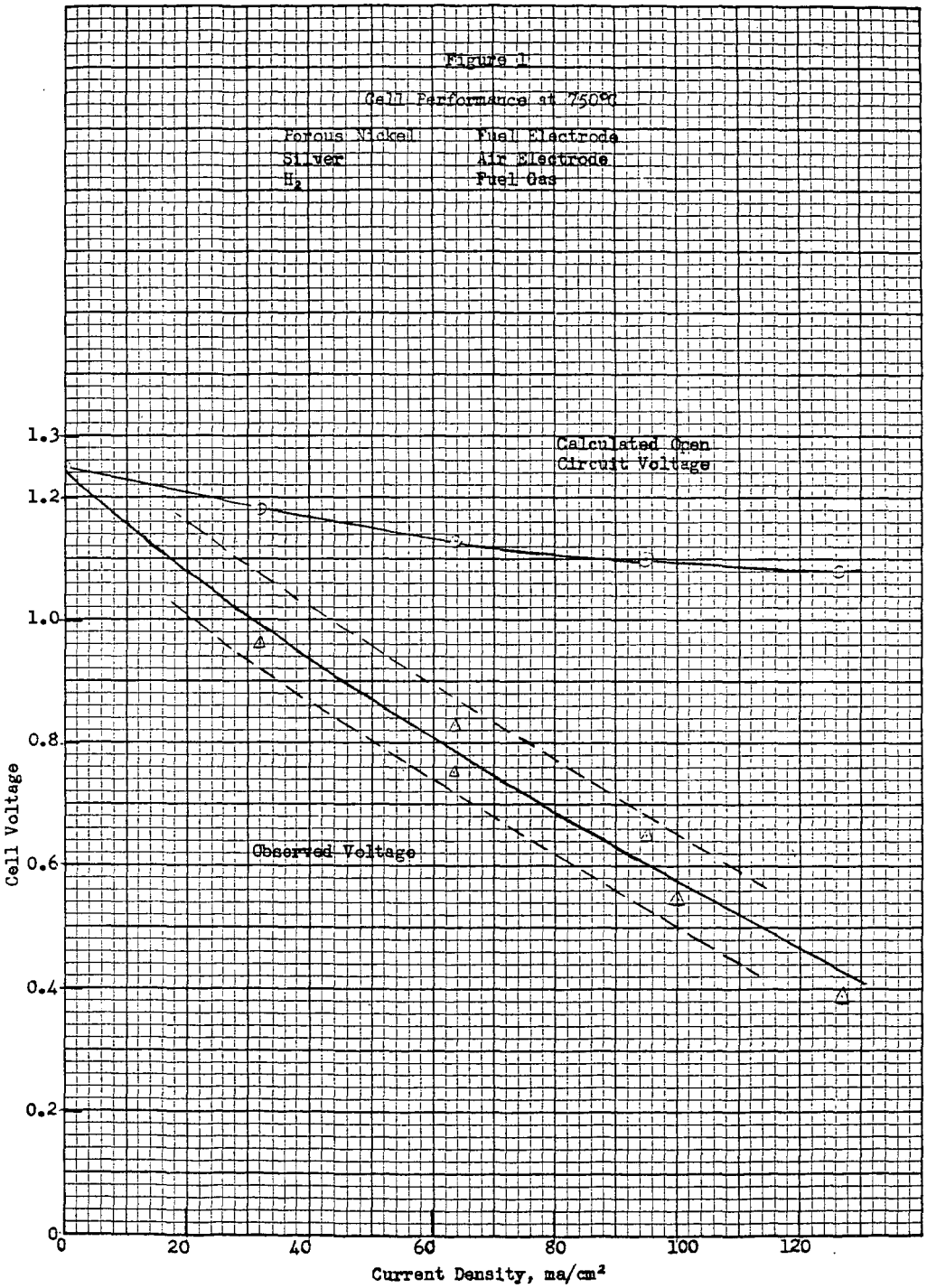

Figure 2

Cell Performance at 700°C

Porous Nickel — Fuel Electrode
Lithiated Nickel Oxide — Air Electrode
H_2 — Fuel Gas

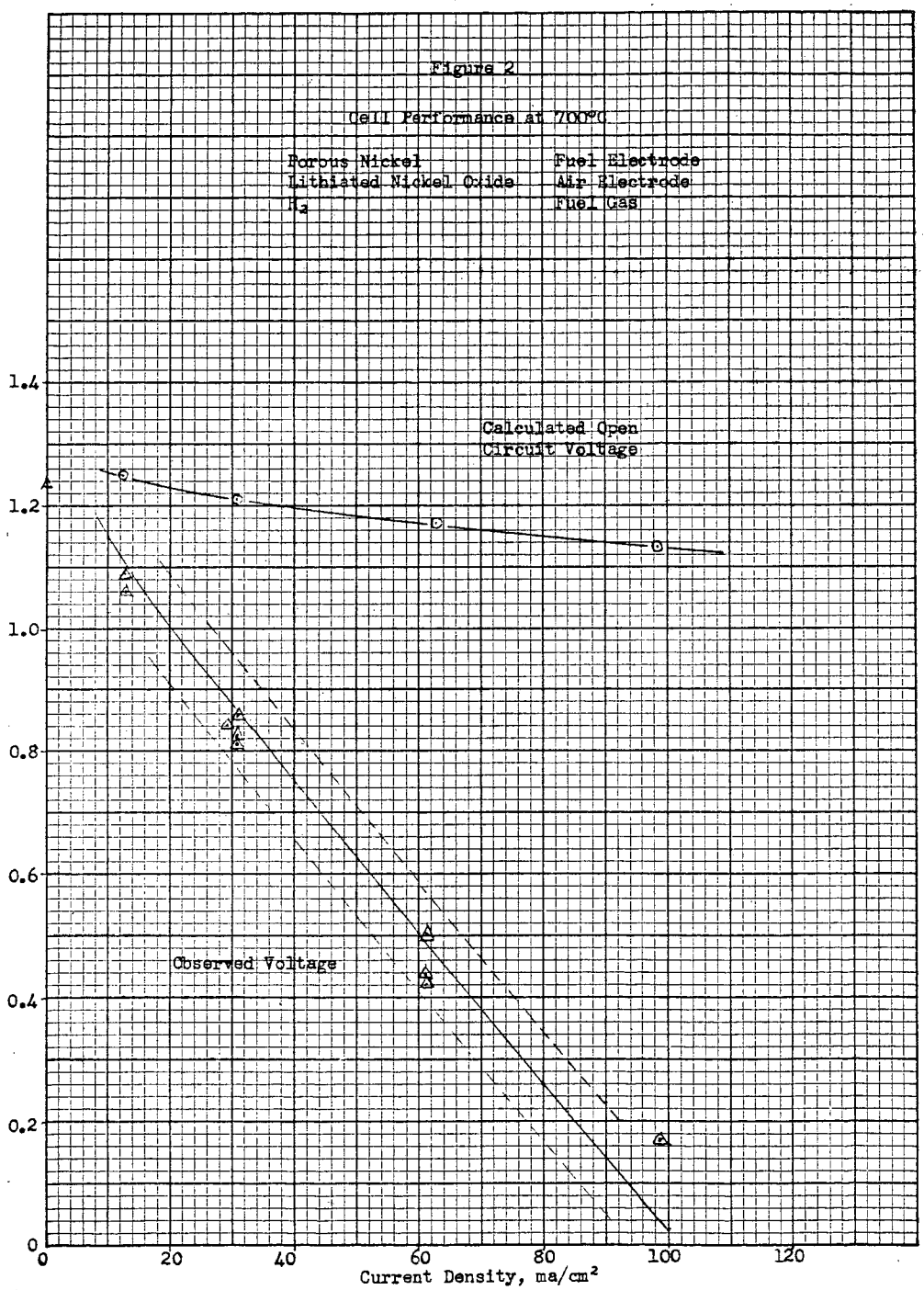

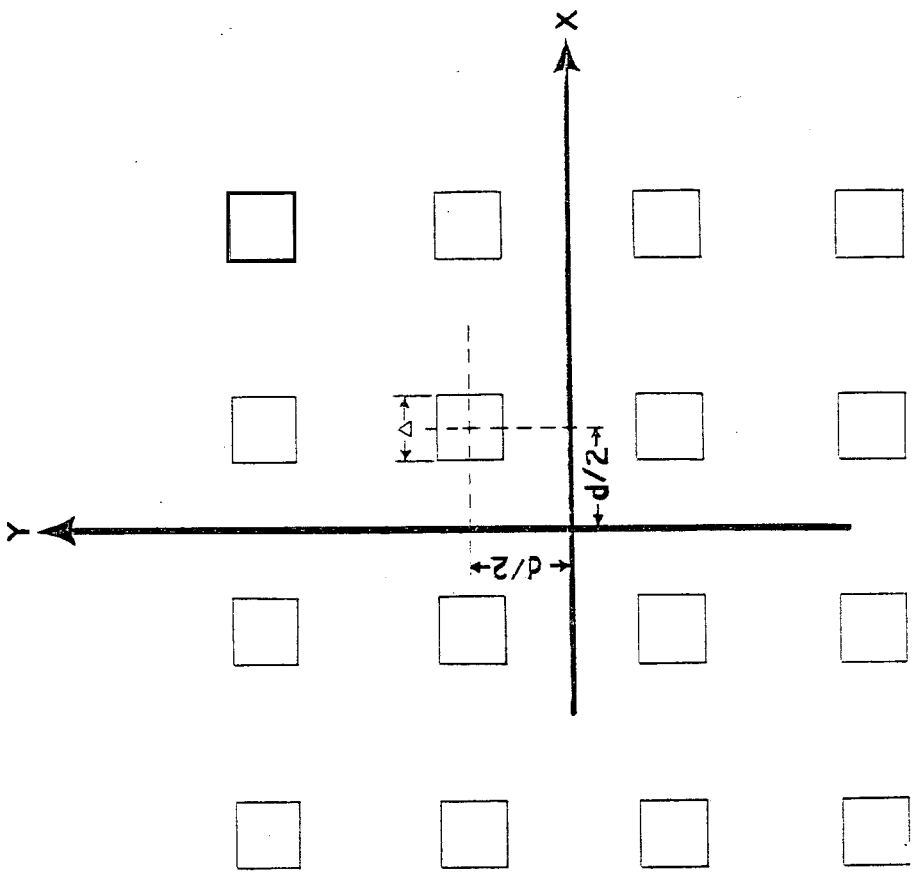

Figure 3

Diagram of Square Mesh Electrode

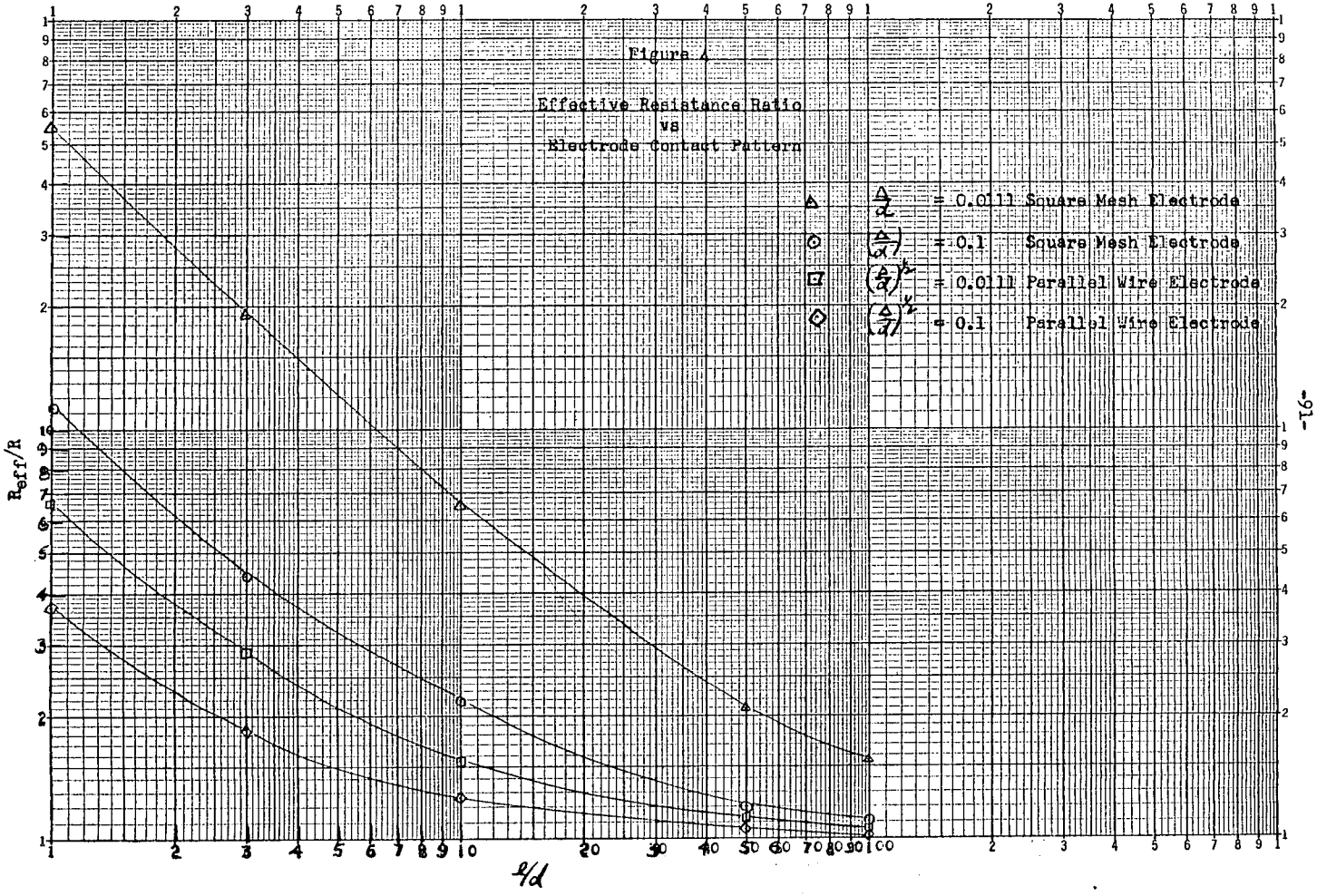
Figure 4
Effective Resistance Ratio
vs
Electrode Contact Pattern
Δ/d = 0.0111 Square Mesh Electrode
(Δ/d)' = 0.1 Square Mesh Electrode
(Δ/d)' = 0.0111 Parallel Wire Electrode
(Δ/d)' = 0.1 Parallel Wire Electrode
Reff/R
ℓ/d

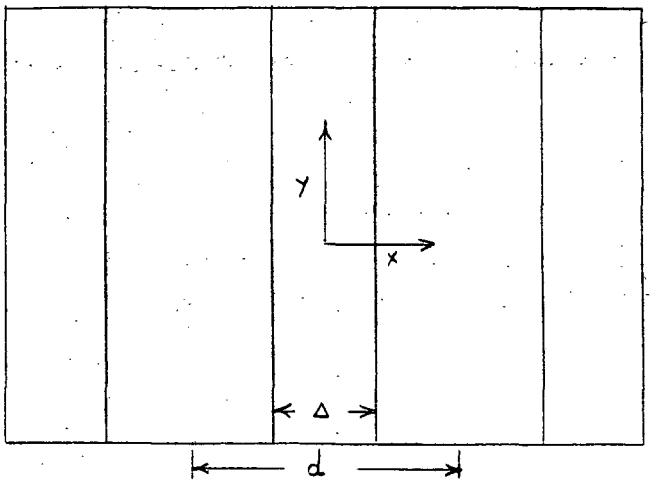

Figure 5. Diagram of Parallel Wire Type Electrode

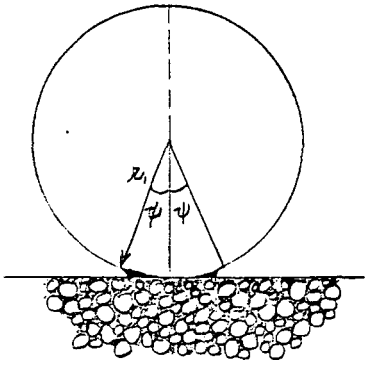

Figure 6. Diagram of Electrode Contact

Figure 7

Flux Factor For Spherical Electrode

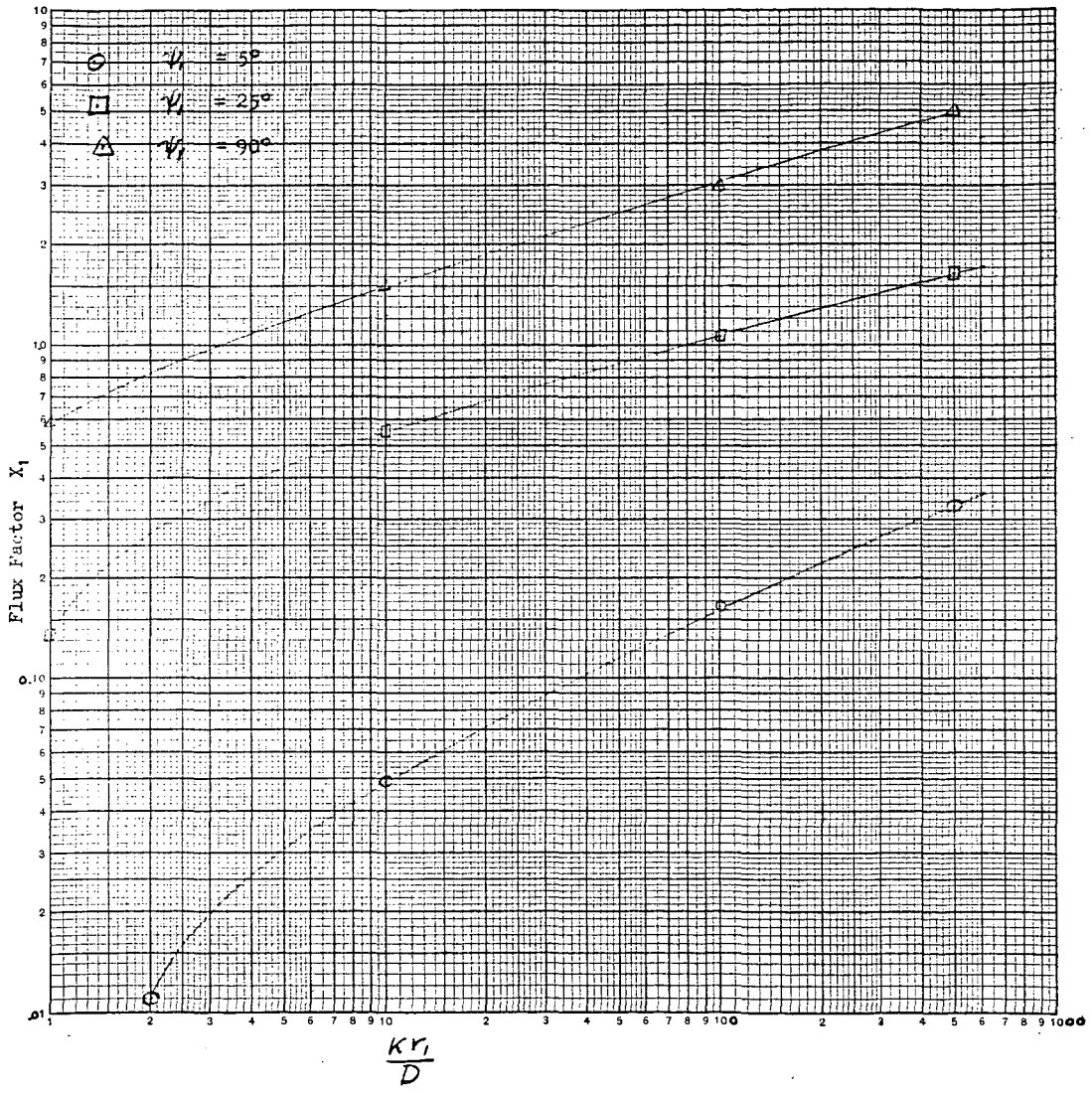

Figure 8

Polarization Due to Slow Formation
Through Spherical Hydrogen Electrode

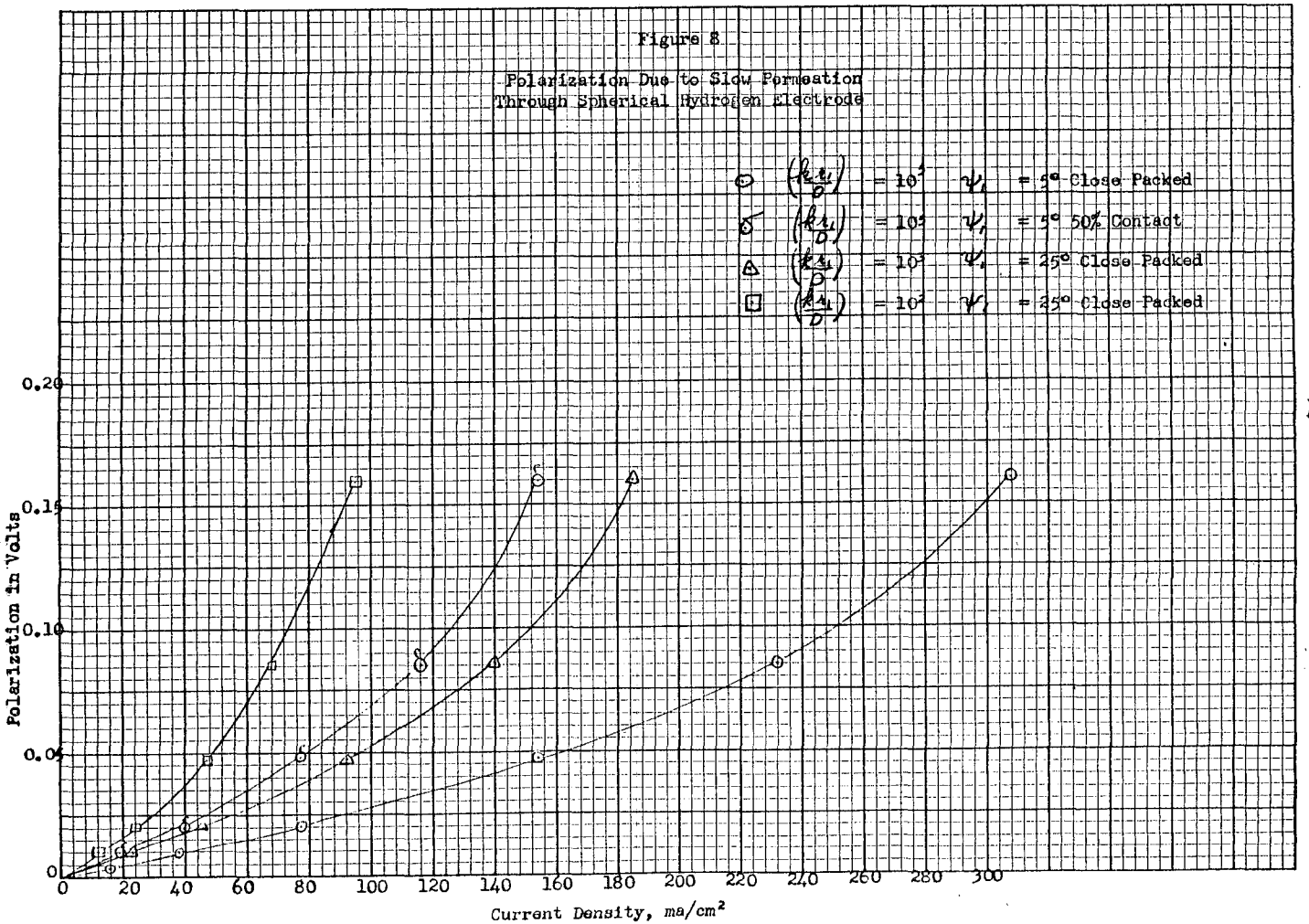

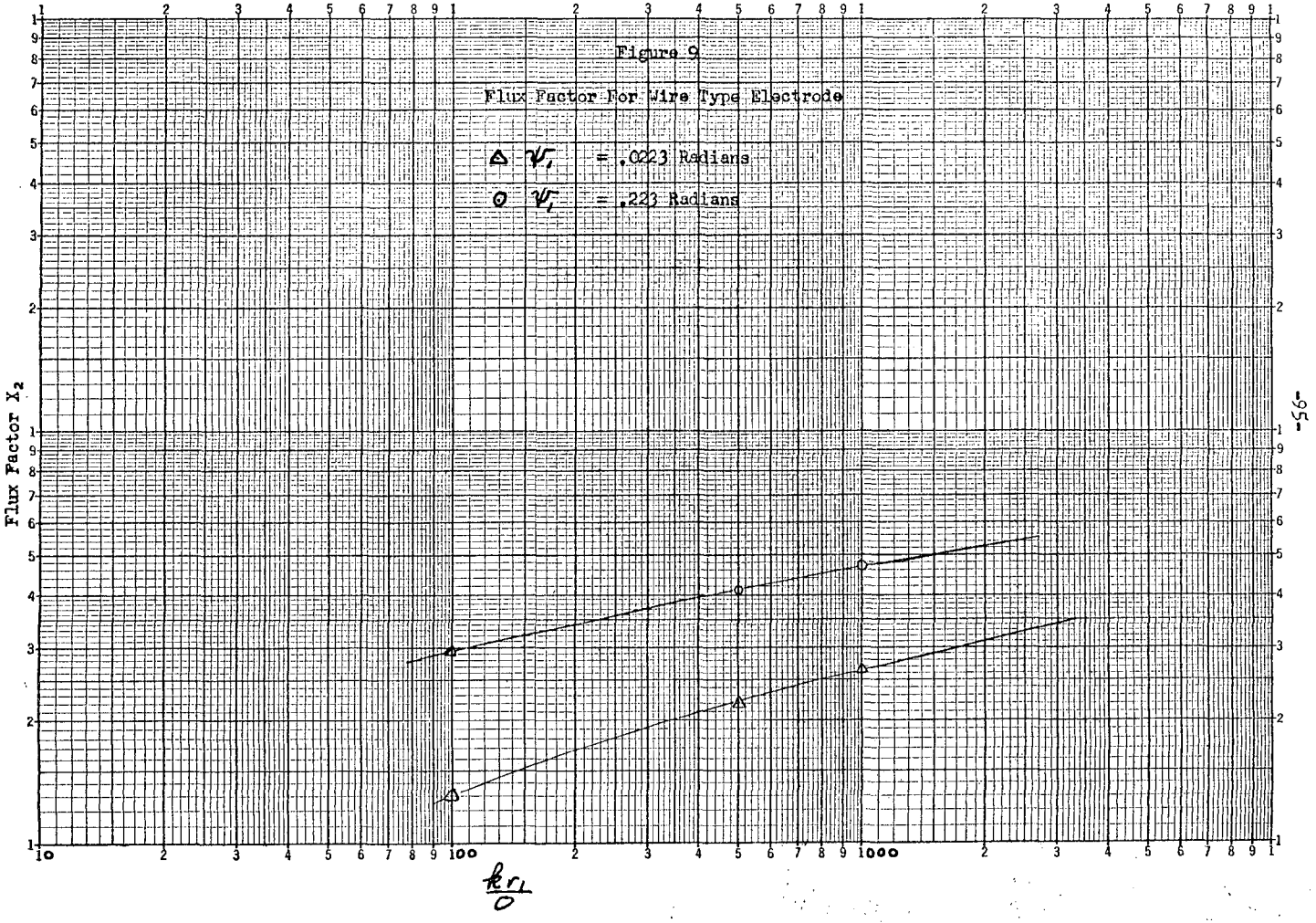
Figure 9
Flux Factor For Wire Type Electrode
Δ ψ₁ = .0223 Radians
○ ψ₁ = .223 Radians
Flux Factor X₂
kr₁/0
10
100
1000

MOLTEN ALKALI CARBONATE CELLS WITH GAS-DIFFUSION ELECTRODES*

by

David L. Douglas
Research Laboratory, General Electric Co.
Schenectady, New York

ABSTRACT

The application of gas-diffusion electrodes to high temperature fuel cells offers the possibility of obtaining the large current densities associated with such electrodes in low temperature cells. In addition the high internal resistance, electrolyte contamination and fragility encountered in the magnesia diaphragm cells are avoided. The problems which arise in connection with design and construction of gas-diffusion electrodes are control of pore size distribution and selection of materials.

An apparatus has been assembled to study the performance of small gas-diffusion electrodes immersed in a molten mixture of lithium, sodium and potassium carbonates. A reference electrode, consisting of a porous plug of gold sintered into a gold tube, permits study of the polarization characteristics of the individual electrodes. This is operated as an unloaded cathode (oxygen electrode). Gas-diffusion electrodes have been fabricated successfully using commercially available porous nickel and stainless steels and various sintered silver powders. Nickel shows very little polarization as a hydrogen electrode at temperatures above 500 C. Porous 431 stainless steel as a carbon monoxide electrode shows comparable polarization losses at 600 C. The data suggest that both the hydrogen and carbon monoxide electrodes suffer some activation polarization. In agreement with other workers we have found that silver makes an oxygen electrode showing negligible polarization above 600 C.

The cell assembly, although having large electrode separation, yields power densities at 600-650 C. comparable to those obtained from magnesia diaphragm cells operated at higher temperatures. It is anticipated that these will improve greatly when parallel close-spaced electrodes are used. No life tests have been carried out, but cells have been operated continuously for 100 hrs. Individual electrodes have operated without failure for several hundred hours. It appears that the operating life of electrodes will be limited by corrosion processes at the electrodes.

* Manuscript not received in time for preprinting.

Not for Publication
Presented Before the Division of Gas and Fuel Chemistry
American Chemical Society
Atlantic City, New Jersey, Meeting, September 13-18, 1959

Finding Commercial Uses for the Coal Acids

By

R. S. Montgomery

The Dow Chemical Company, Midland, Michigan

When we began our work on the mixed acids obtained by the caustic-oxygen oxidation of bituminous coal, our first concern was to find commercial applications for them. Just as with any other research chemical, the important question was, "What are they good for?". Basically, the coal acids are a complex mixture of polyfunctional aromatic acids with benzene, naphthalene, and biphenyl as the chief nuclei. (1) The average molecular weight is about 270 and the average equivalent weight about 81. Therefore, the average functionality is about 3.3. They are made by oxidizing a suspension of bituminous coal in aqueous sodium hydroxide by means of gaseous oxygen at a temperature of about 290°C. and a total pressure of about 1800 p.s.i.g. (2) In this paper, I plan to discuss our general plan of attack on the problem of finding out "What are they good for?".

INITIAL WORK

The most obvious line of attack and the one generally used at the outset in problems of this nature is to try to use the new chemical in applications where similar materials are now being used. A model compound of similar structure is selected and then one systematically attempts to substitute the new compound for this compound in all the areas where it is being used. The only polyfunctional aromatic acid of much commercial importance is phthalic acid and so it is natural to select this acid as our "model compound". This leads us to an investigation of the possible use of the coal acids in plasticizers, plating baths, synthetic lubricants, alkyd resins, and the like. We investigated these uses as did other investigators a good deal prior to us. (3)(4)(5) In general, however, this approach was not very profitable mainly because the coal acids are really not very similar to phthalic acid. In the first place they are a complex mixture rather than a single chemical species. In addition, they are water-soluble, rather dark colored, and have higher functionalities and molecular weights than does phthalic acid. Because of this, the coal acids appear to be inferior to phthalic acid in all the applications where phthalic acid is commercially used.

SEPARATION

The next logical line of attack on this problem is to attempt to separate the mixture into its components. If this is not feasible, perhaps the mixture could be fractionated into simpler mixtures or perhaps at least the dark colored components could be removed. Previous investigators had attempted to separate the mixture by distillation of the esters and by solvent fractionation. (6) We investigated these methods (7)(8) and also investigated a fractionation based on differences of acid strengths (8) and even partition chromatography. (9) None of these methods was suitable for the commercial separation of the components and only the fractionation based on the different acid strengths appeared to be of any commercial importance. With this method, a reasonable fractionation can be obtained as can be seen from Figure 1 but the fractions are still dark-colored and are still complex mixtures. The dark-colored components could not be removed although some of the fractions obtained by the distillation of the esters, chromatography, and solvent fractionation were lighter in color

than others. Treatment of the mixture with hydrogen, hydrogen peroxide (10), carbon, and sodium hypochlorite were all quite ineffective although the hypochlorite treatment did give some improvement.

THERMOSETTING RESINS

After the only very limited success of these two lines of attack, some new point of view was required so we then began to look at the coal acids as a basically new and different chemical and began to try to exploit its unique properties. The properties that seemed the most important were the high functionality, aromatic character, and perhaps the water solubility. Although many applications were investigated from this point of view, I will discuss only the ones that appeared to be of the most interest.

The high functionality of the coal acids suggested that they might be useful in a highly crosslinked, thermosetting resin. Their aromatic character led us to believe that they could also contribute good heat stability and good resistance to oxygen attack. Therefore, we felt that we could, perhaps, make good, relatively heat-resistant binder resins from them and we began to look for applications requiring resins of this kind. In addition, the fact that the acids were water-soluble allowed the uncured mixture or the partially cured resin to be applied directly from a water solution. This lead us to investigate these coal acid resins as foundry binders, plywood and hardboard binders, glass fiber binders, etc. Two of the following papers will be concerned with these applications so I will not go into them any further.

WARP SIZE

Another unique property of the coal acids is their ability to form films. An aqueous solution will dry to a rather tough, pale-yellow film. This behavior is unusual for a material of molecular weight on the order of 270. The viscosity behavior of a concentrated aqueous solution, however, provides an insight into the reason for this property. From Figure 2 it can be seen that the coal acids in dilute solution behave as individual monomeric units of about 270 molecular weight but as the solution becomes more concentrated, the viscosity increases more rapidly than can be accounted for by just the increased concentration. The molecular weight increases as the concentration increases until at very high concentrations we have, in effect, a high polymer. This is probably due to the formation of hydrogen bonds as the monomeric units are brought closer and closer to each other when the solution becomes more concentrated and can be considered as actually a kind of reversible polymerization. Perhaps then, the coal acids could be used in applications where water-soluble polymers are used. We investigated several of these applications and the most promising appeared to be textile warp sizing. This specific application will be discussed in a following paper so I will not say much about it but I would like to emphasize the fact that this use is based on the unique physical behavior of the coal acids and would not be expected on a basis of the physical properties of other known aromatic acids.

SLURRY THINNING

Another application based on the unusual water solubility of the coal acids is that of slurry thinning. It was already known that the sodium salts of the coal acids were useful as slurry thinners for weighted drilling muds. (11) Normally only the salts of large molecular weight organic acids have the required solubility for this application but in this case the acids themselves can be used. The coal acids themselves have shown a much wider applicability than did their sodium salts. For instance, the coal acids are useful for thinning ordinary drilling mud as well as weighted drilling mud. Figure 3 shows the viscosity of bentonite drilling mud as a

function of the amounts of both the coal acids and their sodium salts. This again is an example of a use based on the unique properties of the coal acids.

CONCLUSIONS

In conclusion, I would like to re-emphasize the fact that very often, as in this case, the more conventional ways of investigating the utility of a new material may be unproductive but a fresh point of view may provide us with an important new use based on one or more unique properties of the material. In the case of the coal acids, their use in thermosetting resins, as water-soluble film formers, and as slurry thinners are all based on unique properties and would not be predicted on a basis of the properties of other aromatic acids.

LITERATURE CITED

(1) Montgomery, R. S., Holly, E. D., and Gohlke, R. S., FUEL, Lond., 35, 60 (1956)

Montgomery, R. S., and Holly, E. D., ibid, 36, 63 (1957)

(2) Franke, N. W., Kiebler, M. W., Ruof, C. H., Savich, T. R., and Howard, H. C., Ind. Eng. Chem., 44, 2784 (1952)

(3) Montgomery, C. W., Gilbert, W. I., and Kline, R. E., U. S. Patent 2,516,640 (1950)

Montgomery, C. W., Gilbert, W. I., and Kline, R. E., U. S. Patent 2,568,965 (1951)

(4) Berman, N. and Howard, H. C., Anal. Chem., 21, 1200 (1949)

(5) Franke, N. W., and Kiebler, M. W., Chem. Inds., 58, 580 (1946)

(6) Ruof, C. H., Savich, T. R., and Howard, H. C., J. Am. Chem. Soc., 73, 3873 (1951)

(7) Holly, E. D., Montgomery, R. S., and Gohlke, R. S., FUEL, Lond., 35, 56 (1956)

(8) Montgomery, R. S., and Sienknecht, P. J., Ind. Eng. Chem., 47, 1274 (1955)

(9) Holly, E. D., and Montgomery, R. S., FUEL, Lond., 35, 49 (1956)

(10) Montgomery, R. S., and Bozer, K. B., ibid, in press.

(11) Salathiel, R. A., U. S. Patent 2,545,169 (1949)

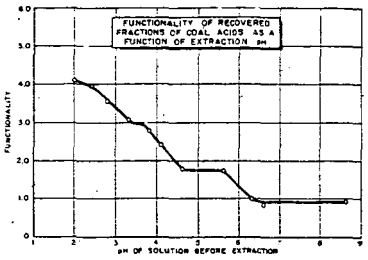
FUNCTIONALITY OF RECOVERED FRACTIONS OF COAL ACIDS AS A FUNCTION OF EXTRACTION pH
FUNCTIONALITY
pH OF SOLUTION BEFORE EXTRACTION

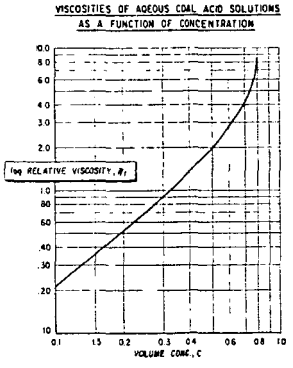
VISCOSITIES OF AQEOUS COAL ACID SOLUTIONS AS A FUNCTION OF CONCENTRATION
log RELATIVE VISCOSITY, η_r
VOLUME CONC., C

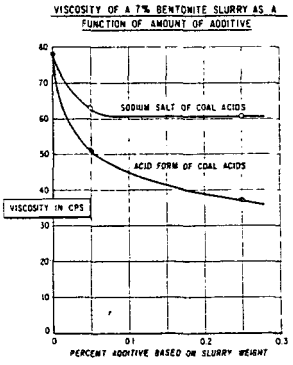
VISCOSITY OF A 7% BENTONITE SLURRY AS A FUNCTION OF AMOUNT OF ADDITIVE
SODIUM SALT OF COAL ACIDS
ACID FORM OF COAL ACIDS
VISCOSITY IN CPS
PERCENT ADDITIVE BASED ON SLURRY WEIGHT

Not For Publication
Presented Before the Division of Gas and Fuel Chemistry
American Chemical Society
Atlantic City, New Jersey, Meeting, September 13-18, 1959

Coal Acids -- A Potential Warp Size for Continuous Multifilament Yarns

By

Keith B. Bozer, Wesley L. Archer, and Robert S. Montgomery
The Dow Chemical Company - Midland, Michigan

Aqueous solutions of the mixture of water soluble aromatic polycarboxylic acids[1] produced by the caustic oxygen oxidation of coal will dry to form a rather tough water soluble film. One possible market for such a material is as a warp size in the textile industry. In this paper we would like to summarize the results of our evaluation of the coal acids for this use.

A warp size can probably best be described as a water soluble coating applied to the warp yarns to increase loom efficiency during weaving. The size is applied to the yarns from an aqueous solution and must be sufficiently water soluble so that it can be completely removed by a dilute detergent solution. In addition, the size must have good adhesion to the yarn and be sufficiently pliable to protect the warp yarns from the flexing, abrasion, and other stresses of the weaving operation.

Just as the above definition implies, the only absolute method for evaluating sizes is to conduct rather extensive weaving trials. However the cost of such a test necessitates some type of preliminary testing to establish a high probability of success. Potential sizes can be evaluated in the laboratory if one simplifies the problem somewhat and looks at the desirable physical properties which are either afforded or enhanced by the presence of a suitable size on the yarn. In the case of a continuous multifilament yarn these properties would include unitization of the yarn and abrasion resistance. It is also necessary to determine if the size has any degradative effects on the yarns physical properties in addition to establishing the ease of application and removal of the size. By comparing the effects of an experimental material and a commercially accepted size it is possible to get an indication of the probability that the experimental material may have for success in a weaving trial.

The coal acids were first evaluated on continuous multifilament nylon yarn. There were two principal reasons for choosing this yarn. First, it is well known that materials having a low pH give the best adhesion to nylon fibers and second, the low viscosity of the size solution suggested that the size might not "lay" the protruding fibrils of a staple yarn in the desired manner. In this evaluation the widely accepted polyacrylic acid size (Acrysol A-1) manufactured by Rohm and Haas was chosen as the control with which the coal acids were compared.

Ease of Application and Removal

Observations made during the preparation of sized samples for testing using the single-end slasher shown in Figure 1 indicated that there would be no problems in applying the coal acid coating to the yarn. While the use of a colored material as a warp size could possibly have certain advantages it has the one major disadvantage in that it must be completely removed from the woven fabric.

Two general methods were used to determine whether the coal acids could be satisfactorily removed from the yarn. The first of these methods was based on the acidic nature of the size. Sized samples of yarn were rinsed with a stream of water for about ten minutes and then after drying were titrated with dilute base to determine the amount of residual acid. The results of this test indicated that the amount of coal acids left on the yarn was below 0.05% size pick-up. A more accurate method was worked out based on the color of the coal acids. In this method samples of the sized yarn which had been washed in an aqueous solution of 0.25% Triton X-100 and 0.25% tetrasodiumpyrophosphate were wound on plastic chips and the color of the yarn determined on a Hunter Color and Color Difference Meter (H. A. Gardener Laboratories, Bethesda, Md.). Samples of yarn sized with Acrysol A-1 and unsized yarn were tested in a similar manner. The results of this evaluation are shown in Table I.

TABLE I

HUNTER COLOR AND COLOR DIFFERENCE METER DATA

Sample	R_d	a	b
Porcelain Standard	77.0	-0.2	+1.8
Unsized Yarn	52.8	-3.0	+3.0
Washed Yarn (Acrysol A-1)	54.9	-2.7	+3.8
Washed Yarn (Coal Acids)	52.6	-3.0	+3.1
Washed Yarn (Coal Acids)	53.3	-3.0	+3.2

KEY: The R_d column indicates the per cent reflectance. The negative numbers in the 'a' column indicate the degree of blueness and the positive numbers in the 'b' column indicate the degree of yellowness.

Although it was impossible to exactly duplicate commercial methods of scouring or size removal, the data in Table I indicates that the coal acids can be completely removed from the yarn.

Yarn Degradation Studies

In certain cases it may be necessary to store a sized warp for prolonged periods of time. Therefore, it is essential that the size have no adverse effects on the physical properties of the yarn. The tensile strength and per cent elongation of nylon yarn which had been aged after being sized with Acrysol A-1 and coal acids were determined and found to be comparable.

Abrasion Tests

The most widely accepted method of laboratory evaluation of experimental sizing materials is that of determining the abrasion resistance of the sized yarn. However, the type of abrader and test may vary considerably with the investigator and the type of yarn used [2]. The method which we employed in evaluating the coal acids, and which appears to work quite well on continuous multifilament yarns, is based on the Duplan Cohesion Tester (Geier and Bluhm Inc., Troy, N. Y.). See Figure 2. The purpose of a warp size is to reduce the number of breaks in the warp yarns during weaving but this yarn break point is not necessarily a good end point on an abrasion tester. This is particularly true with continuous multifilament yarn where the yarn itself may not break from abrasion alone for several thousand cycles while a good size may well be completely destroyed after 50 cycles. For this reason the "fray-point" was chosen as the end point on the Duplan Cohesion Tester because it clearly shows the point at which the size film is destroyed. The use of this end-point, which is shown in Figure 3,

enables one to measure the degree of unity and abrasion resistance imparted to the yarn by the size. By testing samples of yarn having varying percentages of size pick-up we were able to compare the properties of the commercial and the coal acid sizes. The results of this evaluation are shown in Figure 4. The data shown in Figure 4 indicates that the coal acids and Acrysol A-1 afford a comparable amount of protection to the yarn.

The results of the above tests indicate that the coal acids might be a good warp size for nylon multifilament yarns and suggests further testing in the form of a weaving trial.

Other Types of Yarn

On the basis of the favorable results obtained on nylon, the coal acids were also evaluated on other types of continuous multifilament yarn. In each case a commercial size was used as a control. Evaluations were carried out on Dacron, Orlon and cellulosic type yarns and in general the results obtained were very similar to those obtained on nylon. The results of the abrasion resistance studies on these yarns are shown in Figures 5, 6, and 7. These results indicate that perhaps the coal acids might find rather wide application as a warp size for continuous multifilament yarns.

Weaving Trials

After a small scale weaving trial was conducted successfully on equipment located in the Midland Division a larger and more thorough trial was carried out at North Carolina State, School of Textiles, Raleigh, N. C. In evaluating the coal acids in these weaving trials every attempt was made to handle the experimental material in the same manner as it would be handled commercially. These weaving trials were carried out on continuous multifilament nylon yarn and here again the evaluation was conducted in such a manner that the coal acids could be compared directly with the Acrysol A-1 size.

In general the results of the weaving trial followed very closely those of the laboratory evaluation. It was noted during the sizing operation that the coal acid sized warp parted much easier and subjected the yarn to much less strain than did the commercial size. While the length of the weaving trials was not sufficient to calculate with certainty the efficiency of the sizes there were fewer yarn breaks attributable to 'size failure' in the coal acid warp than there were in the Acrysol warp.

It was in the last stages of the weaving trial, that is the scouring step, that the only serious problem was encountered. During this step the sized fabric was accidentally exposed to live steam before the scouring was started. It was found that temperatures in this range were sufficient to "set" the coal acids or actually cause chemical combination with the yarn which prevented the complete removal of the color from the fabric. Further testing in the laboratory indicated that temperatures of 180°F. or greater would cause varying degrees of discoloration in direct proportion to the time the temperature was maintained. It is not uncommon for slasher drying can temperatures to be maintained in this range but the coal acids have the advantage that their high fluidity will allow drying at lower temperatures (<160°F.) while maintaining normal slasher speeds. The discoloration would probably also be lessened when the coal acids are used on another fiber where the ionic association of the reactive groups in the fiber and size are not so great.

Summary

The coal acids form water soluble films which may be useful as warp sizes for continuous multifilament yarns. The films appear to impart as much or more abrasion resistance to a wide range of multifilament yarns as commercially accepted sizes. The only apparent problem is the tendency of the coal acids to react with, and thereby discolor the yarn at elevated temperatures.

References

(1) Franke, N. W., Kiebler, M. W., Rouf, C. H., Sovich, T. F., and Howard, H. C., Ind. Eng. Chem., 44, 2784-2792 (1952).

(2) Seydel, Paul V., Textile Industries, Vol. 121, No. 3, 110-119 (1957)

lbv

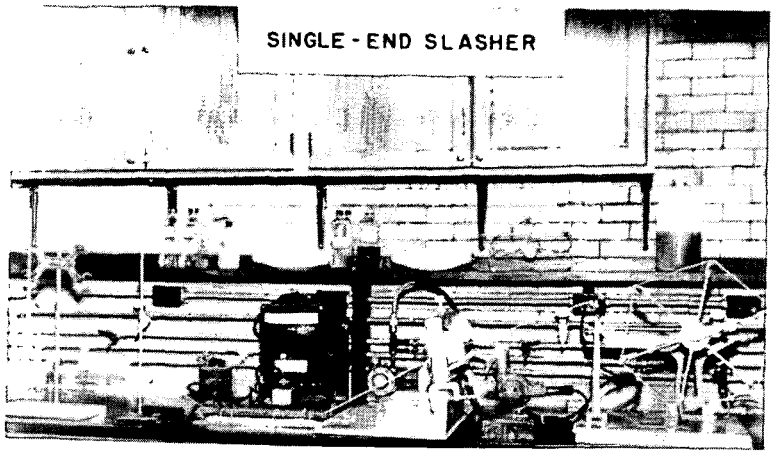

CONE → TENSION POST → SIZE BATH → WRINGER → DRYER → YARN REEL

FIGURE 1

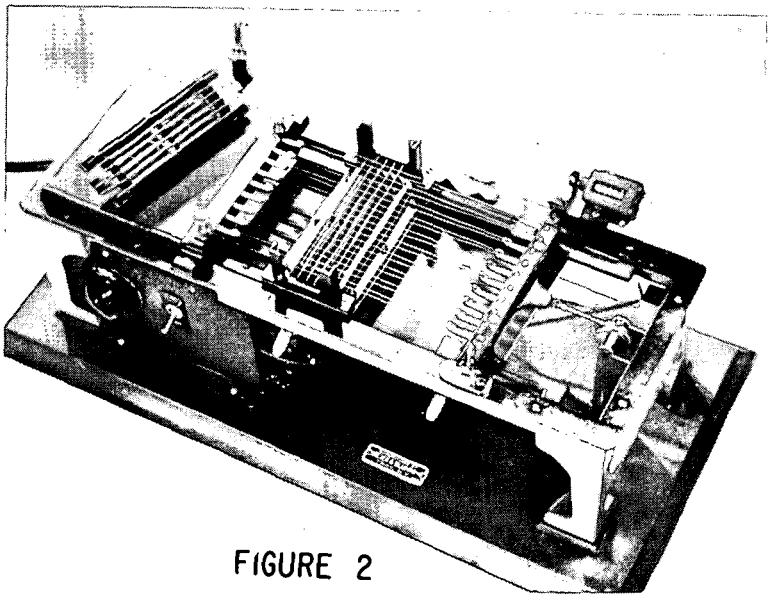

FIGURE 2

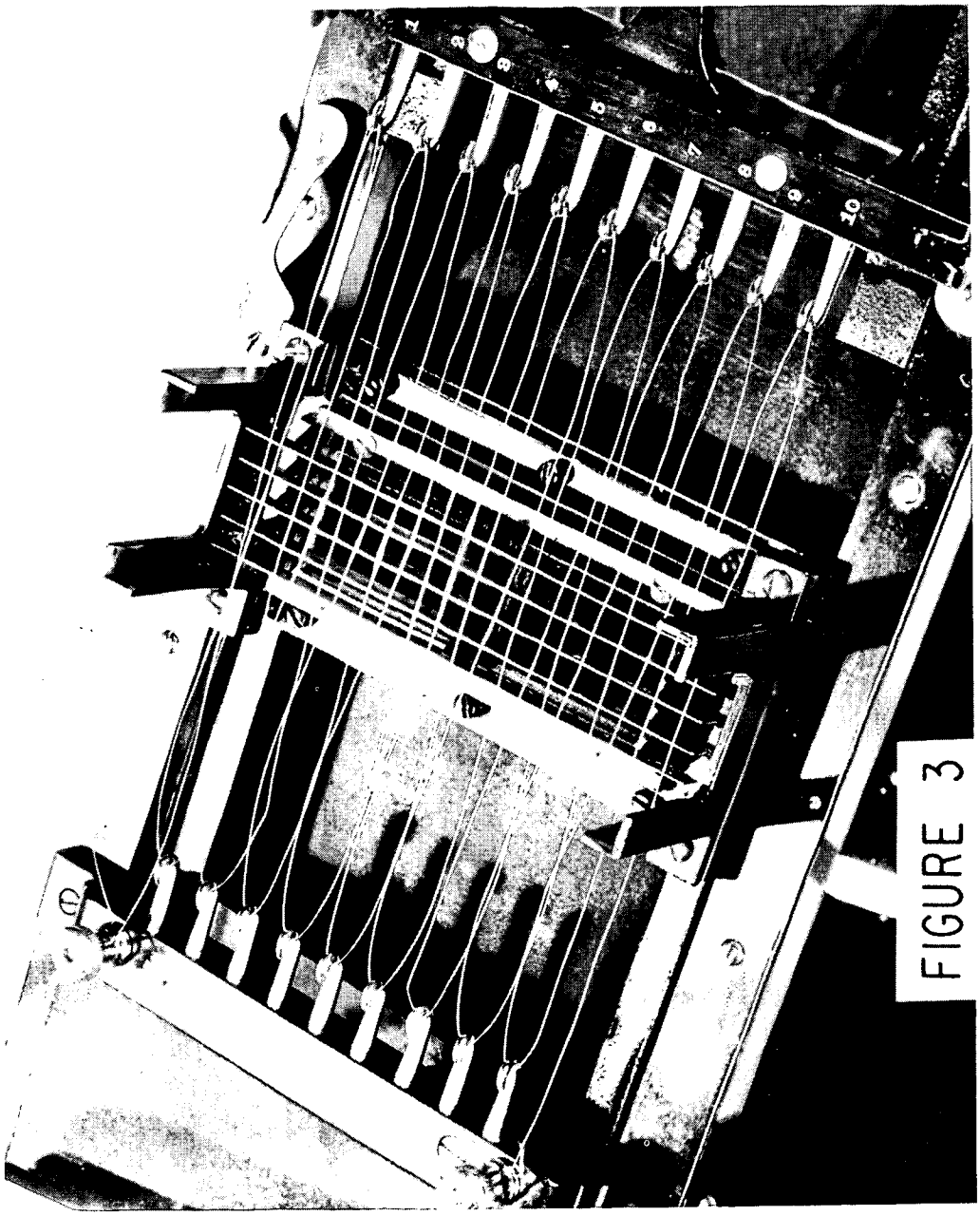

FIGURE 3

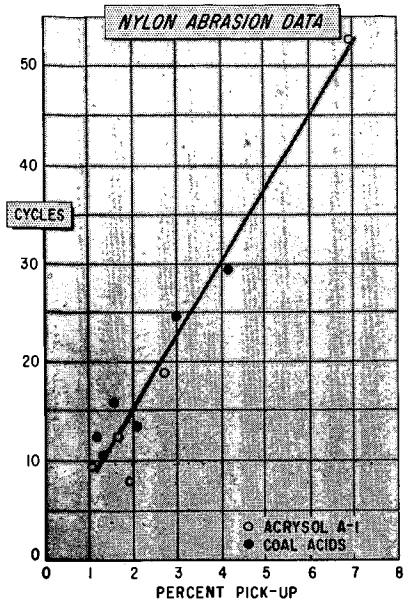

FIGURE 4

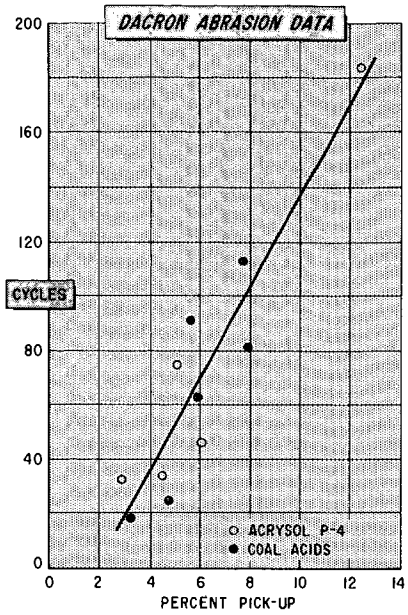

FIGURE 5

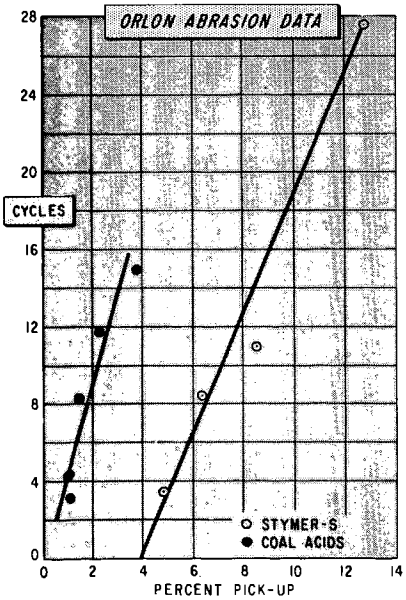

FIGURE 6

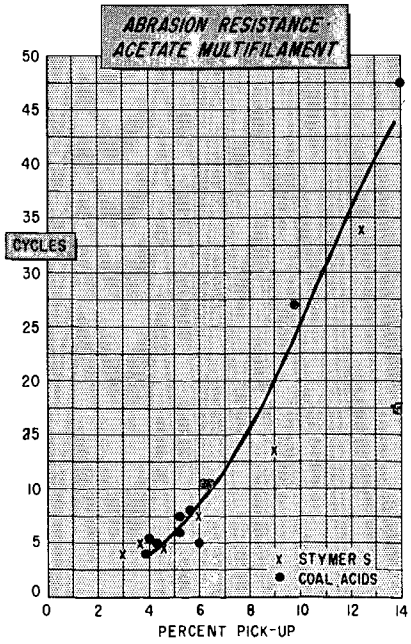

FIGURE 7

Not For Publication
Presented Before the Division of Gas and Fuel Chemistry
American Chemical Society
Atlantic City, New Jersey, Meeting, September 13-18, 1959

Coal Acids - An Intermediate For Thermosetting Resins

By
Wesley L. Archer, Keith B. Bozer and Robert S. Montgomery
The Dow Chemical Company - Midland, Michigan

INTRODUCTION:

Gaseous oxygen oxidation of an alkaline slurry of bituminous coal yields a mixture of water soluble aromatic polycarboxylic acids (1). These coal acids have been shown to have three principle aromatic ring systems, namely benzene, naphthalene and diphenyl (2). The mixture is strongly acidic and has an average functionality of approximately three.

The coal acids afford an interesting and relatively inexpensive raw material. One specific use of these acids is in the preparation of thermosetting resins. The large markets for resins of this type provided an interesting field of investigation and efforts to develop these resins are outlined in this paper.

Coal acids can be reacted with an alkanolamine, alkylene oxide, polyhydroxyl compound or polyamine to give thermosetting resins. Variation of reactants, the equivalents used or the reaction conditions allows a wide spectrum of resins with varying properties. The polyamide, polyester or combination of functional groups possible in these resins are shown in examples 1-5. In examples 1, 2 or 3 an equivalent of hydroxyl or amine reactant

(1) $R(COOH)_3 + HN(CH_2CH_2OH)_2 \longrightarrow R(COOCH_2\text{-})_2\ (CONCH_2\text{-})$

(2) $R(COOH)_3 + HOCH_2CH_2OH \longrightarrow R(COOCH_2\text{-})_3$

(3) $R(COOH)_3 + H_2N(CH_2)_nNH_2 \longrightarrow R(CONCH_2\text{-})_3$

(4) 1 eq. $R(COOH)_3$ + 1 mole $NH(CH_2CH_2OH)_2 \longrightarrow R\left[CON(CH_2CH_2OH)_2\right]_3$

(5) $R(COOH)_2 + CH_2CH_2O \longrightarrow R(COOH)(COOCH_2CH_2OH)$

is used for each carboxylic acid equivalent, while in example 4 one mole of diethanolamine is used per equivalent of acid group. The latter resin will have free hydroxyl groups which could then be crosslinked. Use of a large excess of a glycol reactant with the coal acids also yields a resin with free hydroxyl groups. The preparation of a partially reacted ester with free carboxylic acid and hydroxyl groups is shown in example 5. The resultant water soluble resin intermediate gives a crosslinked structure when cured at elevated temperatures.

A. Preparation and Chemistry of the Resins

Alkanolamine, Polyhydroxyl and Polyamine Resins

The mixture of aromatic polycarboxylic acids (coal acids) obtained from the Coal Research Laboratory of the Carnegie Institute of Technology in Pittsburgh was used in the preparation of some of the resins. The average molecular and equivalent weights are 270 and 82 respectively giving an average carboxylic acid functionality of 3.3. Many of the later resins were prepared from coal acids made at the Dow Chemical Company. These coal acids were shown by equivalent and molecular weight determinations to be similar to the material obtained from the Carnegie Institute of Technology.

A novel and useful feature of these resins is that a mere physical mixture of the coal acids and other reactant in water may be applied directly to the substrate to be bonded. This method of application eliminates the hazard and expense of

organic solvents in commercial applications. The resin adduct in a concentration range of 50-80% solids gives a water solution of workable viscosity and good film forming properties.

A partially cured but still water soluble coal acid resin was prepared from the coal acids and monoethanolamine by heating equivalent amounts of the reactants at 170°C. for 3 hours. Approximately 85% of the water of esterification slowly distilled off giving on cooling a water soluble solid. Titration of this material revealed the presence of nearly all the original amine salt groups. Use of a di or trialkanolamine however yields water insoluble products because of excessive crosslinking of the hydroxyl group.

Another partially cured, but still water soluble resin can be prepared from the coal acids and pentaerythritol. A suspension of an equivalent of pentaerythritol in a 70% solids solution of one equivalent of coal acids in water was stirred and heated at reflux for 3 hours. The resultant solution on titration showed 27% esterification of the pentaerythritol, while after 24 hours of reflux the esterification approaches an equilibrium value of 40%. The partially advanced resin is a viscous solution which does not exhibit any precipitation on standing for prolonged periods.

Alkylene Oxide Derived Resins

Ethylene, propylene and butylene oxide have been reacted with the coal acids in a dioxane media to produce partially reacted esters containing carboxylic acid and hydroxyl groups. These products, which are water soluble in concentrated solutions, can be cured to give a thermosetting resin. The resin of primary interest involves the reaction of one mole of ethylene oxide with two equivalents of coal acids as shown in example 5.

The alkylene oxide addition is generally allowed to proceed until one half of the carboxylic acid groups have reacted giving a resin intermediate which on final cure has no reactive groups. Wide deviation from the 50-50 acid hydroxyl group ratio may give a thermoplastic resin on final cure.

Ethylene oxide adducts with equivalent weights in the range of 162 to 328 have been prepared as have propylene oxide adducts with equivalent weights of 170-440. Reaction with butylene oxide is slower and required the addition of a small amount of sulfuric acid and additional heating at 60°C. to give an adduct with an equivalent weight of 223.

Resin Compatibility with Phenol - Formaldehyde Resins

Preliminary work has shown that various coal acid resin adducts are compatible with the "A or B stage" water borne phenol - formaldehyde resins. However the amine salt character of the alkanolamine or polyamine - coal acid resins limit their compatibility with alcohol borne phenol - formaldehyde resins.

Laboratory investigation has indicated that an actual reaction can occur between the coal acids and the phenol - formaldehyde resin.

Various amounts of coal acids were mixed with both "A" and "B" stage phenol - formaldehyde resins and the mixtures cured. The cured resin mixtures were then titrated in order to determine the amounts of the coal acids that had been incorporated into the cured resin structure. It was found that the "A stage" resin could combine with approximately 43% of its weight of coal acids but the "B stage" resin only 7% of its weight. This can be explained by the fact that the "A stage" resin contains a much larger proportion of free methylol groups than does the "B stage" resin.

B. Reaction Rate Studies

Reaction rate studies of the alkanolamine - coal acid resin adducts have afforded information concerning the relative rates of ester formation as compared with amide - imide formation. The usual methods for kinetic studies are useless in this case because of the highly crosslinked and insoluble nature of the coal acid resins. The most satisfactory solution to the problem was to cure weighed samples of the resin adduct on squares of aluminum foil which were floated on the surface of a Wood's metal bath controlled at a fixed temperature. The resin samples were prepared from a mixture of 1:1 equivalent of alkanolamine - coal acids containing 10% water. The sample after cure was digested in a methanol - water solution and titrated with 1N sodium hydroxide. A plot of pH vs. milliequivalents of alkali revealed two points of inflections, one occurring at approximately pH7 and indicating free carboxylic acid group and the second inflection point at pH 9.5-10.5 which corresponded to the amine salt component.

Samples were run for various time intervals and the milliequivalents of unreacted carboxylic acid groups and/or amine salt groups plotted vs. the cure time in minutes. The semilogarithmic plot approximated a straight line suggesting a first order reaction. This behavior is reasonable, since both reactants are combined into one molecular species by means of the amine salt formation.

A typical plot of an alkanolamine - coal acids reaction is shown in Figure 1. In this case samples of a 1:1 equivalents formulation of the diethanolamine - coal acid resin were cured at 265°C. Line A shows the disappearance of the combined free carboxylic acid and amine salt groups, line B the esterification rate while line C is the rate of formation of the amide or imide. The reaction rate constants and half lives of the mono, di and triethanolamine - coal acid resin reactions are shown in Table I. The slower rates exhibited by the di and triethanolamine resins are probably due to steric hinderance. Use of an acidic catalyst gave the expected reaction rate increase.

Cure rates of the diethanolamine - coal acid resin were determined for temperatures in the range of 240-300°C. to give the Arrhenius plot shown in Figure 2. The slope of the plot is only slight in this temperature range while determinations at 150 and 210°C. gave rate constants far below this range. These lower rate constants may be partially due to a lower heating efficiency of the experimental setup at these temperatures or perhaps indicate a reaction rate threshold effect.

Preliminary work has shown that reaction rates of the coal acid - glycol resins can also be determined provided a lower temperature, e.g. 150°C., is used in order to reduce the evaporation losses of the glycol. Figure 3 is a plot of the reciprocal of the square of the carboxylic acid concentration vs. time as obtained with a coal acid - diethylene glycol resin system. Since the reactants have the same initial concentration, the resultant straight line plot indicates a third order reaction. This is in accord with the mechanism of an acid catalyzed esterification. The catalyzing acid in this reaction is the coal acids because of the strong acidic nature.

A rate study of the coal acid - pentaerythritol resin adduct has proven interesting since the results indicate a first order reaction similar to the alkanolamine resins. The reactants were heated in water to give a partially esterified resin which on titration showed 18% advancement. Samples of the 75% solution were then cured in the normal manner at 230°C. Use of the titration procedure gave a plot shown in Figure 4. A first order reaction is reasonable if one considers that a large portion of the partially cured resin adduct is in the form of a molecular species having both acid and hydroxyl groups. Thus the reaction in this study would be primarily an intramolecular polycondensation and first order. Calculation

of the first order reaction rate constant for this reaction gives a value of 0.175 minutes^{-1} and a half life of 3.95 minutes respectively.

Saponification of Coal Acid Resins

A brief look at the saponification rates of some of the coal acid polyesters may be of interest at this point. The completely cured resin (225°C. for 2 hours) ground to less than 250 mesh was suspended in N/10 sodium hydroxide. The suspension was stirred at room temperature and portions removed at intervals for titration. The saponification rates of the diethanolamine, ethylene glycol and pentaerythritol resins of the coal acids are shown in Figure 5. The lower saponification rates of the diethanolamine and pentaerythritol resins can be explained by steric hinderance. Saponification of the pentaerythritol resin by several different concentrations of sodium hydroxide shows that the rate and extent of degradation is proportional to the alkali concentration.

C. Physical Properties of Coal Acid Resins

1. Physical Strength

Sand briquettes were used as the test media in determining the physical strength of the coal acid resins. The one inch thick sand briquettes were of the figure eight shape and identical to the form adopted by the A.S.T.M. for evaluation of foundry molding sands. Table II lists the tensile strengths of the various resin bonded sand briquettes. All the resins were physical mixtures of one equivalent coal acids and one equivalent reactant in water unless otherwise stated.

The resins in order of decreasing strength are the ethylene oxide adduct, pentaerythritol, glycol and alkanolamine adducts. The alkanolamine type resins can be considerably overcured without imparing their strength, while a glycol resin bonded briquette overcured for 5 minutes at 260°C. suffers a strength loss of some 20%.

2. Heat Stability of Cured Coal Acid Resins

Investigation of the coal acid resins as a glass fiber binder prompted a study of the resin's heat stability. Briefly, the method of test consisted of suspending a powdered sample of the cured resin in a wire screen holder placed in a vertical furnace. A thermocouple placed in the sample continuously measured the temperature of the sample as the furnace temperature was gradually increased and the resin started to burn. The slope of the combustion temperature curve between 700 and 1100°F. was used to express the rate of resin combustibility. The reciprocal slope (Δ temp./Δ time) was used in order to obtain numbers greater than one. If no resin combustion takes place under the conditions used the resin sample temperature will not exceed 700°F. Therefore, the temperature line between 700 and 1100°F. would be due to the resin heat of combustion.

A second heat stability test applied to our resins determined the critical temperature at which the resin would completely burn without added heat. The overall heat stability of the particular resin was shown by combining the slope factor and critical temperature into the expression $\frac{\Delta \text{ temp.}/\Delta \text{ time}}{\text{critical temp.}}$. Some of our combustibility data from this slope method are given in Table III.

The resins in order of decreasing heat stability are diethylene-triamine, diethanolamine, ethylene glycol adduct and phenol-formaldehyde resins. The heat stability of the coal acid - polyamine resin is similar to some melamine type resins.

CONCLUSIONS:

The coal acids undergo polycondensation reactions with alkanolamines, polyhydroxyl or polyamine reactants to give thermosetting resins. Proper choice of reactants, reactant ratios and reaction conditions allows the preparation of a large number of resins with varying properties. The resin adducts may be simple mixtures of the reactants in water or a partially reacted resin which is still water soluble.

The cure process of the various resins can be followed by titration of the still unreacted carboxylic acid or amine salt groups. Thus a method is available for the evaluation of various reactants and conditions in the preparation of the coal acid resins.

Physical properties of these resins that have been studied include their strength and heat stability. The resins in order of decreasing strength are the ethylene oxide adduct, pentaerythritol, glycol and alkanolamine - coal acid resins. Many of the coal acid resins have physical strengths sufficient to allow their use as resin binders. The heat stability of several coal acid resins have been found to be superior to a typical "A stage" phenol - formaldehyde resin.

REFERENCES:

1. Franke, N. W., Kiebler, M. W., Ruof, C. H., Sovich, T. R., and Howard, H. C., Ind. Eng. Chem., 44, 2784 - 2792 (1952).

2. Montgomery, R. S., Holly, E. D. and Gohlke, R. S., Fuel, Lond., 35 (1956) 60
Montgomery, R. S., Holly, E. D., ibid. 36 (1957) 63

lbv
5-1-59

TABLE I

CURE RATES OF ETHANOLAMINE - COAL ACID RESINS AT 265°C.

Resin	Total		Ester		Amide/Imide	
	k min^{-1}	$t_{1/2}$ min.	k min^{-1}	$t_{1/2}$ min.	k min^{-1}	$t_{1/2}$ min.
Monoethanolamine	1.22	0.57	1.67	0.42	0.82	0.85
Diethanolamine	0.68	1.02	0.73	0.95	0.62	1.12
Triethanolamine	0.41	1.68	0.46	1.50	0.28	2.44
Diethanolamine	0.87	0.80	0.96	0.72	0.72	0.98
With 5% poly H_3PO_4						

TABLE II

TENSILE STRENGTHS OF COAL ACID RESIN BONDED SAND BRIQUETTES

Reactant (6% green solids)	Cure Conditions	Tensile Strength, psi.
Monoethanolamine	15 min./260°C.	128 psi.
Diethanolamine	" "	458
Triethanolamine	" "	302
Ethylene glycol (1)	" "	562
Diethylene glycol	" "	690
Propylene glycol	10 min./260°C.	464
Dipropylene glycol	22 min./260°C.	494
Triethylene glycol	18 min./260°C.	580
Ethylene oxide (2)(3)	40 min./225°C.	830
Pentaerythritol (4)	45 min./250°C.	738

Footnotes: (1) 5.5% resin solids
(2) Coal acid - ethylene oxide adduct at approximately 50% reaction.
(3) Thermoplastic after 30 min. cure
(4) Resin composed of 1 eq. coal acid and 0.9 eq. of pentaerythritol and reacted to 16% esterification.

TABLE III

COMBUSTIBILITY RATES OF CURED RESINS

Resin or Coal Acid Reactant	Temp. Time (°F. min^{-1})	Critical Temp. °F.	Slope / Critical Temp. x 10^3 min^{-1}
"B stage" phenol-formaldehyde	200	400°F.	500
50% Diethanolamine	80	680°F.	117
50% "B stage" phenol-formaldehyde Diethanolamine	66.5	700°F.	95
Diethylene-triamine	16-20	690°F.	23
Ethylene glycol	150	625°F.	240

Figure 1

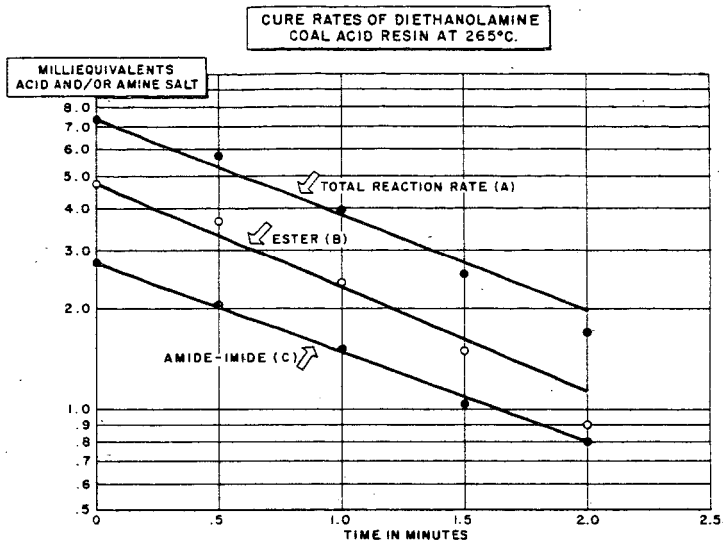

Figure 2

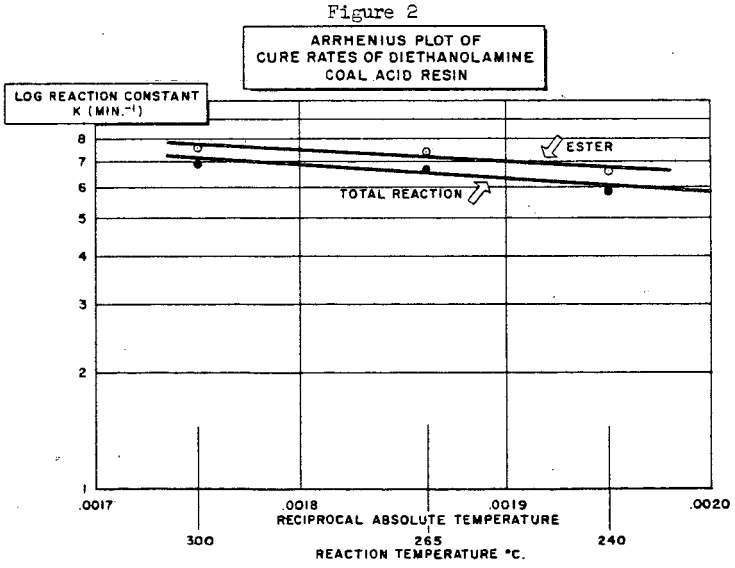

Figure 3

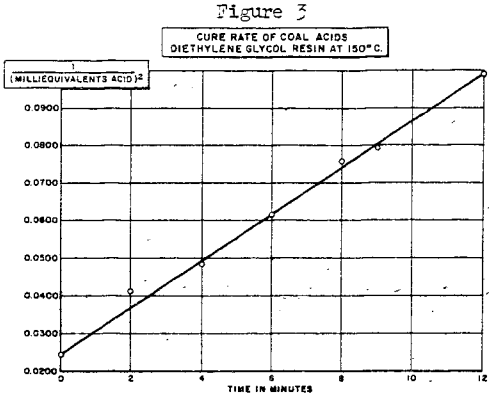

Figure 4

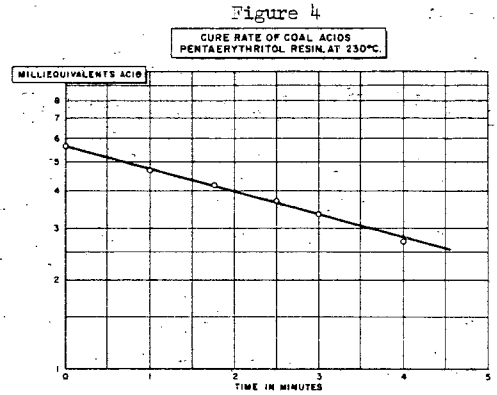

Figure 5

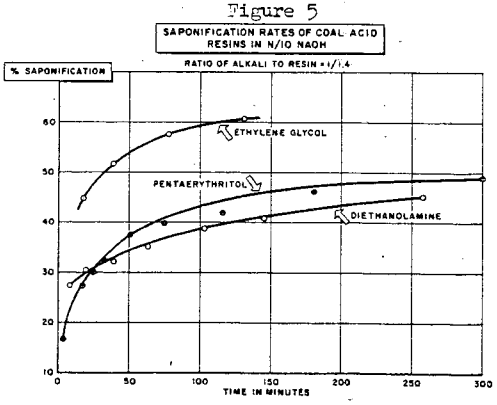

Not for Publication
Presented Before the Division of Gas and Fuel Chemistry
American Chemical Society
Atlantic City, New Jersey, Meeting, September 13-18, 1959

Coal Acids - Raw Material for Foundry Resins

By
Wesley L. Archer, James B. Louch and Robert S. Montgomery

The Dow Chemical Company - Midland, Michigan

INTRODUCTION:

Aromatic polycarboxylic acids derived from the controlled oxidation of coal[1] have been used to prepare thermosetting resins of interest to the foundry industry. The monoethanolamine, diethanolamine, ethylenediamine, diethylenetriamine and pentaerythritol adducts of these coal acids were investigated as shell molding resin binders.

The current uses of a phenol-formaldehyde resin in the foundry industry illustrates some of the market potentials for the new coal acid resins. The largest market is found in shell molding where some 17 million pounds of phenol-formaldehyde resin was used in 1957. The increased use of the phenol-formaldehyde resin with cereal binders in steel cores is another market with good growth potential.

Sand briquettes bonded with the coal acid resins were tested for tensile strength and the resins of particular interest evaluated in shell molding. The coal acid - pentaerythritol preadvanced resin was outstanding in overall performance as a shell molding binder and thus will be the resin of prime interest in this paper.

Resin Preparation

The resin adducts of interest in this investigation were homogeneous solutions of the coal acids and reactant in water. The coal acid - pentaerythritol resin was partially advanced in water to give a still water soluble homogeneous solution. These water solutions afford an easy and economical method of applying the resin to the sand. In most cases, equivalent ratios of the reactants were used in the resin preparation and resin adduct concentrations of 60-70% gave solutions of workable viscosities. The resins as water solutions have an unlimited storage life.

Requirements of a Shell Molding Resin

The first requirement of a shell molding resin is that it must give a free flowing resin coated sand which on heating thermosets to firmly bond the sand grains together. The resultant shell mold must have sufficient heat resistance to withstand the shock of molten metal and hold close tolerances until the metal has set. At the proper time in the metal set cycle the shell must also burn out to give collapse of the shell and a clean casting. The temperature of collapse can be governed by the resin type and concentration, e.g. urea formaldehyde gives a low temperature collapse for magnesium and aluminum castings. Phenolic resins afford higher heat resistance and are commonly used for malleable iron and steel castings.

The potential resin binder must be effectively and easily dispersed in a sand mix by means of a Simpson or similar type muller. Dry blending of the sand and powdered resin has been popular in the past, but it is rapidly being replaced by a more effective liquid resin coating procedure. In this procedure a source of hot air may be used during the mulling operation to dry the resin coated sand until it is free flowing. Maintenance of this free flowing condition during storage is necessary for optimum pattern performance later.

It is important that the resin binder be cured and thermoset within a reasonable period of time. The approximate time and temperature limits are illustrated in the typical shell molding procedure given below.

(1) The dry resin coated sand is dropped onto a preheated (400-500°F.) metal pattern and allowed to remain for 15-35 seconds. This time period known as the coat or dwell time determines the thickness of the shell.

(2) At the end of the proper dwell time the entire pattern is inverted 180 degrees allowing all the excess and unbonded sand to fall back into the dump box. A dough like shell of resin bonded sand is left adhering to the metal pattern.

(3) The metal pattern and partially cured shell is then placed in an electric or gas furnace (800-1400°F.) where the cure is completed in 40-60 seconds.

(4) The thermoset shell mold is then ejected from the metal pattern by hydraulically operated ejection pins.

The fabrication performance and pouring behavior of the shell mold is greatly dependent on the shell having sufficient tensile strength at a reasonable resin concentration, e.g. 3.5-5% resin solids. Factors that affect the tensile strength of the resin bonded sand include the resin's actual composition, the efficiency of the coating operation, the degree of resin flow before thermoset and the temperature range necessary for this flow. All of these factors and the conditions necessary for the optimum tensile strength can be evaluated by preparing briquettes from the dried resin coated sands.

Preparation of the Coal Acid - Pentaerythritol Resin -(ET-400)

Most of the coal acids used in this work were prepared at the Dow Chemical Company. These coal acids were similar to those made by the Carnegie Institute of Technology (2) and had an equivalent weight of 80-85 and average functionality of approximately three.

The first partially esterified coal acid - pentaerythritol resins were prepared by stirring and refluxing the mixture for a period of 3-6 hours. The degree of advancement was determined by titration of the available carboxylic acid groups. The reaction of a 75% solids solution of 1 equivalent coal acids - 1 equivalent pentaerythritol during the first two hours of reflux is rapid. An equilibrium esterification of 38% was obtained after 8 hours. When 0.9 equivalent of pentaerythritol (75% solids solution) is used an equilibrium esterification of 32% is reached after 8 hours. The effect of solids concentration on the esterification rate is shown by the fact that a 90% solids solution of ET-400-85 (contains 0.85 equivalent pentaerythritol) gives 25% esterification at the end of the first twenty minutes of reflux.

The partially advanced resin is a viscous solution which does not exhibit any precipitation on standing if the advancement is greater than 12%. The resin solution at 60-65% calculated reacted solids gave a very workable viscosity.

Physical Properties of the Coal Acid - Pentaerythritol Resins -(ET-400)

Preparation of one quarter inch briquettes from the dried resin coated sand allowed a study of the physical properties of the coated sands as they were related to the resin composition and pretreatment. The sand coating operation was done in a "Kitchen Aid" mixer or in large batches in a Simpson Muller. A source of hot air directed onto the sand mix shortens the time required for the mulling operation. After screening the coated sand through a 42 mesh screen it was dropped into a quarter inch deep briquette mold preheated to 425°F. The coated sand was allowed to stand for 10-15 seconds and then the excess unbonded sand scraped off with a thin metal strip. Curing of the briquette at 650°F. for 2 minutes gave the finished test specimen. These were then tested on a motor driven Dietert Tensile Tester.

A. Optimum Pentaerythritol Concentration in ET-400

Tensile strength determinations have shown that the pentaerythritol concentration can be dropped to 0.9 equivalent pentaerythritol to 1.0 equivalent coal acids without reducing the resin's bonding strength. Use of a 1:1 ratio of hydroxyl to carboxylic acid groups would seem unnecessary since steric hinderance undoubtedly prevents the reaction of some of the carboxylic acid groups.

B. Physical Strength vs. Resin Concentration

A plot of the percent of reacted resin solids on a coarse Ottawa sand vs. the resultant tensile strengths is shown in Figure 1. The briquettes were bonded with an ET-400-9 resin with a preadvancement of 17.5% and cured for 2 minutes at 650°F. A tensile strength of 360 psi. is obtained at the 4% resin level commonly used in commercial shell molds. Naturally, the strength at a certain resin level will vary with the size distribution of the sand, the clay content of the sand, the resin composition and the coating techniques. Each of these factors will be discussed later.

C. Effect of Resin Preadvancement

The tensile strength of the ET-400 resin coated sand has been found to be a function of the resin preadvancement. The preadvancement necessary for optimum tensile strength appears to be in the range of 13-18%. Figure 2 shows the effects of preadvancement on the tensile strengths of two different resin coated sands. This particular data was obtained on small one and a half pound batches of sand coated in a "Kitchen Aid" mixer. The one tensile strength value in Figure 2 marked muller demonstrates that higher tensile strengths may be expected from the more effective coating obtained with a Simpson Muller.

The presence of clay and other nonsilica impurities in the Vasser bank sand could explain the differences in tensile strength of the Vasser bank AFS 100 sand as compared with the high silica content Wedron AFS 116 sand. The clay and silt impurities could indeed decrease the flow of the resin before the thermoset. Thus, flow of the resin coating on a sand grain to the surrounding sand grains and formation of a complete bond would be decreased.

The most important property controlled by resin advancement is the rate and temperature at which the resin flows. The improved flow behavior of the resin on coated sands with less preadvancement is directly reflected in the improved tensile strengths. The temperature at which the resin film on a sand grain will start to flow can be determined and is referred to as the stick point. A lower preadvancement of the ET-400 resin gives a lower stick point and a resultant higher tensile strength.

Preliminary observations have shown that the amount of moisture pickup by the resin coated sand is another factor controlled partially by the degree of resin advancement. Thus, adequate resin advancement is necessary so that the resin coated sand will remain in a free flowing condition before actual use. Sand coated in a Simpson Muller with a resin of at least 15% preadvancement will give a stable free flowing sand. This range of resin preadvancement may also be expected to give nearly optimum tensile strengths.

Shell Mold and Core Fabrication

The ET-400 resin with optimum sand binding properties was then examined in the actual fabrication of shell molds and cores. The small three prong cover plate type shell mold that was prepared on a small dump box machine is shown in Figure 3. Hollow shell cores have also been prepared on a commercial Shalco core blowing machine. Both

pieces of equipment employ the same basic principles of investment, removal of excess unbonded sand and final cure as outlined earlier.

A. Sand Coating Procedure

The proper mulling procedure is second only to the resin in determining the final behavior of the coated sand in shell mold fabrication. The resin formulations for actual shell fabrication were applied to 20 pound batches of sand contained in a Simpson Muller.

A typical coating operation for the Simpson Muller is given below:

(1) Charge 9000 grams of sand and 550 grams of liquid ET-400-9 resin (4% reacted solids on sand) and 20 grams Acrawax (0.22%) to the muller.

(2) Mull for 1 minute.

(3) Hot air supply started and continued until coated sand went through the agglomeration stage.

(4) Mulling continued for an additional 15 minutes with hot air.

(5) Coated sand dumped and screened through a 40 mesh screen.

The Acrawax serves as a lubricant for the final resin coated sand and helps the sand retain its free flowing character. The hot air for the mulling operation was furnished by a small modified hair dryer with a maximum nozzle temperature of 500°F.

During the agglomeration stage it was found necessary to stop the muller several times and manually break up the plastic like sand mass. Coating of 720 pound batches of Nugent AFS 75 sand with ET-400 in a commercial size muller did not give this problem. The entire cycle from resin addition to coated sand discharge required 14 minutes in the commercial setup. Total time for the coating operation in the small Simpson Muller was 35 minutes.

B. Shell Mold Properties

A Nugent AFS 75, coarse Ottawa or Wedron AFS 116 sand coated with 4% of ET-400-9 resin gave good three prong cover plate shell molds at a pattern temperature of 450-500°F., investment time of 15 seconds and cure time of 40-60 seconds. A resin preadvancement of approximately 15% is preferred for maximum tensile strength and pattern performance at a low pattern temperature of 450°F. Moisture stability of the ET-400-9 coated sand appears to be good since no buildup of coated sand on the back side of the shell and/or peel back of a portion of the shell occurs. An excessive amount of moisture also tends to cause the agglomeration of the individual sand particles into units of several particles. These small agglomerates give poor packing of the sand particles at the pattern surface and the resulting poor surface hardness and strength.

The differences in tensile strengths of a high silica sand and bank sand shell mold is again illustrated by the following values. The tensile strength of the 4% ET-400-9 (advanced 16%) coated Nugent sand averaged 315 psi. as compared to the value of 795 psi. for the resin on Wedron sand. Hardness as measured by a Dietert Hardness Tester was 80 for the Nugent shells and 90 for the Wedron sand shells.

Recent work has shown that the addition of a nonionic surfactant, e.g. 0.25% Triton X-100, to the resin coated Nugent or Vasser sand will give a 25% strength increase. Replacement of 30% of the pentaerythritol in the ET-400 resin with a

glycol or ethylene oxide adduct will also give a 25-40% increase in the resin strength. Thus the tensile strength of a modified 4% ET-400-9 coated Nugent sand can be expected to average 400-450 psi.

A field test of the ET-400-9 resin as a shell molding binder has been attempted at a malleable iron foundry. The resin used in this test was one of the earlier ET-400-9 formulations preadvanced to 28.5%. The performance of the resin in the coating of the Nugent sand in 720 pound batches was good. Shell molds of 20 x 30 inches in size were fabricated at a pattern temperature of 500°F., investment time of 34 seconds, and cure time of 50-60 seconds. Figure 4 shows one of the 20 x 30 inch shell molds being ejected from the pattern after cure. Approximately 25 castings weighing 11 pounds a piece were successfully cast without any major metal breakouts. The major point for improvement appeared to be the need for increased tensile strength. Tensile bars prepared from this coated sand gave an average tensile strength of 170 psi. The ability of the newest ET-400 formulation to give some 400 psi. strength on Nugent sand may give the needed additional strength for a completely successful commercial test.

C. Shell Core Properties

Acceptable commercial hollow shell cores (23 inches in length and 2-5 inches in width) have been fabricated on a Shalco core blowing machine using a 3.5% ET-400-9 coated Wedron sand. The resin had been advanced to 28.5% esterification. Shell cores with excellent hardness (90 on Dietert Tester), detail and strength were prepared at 600°F. with an investment time of 5-15 seconds and cure time of 1.5-2.0 minutes. These conditions correspond to cure conditions used with a commercial phenol-formaldehyde resin coated high silica sand.

Core Binders

The foundry industry's interest in improved core binders has encouraged the use of the urea formaldehyde and phenolic formaldehyde resins. Principle use of the phenolic resin in solid foundry cores has been limited mostly to steel cores. The need for a more heat resistant binder for steel cores has limited the resin to a phenolic type. The cheaper urea formaldehyde type resin finds wide use in the nonferrous and ferrous type foundries. Both resins are used in conjunction with various cereal flours and core oil binders.

Preliminary data indicates that several of the coal acid type resins may find utility in foundry cores. Specifically, cores with tensile strengths of 570 psi. have been prepared from an Ottawa AFS 60 sand bonded with 1.0% ET-400-9, 1.0% Mogul B211 flour and 5% water. Core mixes of this type have been successfully core blown with commercial machines. The tensile data of other coal acid resins given in the preceding paper also suggests the possible use of these in the core binder application.

Preparation of briquettes from a moist resin coated sand and allowing the briquettes to stand at room temperature leads to the development of considerable green strength. This green strength is the result of the air drying of the resin film to give a "dry" water plasticized resin film surrounding and bonding each sand particle. The diethanolamine resin adduct for example, yields an optimum strength of 325 psi. at a 6% resin concentration while 6% of the diethylenetriamine adduct gives a green strength of 240 psi. after only 20 hours at room temperature. This green strength property could also be of interest in sand core fabrication.

CONCLUSIONS:

Increasing foundry interest in new synthetic thermosetting sand binders has opened markets for resin binders that have new and improved physical properties. A new type of sand binder for this purpose may be derived from the oxidation products of bituminous

coal. Specifically, thermosetting resins may be prepared from these coal acids and an alkanolamine, polyhydroxyl or polyamine reactant.

The coal acid - pentaerythritol resin (ET-400-9) preadvanced to 13-18% esterification is of particular interest in shell molding work. A 13-18% preadvancement will produce a free flowing sand with optimum tensile strength. Experimental shell molds have been prepared with this ET-400-9 resin at a pattern temperature of 450-500°F., investment time of 15 seconds and cure time of 40-60 seconds. Both high silica content sands and bank sands have been used in the shell mold fabrication. At a 4% resin concentration 315 psi. of tensile strength can be expected with a medium fine, unwashed bank sand. The addition of a surfactant to the resin increases the strength of the resin bonded bank sand to 400 psi. Use of a fine, washed high silica content sand increases the tensile strength to 795 psi.

One attempt to use ET-400-9 as a commercial shell molding binder indicated that a somewhat greater tensile strength is necessary. A new formulation with only 15% advancement may afford the needed strength improvement. Tensile strengths of the original resin bonded sand were 170 psi. as compared to the later tensile strengths of 400 psi. (contains 0.25% surfactant). Commercial shell cores have also been fabricated with ET-400-9.

REFERENCES:

1. Montgomery, R. S., Holly, E. D. and Gohlke, R. S., Fuel, Lond., 35 (1956) 60
Montgomery, R. S., Holly, E. D., ibid. 36 (1957) 63

2. Franke, N. W., Kiebler, M. W., Ruof, C. H., Sovich, T. R., and Howard, H. C., Ind. Eng. Chem., 44, 2784 - 2792 (1952).

Figure 1

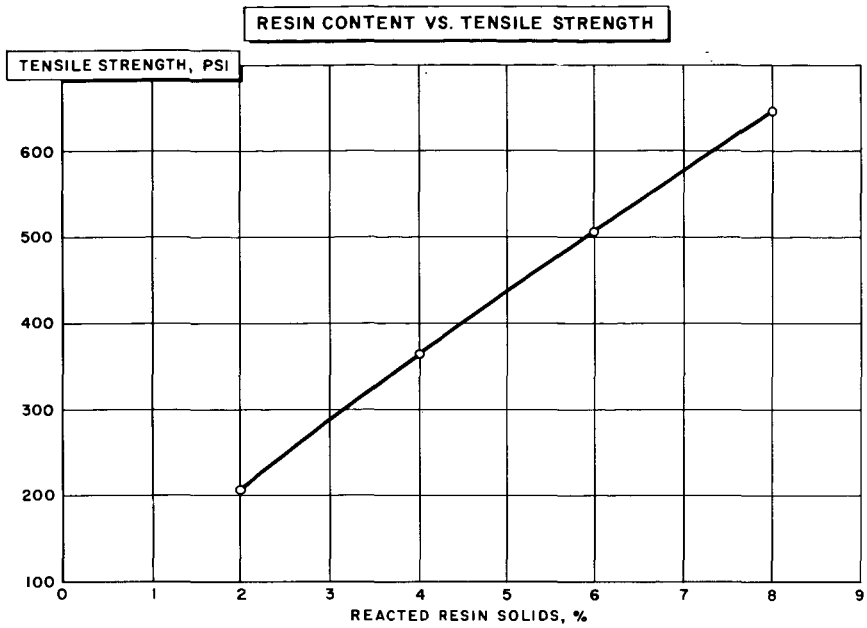

Figure 2

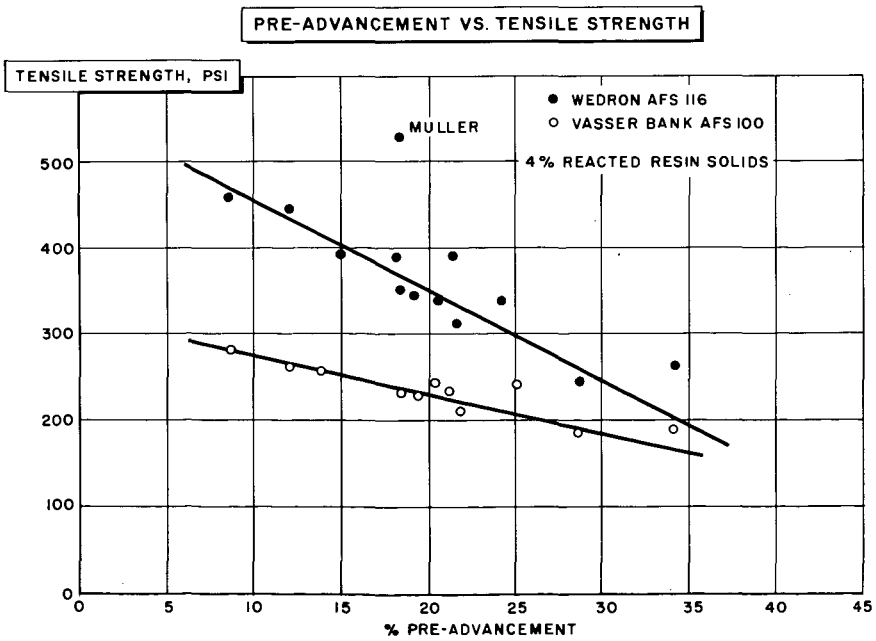

Figure 3

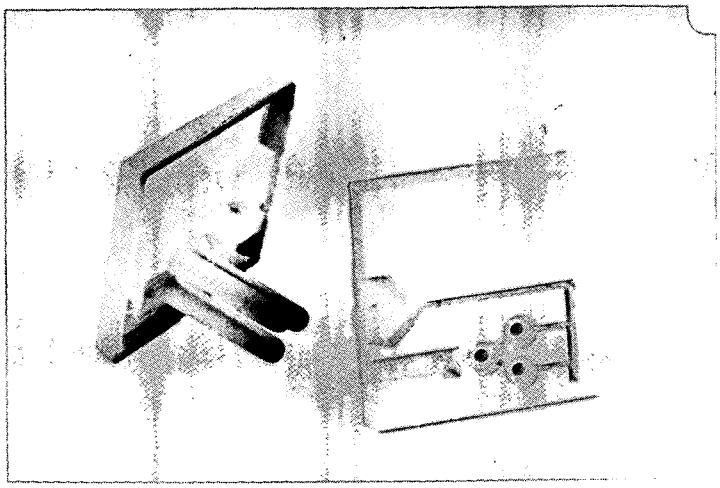

Figure 4

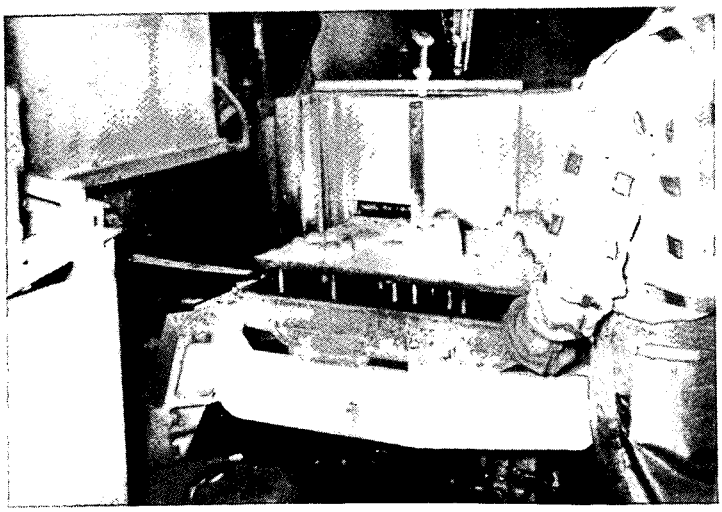

Not for Publication
Presented Before the Division of Gas and Fuel Chemistry
American Chemical Society
Atlantic City, New Jersey, Meeting, September 13-18, 1959

A Mass Spectrometric Study of the Carbon-Carbon Dioxide Reaction

F.J. Vastola and P.L. Walker, Jr.
Fuel Technology Department, The Pennsylvania State University
University Park, Pennsylvania

INTRODUCTION

Carbon dioxide can react with carbon to form carbon monoxide. This is a reversible reaction which can be represented by the equation

$$C + CO_2 \rightleftarrows 2\ CO \quad .$$

Factors such as the type of carbon used and the impurities present in the carbon can drastically affect the rate of the reaction.

There have been a number of mechanisms proposed for this reaction (1-10). Most of these mechanisms postulate the formation of a surface oxide or complex as an intermediate step in the reaction. There is some agreement that the surface complex does not exist at temperatures above 800°C. and, hence, does not play an important role in the reaction carried out at higher temperatures.

In order to investigate the carbon-carbon dioxide reaction with particular emphasis on the role of any surface oxide intermediate, certain factors must be considered. Since the surface oxide is believed to be unstable at temperatures greater than 800°C., the reaction should be carried out at temperatures as much below this point as possible in order to maximize the probability of surface oxide formation. The amount of gas necessary to completely cover a carbon surface is relatively small (approximately 10 micromoles per square meter for carbon monoxide as the adsorbate (11)). Therefore, the relative change in pressure resulting from the formation of a given amount of surface complex can be maximized by operating at low pressures. A sufficient number of the reaction variables have to be measured to be able to compute a complete material balance throughout the progress of the reaction. Furthermore, the measuring system has to be sensitive enough to detect small amounts of reaction in order to minimize the effect of changing surface area during the course of the reaction.

For this investigation, carbon was reacted with carbon dioxide at temperatures from 400°C. to 700°C. and at starting pressures from 2.7 to 16 microns of mercury. The reaction was followed by monitoring the partial pressures of carbon dioxide and carbon monoxide using a mass spectrometer. The sensitivity of the mass spectrometer was sufficiently great to detect surface coverages of 0.01 per cent and reaction of 0.001 per cent of the carbon in the system.

APPARATUS AND EXPERIMENTAL PROCEDURE

Figure 1 shows a schematic picture of the low pressure reactor. The tubing in the system is $1\frac{1}{4}$ inches in diameter; the volume of the system is 16.6

liters. The fused silica reactor tube is set at an angle of 45° so that thermal convection will aid in the mixing of the reacting gases. The system can be evacuated to pressures of 10^{-5} mm. Hg using an oil diffusion pump which is connected to the reactor by stopcock S_1.

There are three pressure measuring devices - an ionization gauge, a thermocouple gauge and a McLeod gauge. Since the mass spectrometer measures partial pressure of all gases present, it also can be used as a pressure measuring device.

The reaction system can be isolated from the mass spectrometer by stopcock S_4. The reaction gases are admitted to the reaction system through stopcocks S_2 and S_3.

The carbon sample is placed in a 1 x 5 cm. fused silica tube sealed at one end. The sample container can be lowered into the reaction tube through a sample port in the upper part of the apparatus. The sample container rests on a fused silica tube, which extends upwards from the bottom of the reaction tube. This support tube also contains a chromel-alumel thermocouple. The cap for the upper port in the reactor contains a Pyrex optical-flat window through which the sample can be observed.

The sample is heated by a 1 KW tube furnace which surrounds the reaction tube. The furnace is $8\frac{3}{4}$ inches long. The temperature of the furnace, as indicated by the thermocouple in the sample support tube, is regulated by an automatic controller-recorder.

The mass spectrometer has been modified so that the reactor can be directly connected to the inlet leak of the spectrometer analyzing tube. Under the conditions used in this investigation, the spectrometer bled off less than two per cent of the total gas present during the course of a run.

A programmed magnetic field controller was constructed to enable the mass spectrometer to sequentially monitor the mass 44 (CO_2^+) ion beam and the mass 28 (CO^+) ion beam every 15 seconds.

In order to determine the time constant of the analyzing system, the reactor was filled with carbon monoxide to a pressure of 8 microns of mercury; and a 5 per cent increment of carbon dioxide was admitted into the reactor. By adjusting the mass spectrometer to monitor mass 44 (CO_2^+), the time taken for the 44 peak to reach a steady state gives an idea of the rate of diffusion and mixing of the gases in the reactor. It was found that the response of the spectrometer was practically instantaneous, with a steady state value obtained within 5 seconds.

The carbon used for this investigation was a highly ground sample of SP-1 spectrographic graphite*. The spectrographic graphite was ground** for 16 hours

---

* The unground SP-1 sample was supplied by the National Carbon Company.

** The SP-1 sample was ground through the courtesy of Mr. S.B. Seeley of the Joseph Dixon Crucible Company.

in a vacuum ball mill in order to increase its surface area, as described recently by Walker and Seeley (12). After grinding, the area of the graphite wear dust was 560 $m.^2/g.$ The grinding process introduced ca. 5 per cent iron into the sample.

The carbon sample was heated to a temperature of 850°C. in vacuum for 3 hours prior to each run. This pretreatment insured that the gases evolved upon the heating of the sample at the end of each run were a result of the reaction and not the past history of the carbon.

RESULTS AND DISCUSSION

Figure 2 shows typical data obtained from the mass spectrometer during a run. This figure illustrates how the spectrometer is calibrated for carbon monoxide, and carbon dioxide just prior to and immediately after the reaction period. Also it shows removal of the surface complex as carbon monoxide upon outgassing the sample following the reaction.

Figure 3 presents the results of this run after data reduction. The reaction rates could be duplicated to within 5 per cent in runs at the same temperature. It was found that the rate of carbon monoxide formation was slightly less than twice the rate of carbon dioxide consumption. This departure from a two to one ratio involves a small amount of carbon monoxide "tied" to the surface of the carbon sample. This complexed carbon monoxide could be recovered by heating the carbon in a vacuum at higher temperatures after the run.

Figure 4 shows the plots of log carbon dioxide concentration versus time for the reaction over the temperature range 400° to 700°C. The experimental data very closely follow a log function throughout the course of the reaction at all temperatures. This indicates that the rate of reaction of carbon dioxide is first order with respect to the carbon dioxide pressure throughout the entire reaction at all temperatures investigated.

With the experimental conditions used in this investigation, two factors can affect the reaction rate, chemical reactivity and the rate of diffusion of the reacting gas through the unconsolidated carbon sample. When the rate of diffusion is large compared to the rate of chemical reaction, the latter will completely control the over-all rate of reaction. Under these conditions the rate of reaction per unit surface area will not be affected by variation in sample size. However, if the rate of chemical reaction is greater than the rate of internal diffusion, an increase in weight of sample reacted will not have a proportional effect on the over-all rate of reaction. Therefore, the rate of reaction per unit surface area will decrease. It was found that the rate of reaction per unit surface area varied with weight of sample reacted.

Table 1 gives the rate constants* for the decrease in carbon dioxide pressure with time per unit surface area versus the sample size.

---

* In a constant pressure reaction system or a constant volume reaction system where only a small amount of the total gas is heated, the rate data obtained should be normalized to a constant concentration basis. For this investigation, 27°C. was taken as the standard temperature. Therefore, the experimental rate constants were multiplied by the ratio of the temperature of the reaction to the standard temperature in degrees absolute.

TABLE 1

EFFECT OF TOTAL SURFACE AREA OF GRAPHITE WEAR DUST ON THE RATE CONSTANT FOR THE DECREASE IN CARBON DIOXIDE PRESSURE IN THE REACTION $C + CO_2 \rightarrow 2\ CO$

Temperature °C.	Rate Constant k, $sec.^{-1}\ m.^{-2} \times 10^6$	
	53 $m.^2$ Surface Area	133 $m.^2$ Surface Area
400	1.21	1.12
500	28.7	23.6
650	116.7	89.0

From Table 1 it can be seen that as the reaction temperature decreases the rate constant becomes less dependent on the sample size. This indicates that there was some diffusion control throughout most of the temperature range investigated, with chemical control being almost complete below ca. 450°C. At the lower temperatures, the activation energy approaches a value of 38 kcal./mole.

Figure 5 shows the per cent of the carbon surface that was covered by complex at the end of a reaction versus reaction temperature. It can be seen that the amount of complex formed increases to a maximum in the 600°C. region and then rapidly decreases. The reason for this trend is apparent when one refers to Figure 2. It is noted that in the outgassing of the sample following a run, the complex which has been formed is quite stable until the carbon is heated to temperatures greater than 600°C. The temperature at which the complex was formed was found to have little effect upon its stability.

The carbon monoxide surface complex could be formed as a product of the carbon dioxide reaction

$$C + CO_2 \rightarrow CO + C(O)$$

or it could be due to the chemisorption of carbon monoxide on the surface of the sample,

$$CO \rightarrow (CO)$$

Here C(O) represents a complex formed upon reaction of CO_2, while (CO) represents chemisorbed carbon monoxide. By exposing the carbon surface to carbon monoxide, the rate of chemisorption can be studied. It was found that the rate of chemisorption increased to a maximum around 600°C. Table 2 shows the amount of carbon monoxide chemisorbed at 600°C. for various pressures and lengths of time. The coverage of 0.125 per cent of the surface in three days indicates that only a small fraction of the total surface will chemisorb carbon monoxide. The relatively small difference between the amount of surface coverage at a pressure of 2.7 microns of carbon monoxide for 30 minutes and a 24 micron pressure of carbon monoxide for 3 days indicates that the majority of this small area is rapidly saturated with chemisorbed carbon monoxide. The chemisorbed carbon monoxide could be recovered by heating the carbon to temperatures greater than 600°C.

TABLE 2

PER CENT OF WEAR DUST SURFACE COVERED WITH CHEMISORBED CARBON MONOXIDE AT 600°C.

	Pressure, (microns of CO)		
Time	2.7	8	24
30 min.	0.054	0.065	0.074
3 days	-	-	0.125

Since the chemisorbed carbon monoxide exhibits the same characteristics as the complex formed during the carbon dioxide reaction, it appears that the complex is chemisorbed carbon monoxide. This chemisorption is a side reaction and does not play a role in the mechanism of the conversion of carbon dioxide to carbon monoxide.

It is recalled that, as a result of the grinding process, the carbon sample used in this investigation contained ca. 5 per cent iron. A ground sample from which the iron was removed did not chemisorb any measurable amount of carbon monoxide. The iron had a very strong catalytic effect on the reactivity of the carbon. The "iron-free" sample had to be heated ca. 300°C. higher than the "iron-containing" sample in order to obtain a comparable reactivity. Although the experimental data indicate that the carbon dioxide is converted to carbon monoxide with no measurable build-up of any intermediate products, the great difference in reactivity between the original "iron-containing" sample and the "iron-free" sample indicates that the iron must play an important role in the reaction mechanism.

A possible mechanism by which the iron could catalyze the reaction would be,

$$y\ CO_2 + x\ Fe \rightleftarrows Fe_xO_y + y\ CO \qquad (1)$$

$$Fe_xO_y + y\ C \rightleftarrows x\ Fe + y\ CO\ . \qquad (2)$$

Both steps one and two in this mechanism are reversible reactions. The equilibrium constant of step one is pressure independent and is approximately one for the range of temperatures used in this investigation. Step two is a pressure dependent reaction; operation at low pressures of carbon monoxide favors the reduction of the iron. If the rate of the forward reaction in step two is sufficiently fast to prevent a significant build-up of iron oxide, the rate of the back reaction in step one would be small. Under these conditions, only the forward reactions of step one and two would play an important role in the over-all reaction scheme.

ACKNOWLEDGEMENT

We wish to express our appreciation to the Mineral Industries Experiment Station of The Pennsylvania State University for supplying the financial support for this research.

REFERENCES

1. Frank-Kamenetski, D.A., Comp. Rend. Acad. Sci. (URSS), 23, 663 (1939); C.A., 34, 4642 (1940).
2. Gadsby, J., Long, F.J., Sleightholm, R., and Sykes, K.W., Proc. Roy. Soc., 193A, 357 (1948).
3. Bonner, F., and Turkevich, J. Am. Chem. Soc., 73, 561 (1951).
4. Brown, F., Trans. Faraday Soc., 43, 1005 (1952).
5. Gulbransen, E.A., and Andrew, K.F., Ind. Eng. Chem., 44, 1048 (1952).
6. Rief, A.E., J. Phys. Chem., 56, 785 (1952).
7. von Fredersdorf, C.G., "Reactions of Carbon with Carbon Dioxide and with Steam", Institute of Gas Technology Research Bulletin No. 19 (1955).
8. Ergun, S., J. Phys. Chem., 60, 48 (1956).
9. Key, A., Gas Research Board Commun. (London), No. G.R.B. 40 (1948).
10. Wu, D.C., "Kinetics of the Reaction of Carbon with Carbon Dioxide", D.Sc. Dissertation, Mass. Inst. Tech., (1949).
11. Emmett, P.H., and Brunauer, S., J. Am. Chem. Soc., 59, 1553 (1937).
12. Walker, P.L. Jr., and Seeley, S.B., Proceedings of the Third Conference on Carbon, U. of Buffalo, 1959, p.481.

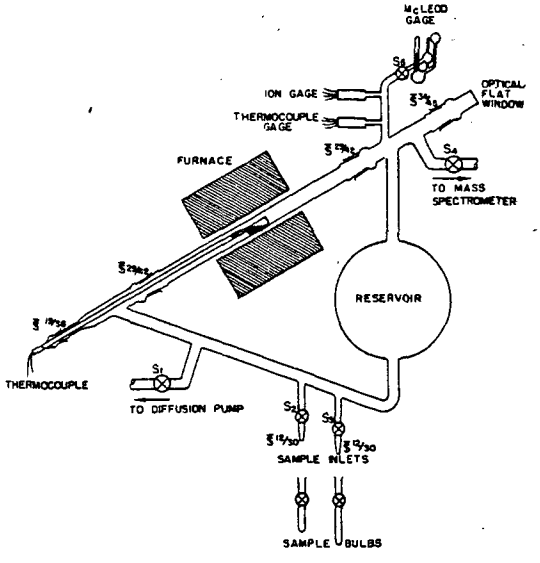

FIGURE 1 - LOW PRESSURE REACTOR

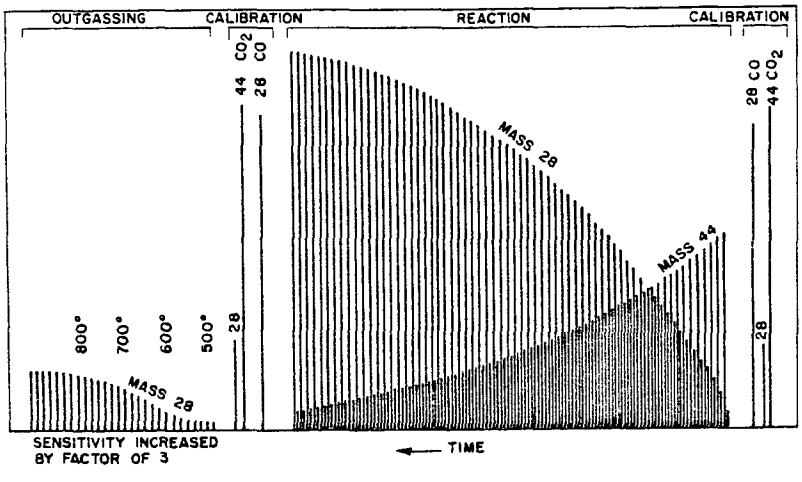

FIGURE 2 - TYPICAL MASS SPECTROMETER RECORD

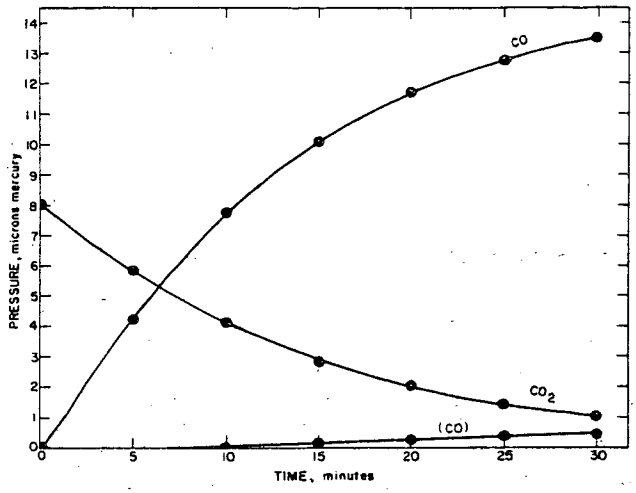

FIGURE 3 - TYPICAL REACTION CURVES

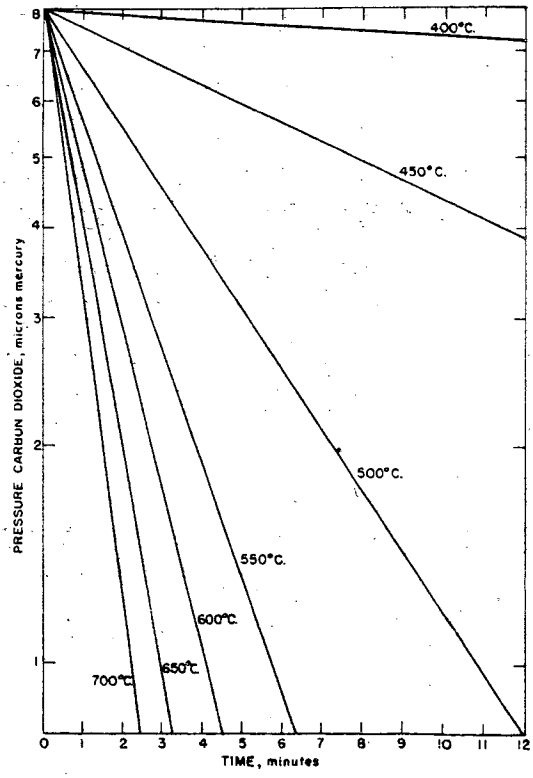

FIGURE 4 - REACTION CURVES FOR GROUND SP-1 GRAPHITE

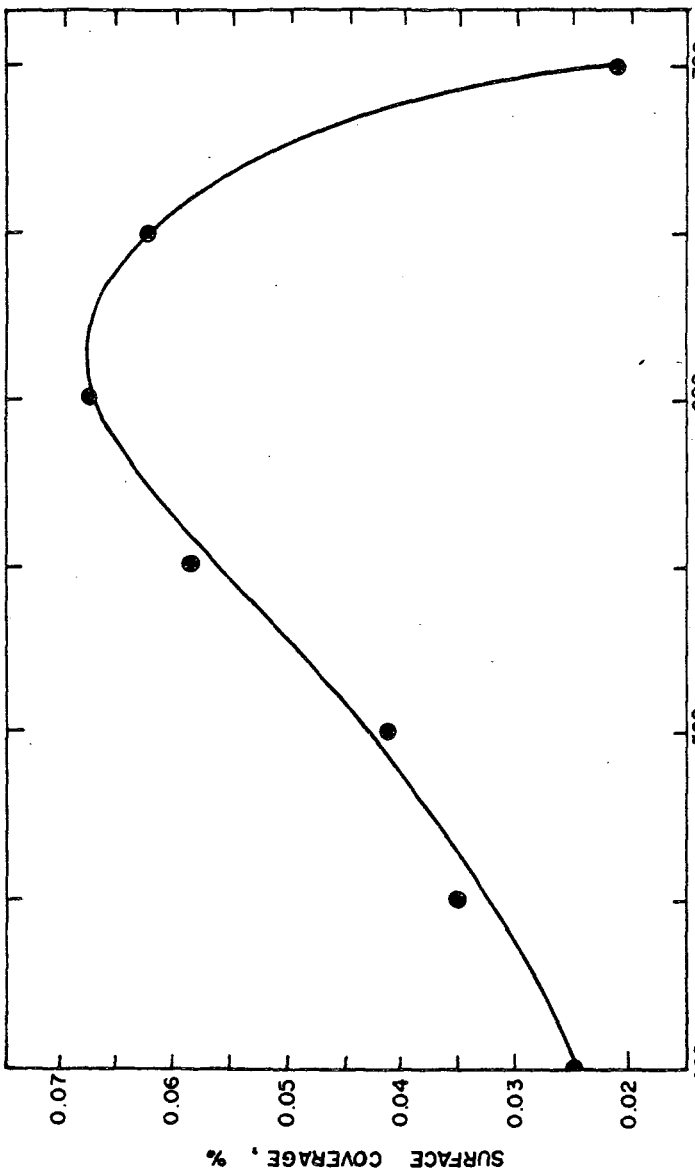

FIGURE 5 – SURFACE COVERAGE OF OXIDE COMPLEX AT END OF REACTION VERSUS REACTION TEMPERATURE

Not for Publication
Presented Before the Division of Gas and Fuel Chemistry
American Chemical Society
Atlantic City, New Jersey, Meeting, September 13-18, 1959

The Impurities in an Acid-Washed 1° Coke-Oven Benzene. Concentration of Impurities by Progressive Freezing

C. F. Glick, A. J. Miskalis, and T. Kessler
Applied Research Laboratory
United States Steel Corporation
Monroeville, Pennsylvania

A knowledge of the impurities in an acid refined 1° coke-oven benzene was required for the logical selection of methods for the purification of this product. Surprisingly little definitive information is available on the impurities, other than thiophene and carbon disulfide, in refined coke-oven benzene. Stinzendörfer (14)* reported that naphthenes of the methylcyclohexane type prevailed in a residual gasoline fraction obtained in the purification of European coke-oven benzene. Anderson and Engelder (6) prepared a sample of saturated nonbenzenoid hydrocarbons from nitration-grade coke-oven benzene by fractional crystallization and fractional adsorption. From the condensation temperatures and refractive indexes of the fractions obtained by efficient distillation of this sample, they inferred the presence of cyclohexane; methylcyclohexane; 3-methylhexane and/or 3-ethylpentane; n-heptane and/or 2,2,4-trimethyl pentane; 1,1-dimethylcyclopentane; and trans-1,2-dimethylcyclopentane and/or trans-1,3-dimethylcyclopentane. A small concentration of toluene was detected, and appreciable concentrations of unsaturated impurities were also indicated. They estimated that the original nitration-grade benzene contained 0.6 volume per cent saturated nonbenzenoid hydrocarbons, 0.004 volume per cent toluene, and 0.1 volume per cent unidentified components.

Anderson, Jones, and Engelder (7) examined the recycle material from the catalytic ethylation of refined coke-oven benzene by the same methods. Any or all of the following paraffins and naphthenes were possible: 2,2-dimethylbutane; 2,3-dimethylbutane; 2-methylpentane; 3-methylpentane; n-hexane; 2,2-dimethylpentane; 2,4-dimethylpentane; 2,2,3-trimethylbutane, 3,3-dimethylpentane; 2,3-dimethylpentane; 2-methylhexane; 3-methylhexane; 3-ethylpentane; n-heptane; 2,2,4-trimethylpentane; cyclopentane; methylcyclopentane; cyclohexane; 1,1-dimethylcyclopentane; trans-1,3-dimethylcyclopentane; trans-1,2-dimethylcyclopentane; cis-1,2-dimethylcyclopentane; cis-1,3-dimethylcyclopentane; and methylcyclohexane. However, the authors observed that some lower-boiling paraffins (2-methylpentane, 3-methylpentane, and n-hexane) appeared to have been introduced during the ethylation process; while most of the naphthenes (except cyclohexane) in the original benzene appeared to have been largely removed. In addition to this serious objection, the inherent limitations of the methods employed in both studies by Anderson and his associates make it virtually impossible, without prohibitive effort, to prove conclusively that any particular compound is present and to measure its concentration accurately.

Kimura and Yasui (11) identified methylcyclohexane and 2,2,4-trimethylpentane in the residue from the commercial chlorination of benzene.

In the present work, the components of virtually the entire impurity content of a conventionally acid-washed 1° coke-oven benzene have been identified positively, and their concentrations have been measured.

* See References

Apparatus

A Perkin-Elmer Model 154-B Fractometer, equipped with a precision temperature controller, was used for the gas-liquid chromatographic separations. Samples were introduced by means of Perkin-Elmer calibrated capillary pipets. The following columns were used:

(1) Two 2-meter by 0.25-inch-diameter stainless-steel-tubing columns of Perkin-Elmer Corporation "A" material (didecylphthalate on Celite 545, proportions unknown).

(2) A 25-foot by 0.375-inch-diameter copper-tubing column of polypropylene glycol 2025 (Union Carbide Chemicals Company) on 30-60 mesh Fisher Column Packing in the proportions 31:69.

(3) A 40-foot by 0.375-inch-diameter copper-tubing column of a mixture of o- and p-benzylbiphenyls on 30-60 mesh Burrell Inert Carrier in the proportions 24:76.

The mass spectrometric analyses were performed with a Consolidated Model 21-103C mass spectrometer.

Reagents

All of the pure compounds for calibration of the gas chromatograph and the mass spectrometer were either standard samples from the American Petroleum Institute or research grade materials from the Phillips Petroleum Company.

The benzylbiphenyl was prepared by the procedure of Goldschmiedt (10). The particular sample of benzylbiphenyl that was used as the stationary phase in gas-liquid chromatography was a mixture of predominantly the o- with the p-isomer, with a crystallizing point of approximately 65°.

Procedure

The benzene selected for this study of impurities was a typical, refined, 1° coke-oven benzene, from the high-temperature carbonization of bituminous coal in modern by-product ovens. This benzene was produced by washing crude benzene-toluene-xylene mixture from coal-tar light oil with 66° Baume sulfuric acid in the conventional manner, neutralizing, and distilling. The benzene had a total distillation range (2) of 79.8 - 80.4 C. Its freezing point (3) was 5.07° C, and its purity (4) was 99.30 mole per cent. Its total sulfur content, determined by a combustion procedure, was 177 ppm. Its thiophene content, determined by the isatin method, was 444 ppm. Its carbon disulfide content by the diethylamine-cupric acetate method was 0.36 ppm. Its bromine index by the proposed ASTM potentiometric titration method was 1.8, which corresponds to 0.00088 mole per cent olefin, if it is assumed that, at worst, all the bromine reacted on an equimolar basis with olefins, and that none reacted with the thiophene. This maximum olefin content is so low that this benzene can be considered to be virtually olefin-free.

Preliminary gas-liquid chromatographic examination of the refined 1° benzene showed that the concentrations of some of the impurities were so small that they must be enhanced to permit certain identification. Schwab and Wickers (13) first introduced the method of progressive or slow fractional freezing for the purification of materials, like benzoic acid, that freeze above room temperature. Dickinson and Eaborn (9) adapted the method to the purification of materials, like benzene, that freeze below room temperature. The principle of either version of

the method is the slow advancement of the solid-liquid interface into the liquid phase. This advancement must be so slow that there is ample opportunity for impurities to be rejected by the freezing solid into the remaining liquid. When most of the sample has frozen, the remaining impure liquid can be removed mechanically, and the purification has been effected. This process requires very simple apparatus and very little effort. The time required compares very favorably with that needed for a careful fractional distillation, and quite small samples can be handled. The efficiency of the purification is impressively high, and the principle is asserted to be superior to zone melting involving a single zone.

If this process can be used to purify a material, then, by the same token, it can be used to concentrate the impurities from that material. To test this argument, part of Dickinson and Eaborn's work was repeated as follows: Approximately 20 ml of thiophene-free ACS-specification benzene was placed in a glass-stoppered test tube, 14 millimeters in internal diameter, 140 mm in length below the tubulure, and approximately 22 ml in volume. This tube, suitably counterweighted, was lowered by a miniature windlass (driven by an electric clock motor, 1 revolution per hour) at a rate of 3 cm per hour into an ice-water bath maintained at constant level. At the beginning of the experiment, the tip of the tube was touched briefly with a small piece of dry ice to start crystallization and avoid supercooling. Approximately 90 per cent of the sample was frozen after 3 hours. The liquid 10 per cent was withdrawn with a hypodermic syringe, the solid was melted, and the process was repeated until six freezings had been performed. The starting material, the six liquid portions withdrawn, and the final purified material were all subjected to gas-liquid chromatographic analysis on the Perkin-Elmer "A" column at 80.5° C. The chromatogram of the liquid withdrawn after the first freezing displayed six impurity peaks, which were 1.13, 1.50, 4.26, 4.50, 2.17, and 6.04 times as large as the corresponding peaks in the chromatogram of the original benzene. For each liquid portion withdrawn after each successive freezing, the impurity peaks became smaller. The purified material left after the sixth freezing was pure benzene by this test; there were no impurity peaks whatever in its chromatogram. Dickinson and Eaborn's preparation of pure benzene was therefore confirmed, and the application of their technique to the preparation of concentrated impurities is valid. Some time after this work was done, Matthews and Coggeshall (12) also demonstrated the application of progressive freezing to the concentration of impurities from organic compounds.

One obvious extension of the progressive-freezing technique is its application in cascade. For this purpose, a large glass-stoppered test tube (27 mm in internal diameter, 380 mm in length below the tubulure, approximately 230 ml in volume) was substituted for the smaller test tube. This tube, suitably counterweighted, could be lowered into an ice-water bath, maintained at constant level, by the same windlass arrangement at 5 centimeters per hour. Approximately 90 per cent of a 200-ml sample of the refined 1° coke-oven benzene was progressively frozen in this apparatus in 8 hours. The remaining 20 ml of liquid ("10 per cent off, first pass, first freezing") was withdrawn by syringe and subjected to another progressive freezing in the smaller test tube. Again 90 per cent was frozen and the remaining 2 ml of liquid ("10 per cent off, first pass, second freezing" or "concentrated impurities") was withdrawn. The original refined 1° benzene and the 10 per cent portions withdrawn in the first and second freezings were chromatographed on the polypropylene glycol 2025 column at 121° C. The resulting chromatograms, Figure 1, show the increases in concentrations of impurities that are achieved by cascade operation. In this figure, the three chromatograms have been displaced vertically from each other to a slight extent for the sake of clarity. The encircled numbers designate the various peaks. The attenuation factors are marked near the peaks. In Table I, the heights of the easily measurable impurity peaks in these three chromatograms are tabulated. The first freezing produced a two- to threefold increase in most of the peaks; the second freezing produced a nearly

twofold increase over the first. Cascade operation therefore produced approximately a fivefold increase in most of the peaks. The cascade method was therefore adopted for the production of "concentrated impurities" from the refined 1° benzene.

In view of the extremely small concentrations of some of the impurities in the refined 1° benzene, all the qualitative analyses were performed on the concentrated impurities. The benzylbiphenyl column, originally described by Desty and Whyman (8), was used for all the gas-liquid chromatographic separations, because of its superior resolving power for aromatics and paraffins. This column was operated at 121° C, and 500 µl (nominal) of sample was introduced. A typical chromatogram is shown in Figure 2. The very large sample volume was used to supply detectable amounts of the minor impurities, such as those in peaks 1 and 6. To obtain additional information to supplement the chromatographic data, so that qualitative identifications could be made with certainty, each peak in the chromatogram was collected in a trap cooled in liquid nitrogen. The contents of each trap were then analyzed by mass spectrometry. In each case, the mass spectrum of the contents of the trap was first corrected for the very small contribution of the "column blank"--the very small amount of the stationary phase and/or its decomposition products that is vaporized constantly from the chromatographic column and is caught in the trap when it is cooled. The hydrocarbon-type analysis developed originally by Brown (5) was next applied to each mass spectrum to facilitate its interpretation. When the relative retention volume for a chromatographic peak was used to narrow the choice of possible components contributing to that peak, it was then usually rather simple to confirm or reject each of the possible components from the mass spectrum. The relative retention volumes of a small number of pure hydrocarbons were determined under the conditions prevailing in the qualitative analysis, that is, on the benzylbiphenyl column at 121° C, "flooded" with 500 µl of benzene. From these data and the published values for a large number of compounds at 78.5° C (8), the relative retention volumes at 121° C for these compounds could be estimated with sufficient accuracy for the preliminary qualitative analyses. Once the presence of a compound had been established by the preliminary chromatographic and mass-spectrometric data, its presence was further confirmed by direct experimental measurement of its relative retention volume on the benzylbiphenyl column at 121° C, "flooded" with 500 µl of benzene. Similarly, published mass spectra (1) were used for the preliminary interpretations, but once the presence of a compound had been thus established, its mass spectrum was determined by direct experimental measurement with the Model 21-103C spectrometer. The qualitative compositions of the substances producing the peaks in the chromatogram in Figure 2 are shown in Table II. As more than one compound contributed to each impurity peak and as progressive freezing affected the concentrations of the compounds contributing to any peak to different unknown extents, it was obviously necessary to perform the quantitative analysis directly on the original 1° benzene.

The quantitative analyses were performed by collecting quantitatively in a cold trap the substance producing each peak in the gas chromatogram of a known amount of the original 1° benzene (similar to Figure 2, but with smaller impurities peaks). The time intervals marked above the chromatogram in Figure 2 are identical with those used in the trappings for the quantitative analyses. The entire contents of the trap were then admitted to the mass spectrometer and analyzed quantitatively. Since the concentrations of the several impurities varied over a very wide range, not all of the peaks could be trapped from a single sample of the 1° coke-oven benzene. The amount of sample used in each case is shown in Table II. For a very minor impurity, 500 µl (nominal), which is the practical maximum accommodated by the chromatographic column, would provide too small an amount of impurity for spectrometric analysis. In that case, a sufficient number of 500-µl (nominal) portions of the 1° benzene was chromatographed in succession to supply the necessary amount of impurity for the spectrometric analysis. When the desired chromatographic peak appeared in each chromatogram,

the same collecting trap was applied to the vent line of the chromatograph until the necessary total amount of that impurity had been collected.

Because this whole procedure can be no more accurate and precise than the quantitative operation of the cold traps, these were studied carefully. The first traps used were simple U-shaped lengths of capillary tubing 2 mm in internal diameter and 18 inches in length, provided with vacuum stopcocks near each end and a standard taper joint at one end (8). Six such traps were used with a manifold arrangement connected to the vent line of the chromatograph. The possibility of absorption of minor components by stopcock grease and occasional plugging of the capillary by frozen condensate led to the adoption of a simpler system, which was used for all the final quantitative analyses. A short glass Y-tube was butted against the end of the vent line of the chromatograph. The butt joint was held in place with Tygon tubing. The traps were of the conventional concentric tube design, 175 mm long, with the inner tube 6 mm in external diameter and the outer tube 16 mm in external diameter. The inner tube ended 15 mm above the bottom of the outer tube. One of these traps was connected to each arm of the Y-tube with a section of Tygon tubing just long enough to permit the application of a hosecock clamp. A drying tube filled with Ascarite was connected with a similar short length of Tygon tubing and clamp to the exit tube of each trap to minimize back-diffusion of moisture and carbon dioxide into the trap when it was chilled. Each trap was purged at room temperature with helium before use. As there were no stopcocks in the system, grease was eliminated. By connecting the traps to the Y-tube and manipulating the clamps at the proper times, any peak could be collected in a trap. Although this arrangement was not quite as fast or convenient as the manifold with stopcocks, it did eliminate the possibility of partial loss of components by absorption in stopcock grease. The traps were immersed to only about one-half to two-thirds of their length during use. As soon as the trapping was completed, the liquid nitrogen level was raised so that the entire length was immersed. By this procedure, loss of trapped material by warming of condensate in the upper part of the trap should be eliminated. The trap was butted to the mass-spectrometer inlet system with Tygon tubing, and its entire contents were analyzed quantitatively in the usual way.

The performance of this entire procedure was tested by introducing known amounts of pure compounds or known mixtures into the gas chromatograph, collecting the components in the chilled traps connected to the chromatograph vent line, and measuring the amounts collected by mass spectrometry. Pure n-heptane was used first. In seven tests, the recovery achieved was 80, 94, 114, 106, 109, 108, and 101 per cent of the amount introduced. A mixture comprising 62.7 volume per cent n-heptane and 37.3 volume per cent cyclohexane (mass spectrometric analysis) was tested next. Each component was trapped individually. In duplicate tests, 108 and 108 per cent of the heptane and 101 and 101 per cent of the cyclohexane introduced were recovered. From these data, the apparent recovery achieved with the procedure might be estimated at 100 $\pm$ 10 per cent, although, for reasons unknown, recoveries outside these limits, particularly on the low side, may be observed occasionally.

Positive errors (recoveries higher than 100 per cent) may be caused by 1) excess liquid sample clinging to the outer surfaces of the capillary pipette with which samples are introduced into the gas-liquid chromatograph, and/or 2) error in the calibration of the very small capillary pipette (0.5 μl) with which pure liquids are introduced into the mass spectrometer for calibration. The first error is variable; the second is constant. The first error was minimized by touching only the very tip of the pipette to the surface of the liquid sample, removing the pipette from contact with the liquid, and waiting perhaps 15 seconds before introducing the sample into the chromatograph. By this procedure, the excess liquid is minimized at the outset, and the very small excess that cannot

be avoided has time to evaporate. The second error is caused by the difficulties during calibration of filling with mercury the very tiny volume of the mass spectrometer pipette and emptying it completely. Beyond exercising the utmost care in all the manipulations and replicating the calibration with good repeatability, the authors know of no obvious improvement.

Negative errors (recoveries lower than 100 per cent) may be caused by 1) failure to introduce the entire sample into the chromatograph, 2) less than quantitative trapping, and 3) losses in introducing the trapped sample into the mass spectrometer. Gross errors of the first kind can be detected immediately by variations in the peak heights in the chromatogram, and the test can be rejected. The second error is difficult to isolate and study. Packing the trap or increasing the contact of the vapor with the trap walls in other ways might increase the efficiency of trapping, but might also make it more difficult to vaporize all the condensate into the mass spectrometer or to clean the trap for reuse. The third error was minimized by eliminating stopcock grease from the spectrometer inlet system by butting the trap to it with Tygon tubing.

Two special modifications of the standard concentric cylindrical traps were made. When peak No. 9 (Figure 2), the small peak on the long tail of the very large peak No. 8, was trapped, sizable amounts of the material of peak No. 8 were collected and plugged the ordinary trap. A special trap was therefore made to avoid this difficulty, with the external tube 24 mm in outside diameter and 115 mm long, and the internal tube 15 mm in outside diameter and 100 mm long. This trap was amply large to accommodate all the material collected. When peak No. 8 was collected, this trap was still large enough, but in this case it was desirable to introduce the collected material into the mass spectrometer as a liquid. For this reason, a small tip, 8 mm in diameter and 35 mm long, was blown into the bottom of one of the special traps. After the material from peak No. 8 had been collected in this trap, the frozen condensate was melted into the small tip, which was then broken off to make the liquid available.

All the quantitative analyses were performed in duplicate at least. In view of the fact that those errors (described above) that are most difficult to control all tend to cause less than quantitative recoveries, replicate analyses that gave low results were regarded with suspicion and repeated.

Results and Discussion

The qualitative and quantitative analyses of the mixtures producing each of the ten peaks in the chromatogram of the 1° coke-oven benzene on the 40-foot benzylbiphenyl column at 121° C are tabulated in Table II. In every case, the residual mass spectrum remaining after the contributions of these components had been calculated was examined. For peaks No. 1, 2, 3, 4, 5, 8, 9 and 10, these residuals were within the expected mass spectrometric error, that is, no residual peak was larger than 3 per cent of the largest peak in the mass spectrum and was usually appreciably less. For these mixtures, it is highly probable that no additional components (beyond those listed in Table II) would be identified at concentrations exceeding approximately 0.005 mole per cent (in each mixture) in any more exhaustive investigation. For peak No. 7, the largest residual mass peak was 4.3 per cent of the height of the largest peak in the spectrum. Moreover, residual peaks occurred at masses 43, 57, 69, 71, 85 and 97, which were 3 to 4 per cent of the height of the largest peak. It is highly probable that some unidentified alkanes and/or naphthenes, present at a total concentration of less than approximately 0.03 mole per cent, account for these peaks. This is approximately 4 per cent of the total 0.70 mole per cent impurity determined cryoscopically.

The type analysis calculated from the mass spectrum of peak No. 6 showed 86 per cent naphthenes and 13 per cent alkanes, with an average carbon number of 8. From the mass spectrum, the naphthene is very probably a trimethylcyclopentane. The specific isomer could not be identified, however, because only six of the possible eight geometric isomers of trimethylcyclopentane (excluding stereoisomers) have been prepared in the pure state and their mass spectra published. The relative retention volume of peak No. 6 also confirms the hypothesis that the naphthene is a trimethylcyclopentane. The impossibility of identifying the naphthene specifically also makes it impossible to identify the accompanying alkane specifically. From the mass spectrum and the relative retention volume, the alkane is very probably an octane. The estimates of the concentrations of the naphthene and the alkane were made from average published values for the mass spectrometric sensitivities for trimethylcyclopentanes and octanes, respectively. These are only estimates, but peak No. 6 in any case accounts for only about 1.5 per cent of the total impurities.

Appreciable concentrations of impurities might be obscured by the very extensive benzene peak (similar to peak No. 8, Figure 2). The material producing this peak was therefore collected and analyzed as previously described. This material was benzene of even higher purity than the benzene of 99.93 mole per cent purity that was used for calibration. The probability of any appreciable concentration of impurities being obscured by the benzene peak is therefore slight.

The chromatograms of "concentrated impurities" on the polypropylene glycol 2025 (Figure 1) and the benzylbiphenyl (Figure 2) columns exhibited three and one peaks, respectively, arriving before peak No. 1. As the total concentrations of the component(s) producing these peaks are very probably appreciably less than one part per million, no attempt was made to collect and identify them.

It can be seen from Table II that most of the 2-methylhexane was found in peak No. 2, but that a small amount was also found in peak No. 3. This is a direct consequence of the fact that the 2-methylhexane had not been completely eluted with the other components of the first peak, before the components of the second peak of the pair began to elute. Similarly, most of the n-heptane was found in peak No. 4, but a small amount was found in peak No. 5. However, as long as both peaks of each pair are trapped from the same sample introduction, no error is caused by this partial failure to resolve the components. This procedure was followed in each of these cases.

In Table III, therefore, the qualitative and quantitative analyses of the impurities have been tabulated on a cumulative basis, without regard to the distribution of a component between two peaks. The concentrations are expressed as volume, weight, and mole per cent, all based on the whole benzene sample. A total of 20 impurities was identified -- 8 alkanes, 8 naphthenes, 1 aromatic, and 1 heterocyclic compound with certainty; and 1 alkane and 1 naphthene with good probability. Neither olefins nor carbon disulfide were detected, as was expected from their very low concentrations. The 501 ppm thiophene determined here agrees fairly well with the 444 ppm found by the isatin method. The average 4.4 per cent of the impurities unaccounted for agrees well with the approximately 4 per cent unaccounted for in peak No. 7.

For all the specifically identified components present in concentrations exceeding 0.007 mole per cent (1 per cent of the total impurity), the average repeatability of the determinations was $\pm$ 3.9 per cent; the worst repeatability was $\pm$ 9.9 per cent. For all the specifically identified components present in concentrations less than 0.007 mole per cent, the average repeatability was $\pm$ 8.3 per cent; the worst repeatability was $\pm$ 24.2 per cent. Over-all repeatability, calculated from the total impurities found, was $\pm$ 2.7 per cent. The accuracies

of individual analyses cannot be estimated; in fact, the only indication of accuracy is the total average recovery, 95.6 per cent of the total impurity measured by the cryoscopic method, which is usually highly accurate for a sample of this kind.

The occurrence in coke-oven benzene of 2,2-dimethylpentane; 2,4-dimethylpentane; 2-methylhexane; 3,3-dimethylpentane; 2,3-dimethylpentane; 3-methylhexane; 3-ethylpentane; 1,trans-2 dimethylcyclopentane; 1,trans-3 dimethylcyclopentane; and 1,cis-2 dimethylcyclopentane, which had been identified tentatively by Anderson and his associates (6, 7), has now been established definitely. 1,trans-2, cis-4 trimethylcyclopentane has been identified in coke-oven benzene for the first time. (The occurrence of another trimethylcyclopentane is highly probable.) Eleven new products of the high-temperature carbonization of bituminous coal have therefore been established with certainty.

Acknowledgments

The authors gratefully acknowledge the assistance of J. E. Friedline, who helped to record many of the mass spectra; of the Chemical Service Section, Coal, Coke, and Chemicals Division, Applied Research Laboratory, for the ASTM analyses; and of the U. S. Steel Fellowship at the Mellon Institute for the preparation of the benzylbiphenyls and for the development of the combustion method for total sulfur.

Literature Cited

1. American Petroleum Institute, Research Project 44, Petroleum Research Laboratory, Carnegie Institute of Technology, Pittsburgh, Pa., "Catalog of Mass Spectral Data".

2. Am. Soc. Testing Materials, Philadelphia, Pa., "Fuels, Petroleum, Aromatic Hydrocarbons, Engine Antifreezes," Designation D850-55, p. 1252, 1955.

3. ibid, Designation D1015-55, p. 465, 1955.

4. ibid, Designation D1016-55, p. 480, 1955.

5. Am. Soc. Testing Materials Committee D-2 on Petroleum Products and Lubricants, "Proposed Method for Hydrocarbon Types in Gasoline by Mass Spectrometry," 1956.

6. Anderson, J. R., and Engelder, C. J., Ind. Eng. Chem., 37, 541 (1945).

7. Anderson, J. R., Jones, A. S., and Engelder, C. J., ibid, 37, 1052 (1945).

8. Desty, D. H., and Whyman, B. H. F., Anal. Chem., 29, 320 (1957).

9. Dickinson, J. D., and Eaborn, C., Chemistry and Industry, 1956, 959.

10. Goldschmiedt, G., Monatsh. Chem., 2, 433 (1881).

11. Kimura, S., and Yasui, H., J. Chem. Soc. Japan, Pure Chem. Sect., 75, 163 (1954).

12. Matthews, J. S., and Coggeshall, N. D., "The Removal of Impurities From Organic Compounds by Progressive Freezing," Pittsburgh Conference on Analytical Chemistry and Applied Spectroscopy, March 3-7, 1958.

13. Schwab, F. W., and Wickers, E., J. Res. Nat. Bur. Standards, 32, 253 (1944).

14. Stinzendorfer, H., Oel u. Kohle, 38, 193 (1942).

Table I

Enhancement of Concentrations of Impurities in 1° Coke-Oven Benzene by Cascade Application of Progressive Freezing

Peak Number (Figure 1)	Chromatogram Peak Height, arbitrary units		
	Original 1° Benzene	"10% Off, First Pass, First Freezing"	"10% Off, First Pass, Second Freezing" "Concentrated Impurities"
1	0.2	0.7	1.7
2	9.6	25.7	53.6
3	13.4	35.4	74.2
4	47.4	124	251
5	20.2	53	99
6	--	--	3.7
7	2	8	19
9	--	4.3	6.0
10	0.4	1.0	2.8

Table II

Qualitative and Quantitative Analyses of the Individual Peaks in the Gas-Liquid Chromatogram of 1° Coke-Oven Benzene

Peak No. (Figure 2)	Total Volume of Sample, µl	Component	Analysis, Mole % Based on Benzene Sample		
			Trial 1	Trial 2	Average
1	1514.4	2,2-dimethylpentane	0.000130	0.000116	0.000123
		2,4-dimethylpentane	0.000747	0.000454	0.000601
2	1009.6	2-methylhexane	0.0231	0.0221	0.0226
		3,3-dimethylpentane	0.000870	0.000827	0.000849
		methylcyclopentane	0.00597	0.00599	0.00598
3	1009.6	2-methylhexane	0.000308	0.000425	0.000367
		methylcyclopentane	0.000671	0.000648	0.000659
		2,3-dimethylpentane	0.0156	0.0134	0.0145
		3-methylhexane	0.0251	0.0232	0.0242
4	169.4	n-heptane	0.0880	0.0844	0.0862
		1,1-dimethylcyclopentane	0.00697	0.00682	0.00690
		3-ethylpentane	0.00523	0.00406	0.00465
5	169.4	n-heptane	0.00490	0.00529	0.00510
		cyclohexane	0.0644	0.0613	0.0629
		1,trans-2 dimethylcyclopentane	0.0550	0.0447	0.0499
		1,trans-3 dimethylcyclopentane	0.0448	0.0487	0.0468
6	1514.4	a trimethylcyclopentane (?)	~0.00690	~0.00950	~0.00820
		an octane (?)	~0.0010	~0.0010	~0.0010
7	169.4	methylcyclohexane	0.229	0.214	0.222
		1,cis-2 dimethylcyclopentane	0.0196	0.0181	0.0189
		1,trans-2,cis-4 trimethylcyclopentane	0.00744	0.00677	0.00711
8	169.4	benzene	Pure benzene		
9	169.4	benzene		0.4777	
		thiophene	0.0466	0.0465	0.0466
10	1009.6	benzene	0.0862	0.0959	0.0911
		toluene	0.0330	0.0338	0.0334

Table III

Qualitative and Quantitative Analyses of the Impurities in 1° Coke-Oven Benzene

Peak No. (Figure 2)	Normal Boiling Point of Pure Component, °C	Component	Analysis, Based on Benzene Sample: Mole Per Cent Trial 1	Mole Per Cent Trial 2	Average Mole %	Average Vol %	Average Wt %
1	79.205	2,2-dimethylpentane	0.000130	0.000116	0.00012	0.00021	0.00016
	80.51	2,4-dimethylpentane	0.000747	0.000454	0.00060	0.0010	0.00077
	90.05	2-methylhexane	0.0234	0.0225	0.0230	0.0381	0.0295
	86.071	3,3-dimethylpentane	0.000870	0.000827	0.00085	0.0014	0.0011
2 & 3	71.812	methylcyclopentane	0.00664	0.00648	0.00656	0.0083	0.0071
	89.79	2,3-dimethylpentane	0.0156	0.0134	0.0145	0.0235	0.0186
	91.95	3-methylhexane	0.0251	0.0232	0.024	0.039	0.031
	98.428	n-heptane	0.0929	0.0897	0.0913	0.150	0.117
	87.84	1,1-dimethylcyclo-pentane	0.00697	0.00682	0.0069	0.010	0.0087
	93.468	3-ethylpentane	0.00523	0.00406	0.0047	0.0075	0.0060
4 & 5	80.738	cyclohexane	0.0644	0.0613	0.063	0.077	0.068
	91.87	1,trans-2 dimethyl cyclopentane	0.0550	0.0447	0.050	0.063	0.054
	90.77	1,trans-3 dimethyl cyclopentane	0.0448	0.0487	0.047	0.060	0.051
6		a trimethylcyclo-pentane (?)	~0.0069	~0.0095	~0.0082	~0.014	~0.012
		an octane (?)	~0.0010	~0.0010	~0.0010	~0.0018	~0.0015
	100.934	methylcyclohexane	0.229	0.214	0.222	0.319	0.279
	99.53	1,cis-2 dimethyl					
7		cyclopentane	0.0196	0.0181	0.019	0.027	0.024
	109.28	1,trans-2,cis-4 tri-methylcyclopentane	0.00744	0.00677	0.0071	0.012	0.010
9	84.1	thiophene	0.0466	0.0465	0.0466	0.0411	0.0501
10	110.623	toluene	0.0330	0.0338	0.0334	0.0396	0.0392
Total			0.685	0.652	0.670	0.933	0.808
% of the total 0.70 mole % impurity accounted for			97.9	93.1	95.6		
% of the total 0.70 mole % impurity unaccounted for			2.1	6.9	4.4		

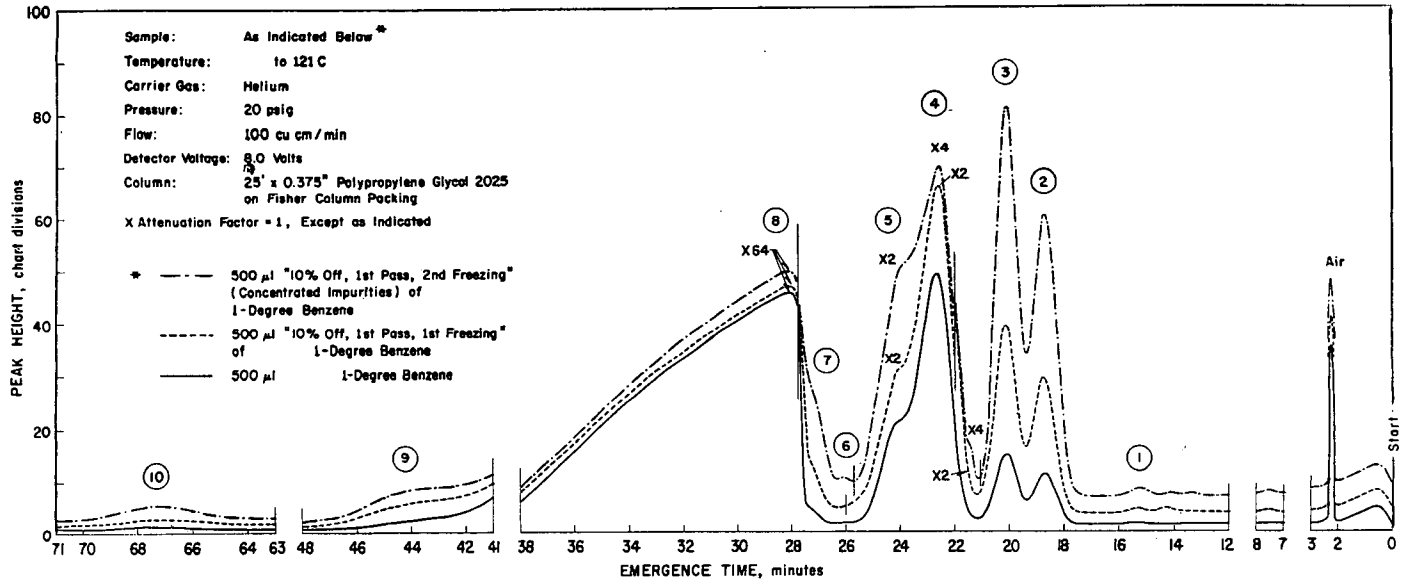

Figure 1. Gas-Liquid Chromatograms Showing Enhancement of Concentration of Impurities in 1-Degree Benzene

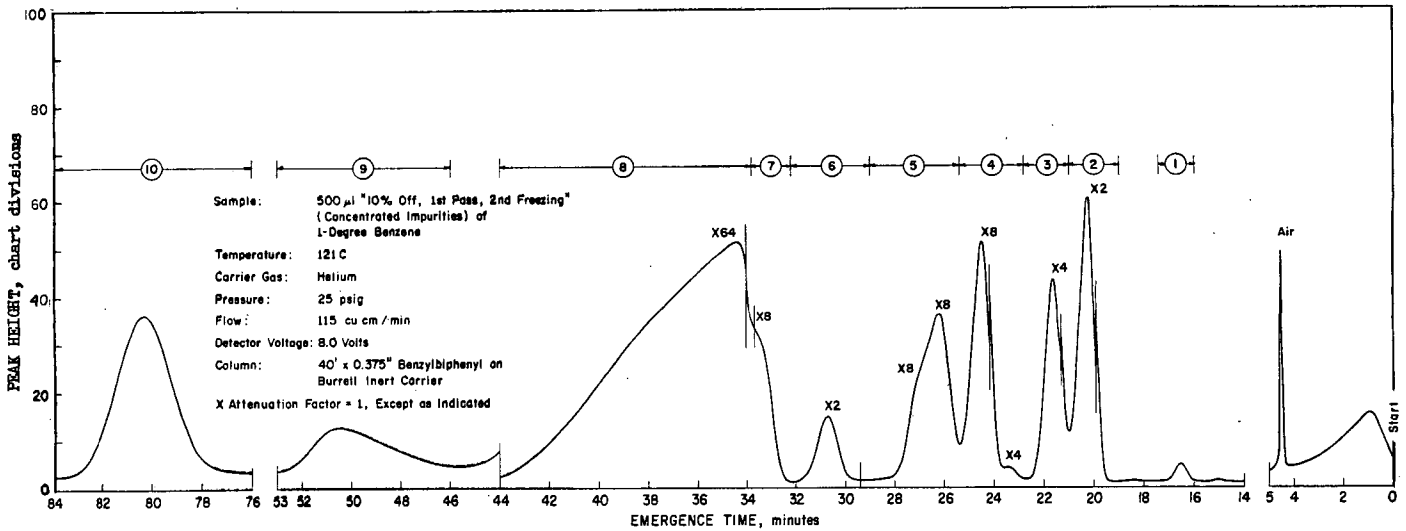

Figure 2. Gas-Liquid Chromatogram of Concentrated Impurities From 1-Degree Benzene